Complex self-organized dynamics in oscillator networks and methods of its control

vorgelegt von
Diplom-Physiker
Santiago Gil

Von der Fakultät II - Mathematik und Naturwissenschaften
der Technischen Universität Berlin
zur Erlangung des akademischen Grades

Doktor der Naturwissenschaften
— Dr. rer. nat. —

genehmigte Dissertation

Promotionsausschuss:

Vorsitzender: Prof. Dr. H. Stark
Gutachter: Prof. Dr. H. Engel
Gutachter: Prof. Dr. A. S. Mikhailov

Tag der wissenschaftlichen Aussprache: 26.1.2010

Berlin 2010
D 83

"Dios mueve al jugador, y éste, la pieza.
Qué dios detrás de Dios la trama empieza
De polvo y tiempo y sueño y agonías?"

— Jorge Luis Borges
Ajedrez

"Nos callamos un rato
cómplices en saber que la bestia humana
sólo sonreirá cuando verdad y belleza sean una sola cosa"

— Mario Trejo
El insomne insumiso o sobre los
alcances de hablar de ciertos temas

Kurzfassung

Modelle von Phasenoszillatoren sind ein Universalwerkzeug, um die kollektive Dynamik in periodischen Systemen zu untersuchen. Dabei führen Wechselwirkungen zwischen gewöhnlich regulär periodischen Elementen zu einer Vielzahl an Verhalten. Dazu zählen auch Chaos und Inkohärenz, welche für etliche Anwendungen unerwünscht sind. Die Zielsetzung dieser Arbeit ist die Untersuchung von Methoden zur Kontrolle von Chaos und Unordnung in Systemen wechselwirkender Oszillatoren und die damit einhergehenden dynamischen Aspekte.

Dazu werden Systeme gekoppelter Phasenoszillatoren betrachtet, bei denen die paarweise Wechselwirkung von einer Phasenverschiebung zwischen den Elementen abhängt. Diese Phasenverschiebung kann in einem global gekoppelten System von identischen Oszillatoren zu Desynchronisation führen. Hierbei wird der Einfluss von externem gemeinsamen, auf alle Elemente wirkendes Rauschen untersucht. Ist dieses Rauschen schwach, beobachten wir die Ausbildung von Clustern im System; starkes Rauschen hingegen führt zu Synchronisation.

Betrachtet man statt der globalen Kopplung ein Zufallsnetzwerk, geht die Desynchronisation in Chaos über. Die Auswertung des Lyapunov-Spektrums liefert in diesem Fall einen hochdimensionalen chaotischen Attraktor, welcher analog zur Phasenturbulenz in oszillatorischen Medien ist. Turbulenz kann durch die Einfuehrung von globalem Feedback unterdrückt werden. Dabei kann ein Übergang zu synchronen Oszillationen herbeigeführt werden. Entlang dieses Übergangs zeigen solche Systeme verschieden komplexe Dynamik, wie die Ausbreitung von Phasenrutschen (*phase slips*) oder zeitweilige Turbulenz. Dabei entstehen kohärente Muster, die als selbst-organisierte aktive Unternetzwerke auftreten, deren Größe und Verhalten kontrolliert werden können.

Die vorliegende Arbeit verwendet Methoden, welche selten in der Analyse von Netzwerken von Phasenoszillatoren benutzt werden. Dadurch können dynamische Muster gefunden und beschrieben werden, die bislang möglicherweise übersehen worden sind. Damit wirft diese Arbeit ein neues Licht auf selbstorganisierte Dynamik, welche am Übergang zwischen Unordnung und Synchronisation auftritt.

Abstract

Models of phase oscillators are a universal tool for the study of collective dynamics in periodic systems. The interactions of otherwise regular periodic elements may produce various kinds of behavior, amongst which chaos and incoherence may not be desirable. The objective of this work is to study possible methods to control chaos and disorder in systems of interacting oscillators, and to study the different kinds of dynamical states that can be induced in the process.

Systems of coupled phase oscillators are considered, which include phase shifts in the interactions between each pair of elements. This phase shift can lead to a desynchronization transition in a globally coupled system of identical oscillators. Under these conditions, we investigate the effect of external common noise acting on all elements. We observe that when such noise is weak, it gives rise to the formation of clusters in the system, whereas strong noise intensities bring the system to a synchronized state.

When the all-to-all coupling is replaced by a random network, desynchronization gives way to chaos. Analysis of the Lyapunov spectrum reveals a high-dimensional chaotic attractor which is analogous to phase turbulence in oscillatory media. By introducing global feedback, turbulence can be suppressed and a transition to synchronous oscillations can be induced. Along this transition, different kinds of complex dynamics can be observed, such as propagation of phase slips or intermittent turbulence. Emerging coherent patterns take here the form of self-organized active subnetworks whose size and behavior can be controlled.

This work exploits methods rarely used in the analysis of phase oscillator networks to uncover dynamical patterns that may have previously been overlooked. As such, it sheds new light on the kinds of self-organized dynamics that can be found between the boundaries of disorder and synchronization.

Contents

Introduction

The universe is abundant in systems of periodic nature. The repeated occurrence of events at regular intervals can be found ubiquitously at all scales, from atomic to astronomical; and oscillating quantities can be measured all around us. Oscillations are one of the most pervasive kinds of dynamical behavior in the physical world. Life itself seems to be dependent on the preservation of specific cycles.

The second law of thermodynamics states that a closed system will always approach an equilibrium state of maximal disorder. This should mean that all oscillations would be damped, and all activity would die out. However, the world is full of systems that are not closed. In fact, many systems, such as living systems, cannot be understood if not through its interaction with the environment, continually exchanging energy and matter. In this manner, systems that would go to a rest state in isolation can be kept active by providing them with chemical reactants, applying electrical currents, light or other kinds of energy.

Within the theory of dynamical systems, the appearance of oscillations can be understood in different ways. One common type of oscillations is that which is characteristic for Hamiltonian systems: in the absence of dissipation, oscillations are maintained due to the conservation of kinetic energy. This is the case, for example, of a frictionless pendulum.

A much more interesting situation is encountered when self-sustained oscillations develop as a result of an instability of the stationary state. In this kind of systems, oscillations are not an effect of energy conservation, but the consequence of the presence of a periodic attractor. This means that, by maintaining a flow of energy through the system, it can not only be brought to an active state of sustained oscillations, but these oscillations can also be stable. Small perturbations from this attractor do not drive the system to another state, and it relaxes back to its oscillatory dynamics.

The widespread use of phase oscillator models in diverse research areas is an example of the philosophy that is predominant in the science of complex systems. The underlying idea is that the validity of results found in a certain model may extend far beyond the specific system or object under consideration [1]. The behavior

of a generic model may tell us something about a large class of systems, for which this model may be a valid approximation. Indeed, phase oscillator models have been used to address such diverse problems as pathological synchronization in the brain and the design of therapies for it [2, 3], arrangements and control of traffic lights [4], pattern formation in oscillatory chemical reactions [5], optimization of telecommunication systems [6, 7], and many more.

The importance of phase oscillators models lies in that, while being extremely simple, they capture essential features of many different systems with periodic behavior. Let us, for example, consider systems of very diverse nature as an enzyme, a neuron or a machine in a factory. Each of them may be hard to describe mathematically, and this difficulty arises for different reasons. In the case of an enzyme, interactions between all atoms in the molecule may not be known, and single molecule experiments to study their behavior with enough precision may not be feasible. The generation of action potentials in a neuron is the result of the collective action of millions of ion channels and pumps along the membrane. And although we can know exactly what the function of each piece of a machine is, and recognize their interactions fully, the numerical simulation of a single machine may require extreme computational power, in many cases impossible to reach in real time.

Nevertheless, these three kinds of systems have clear features in common, namely that all of them operate by repeating an operational cycle. The system proceeds through a sequence of stages, each of which has a specific functionally within its operation. All of these systems operate by receiving a certain input, be it chemical reactants and ligands, action potentials in the dendrites or material flow intake. The system then goes through some conformational changes —electrochemical, physical or mechanical— to process these inputs in a specific way. A certain output is produced and released or emitted, and another conformational change will take place to restore the system to its initial configuration, where it may idle for some time (refractory period). Although variations on this cycle may exist from system to system (indeed, a machine may have several inputs and outputs), what is important for our consideration is that their operation, from a functional viewpoint, requires the repeated and periodic execution of a regular operational cycle.[1]

If we consider the operational cycle of such systems as a circle, then the progress along this cycle can be represented by an angle variable that increases at constant rate, being zero at the beginning of the cycle and covering all the circle when the end is reached. Such a variable would be known as the *phase* of the cycle, and the mathematical object representing the operational progress of the system is known as a *phase oscillator*. In this view, the complicated internal dynamics of a system is reduced to a single variable description characterizing its current stage along the operational cycle.

Of course, enormous amounts of information about the system and its state may be lost in such a drastic simplification. But this is a loss that we may be better off with if we want to gain in tractability and computability. What is important in this representation, is that very general models can be devised with such an approach,

[1] The idling time may in principle be variable, since it depends on the input. However, an average idling time in normal functioning may be considered, and taken to be part of the operational cycle.

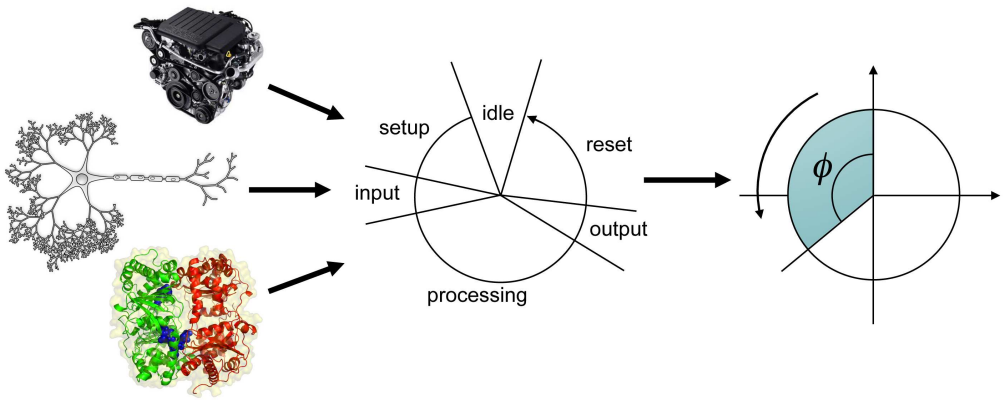

Figure 1: Operational cycle of different systems

which allow us to dispense with the specific details of a particular system, and draw general conclusions about the behavior of systems of periodic nature. Phase oscillators may be an overly simplistic way to describe a system, but they provide a solid mathematical framework to formulate a generic representation of systems of periodic nature.

A line of research has been built around the idea that the information processing and memory storage capabilities of the brain are emergent properties which are codified in a specific configuration of the synapses that connect the neurons and transmit information between them. In the neural computation and neural networks approach, so fully is the computing capability trusted to the structure of these connections, that in many of these studies, the details of neuronal properties and dynamics are ignored, and the brain is reduced to a network of switches. In this view, the capacity of the brain to learn, store and process information and assimilate new cognitive functions is rooted in the plasticity of the synapses (Hebbian learning), and therefore, it is the specific neuronal network what determines the functioning of a brain.

In other systems, such as a factory, the interactions between machines are also of crucial importance, so that the functioning of the system may require an explicit and very specific pattern of interactions defining the transmission of information, material flows or distribution lines that are necessary for operation. In the analysis of such system, a precise description of the dynamics of each machine may prove to be a distraction, and in the larger picture, it might be wise to overlook such details. Just like in the neural networks approach, much insight might be gained from the studie of greatly simplified models.

Thus, we see that very different systems essentially represent networks of interacting periodic elements. For this reason, our emphasis is placed on the interactions between elements, more than the elements themselves. We intend to investigate the interaction of extremely simple elements like phase oscillators, in the hope that such simplicity will account for more generality in the results we observe. It is in this spirit that we choose as the object of our study networks of interacting phase

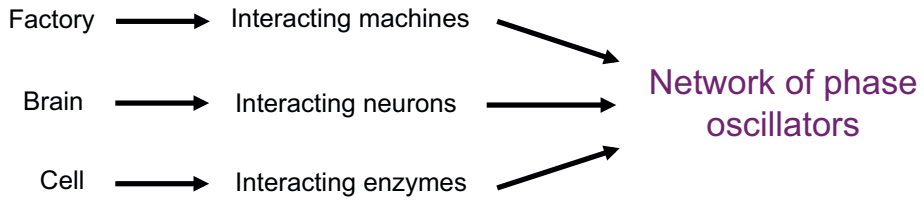

oscillators.

Through the interactions of a large number of simple elements, a great variety of dynamical states can emerge. In the context of periodic elements, such states can range from global synchronization to spatio-temporal chaos. For many man-made and natural systems, it may be a task of fundamental importance to device control methods for such dynamical states [8]. This goal is particularly clear when considering a production system, in which a specific dynamical pattern should be attained and preserved for the proper functioning of the system.

A desirable aspect of a control mechanism is the requirement to determine and manipulate only a small number of parameters. Control systems that depend on permanent measurements of the current state of the system for the calculation of a large number of corrective parameters are not only computationally expensive, but they also suffer from a high probability of failure [9].

A promising way to meet these requirements is to select systems that are self-correcting, i.e., whose stationary states are reached through a self-organized dynamical process. In this case, a system can adapt to perturbations maintaing its original state [10].

A particular implementation of a self-correcting mechanism as a method of control is that of taking a signal produced by the system and applying it back to the system as external forcing. This is what is usually referred to as a feedback mechanism. Although this signal might still need to be processed in some way for the successful implementation of a control mechanism, such a strategy may provide a solution for which no supervision or intervention is needed.

We will consider the simplest case, in which the feedback is determined by monitoring the average signal of the system and applying it back directly as an external force. In this way, only one parameter, namely the intensity of the feedback, is left for us to determine.

In the early 1990s, much excitement in the scientific community grew around the concept of the Edge of Chaos [11, 12]. In a number of different studies, it was found that, when approaching chaos, many systems presented fascinating properties, such as, e.g., the capability of universal computation [13].

Lack of general conclusions, and occationally even irreproducibility of some results made the enthusiasm wane, and critics declared such claims as lacking substance [14]. The notion of the 'Edge of Chaos' as a mysterious realm where evolution is maximized and life is permitted has fallen out of favor. We intend no endorsement to these claims, but we would like to appeal to a rather intuitive idea: that

between the rigidity of order and the irregularity of randomness is where a system may respond to perturbations in its most adaptive way, allowing for flexibility and coherence in its internal organization.

In the scientific literature on systems of interacting phase oscillators, many studies can be found which concentrate on the conditions that allow for and preserve synchronization [15]. Spontaneous synchronization of an ensemble of oscillatory elements with no kind of hierarchical organization is a remarkable phenomenon, but as a dynamical behavior, it essentially consists of all elements acting as one. On the other extreme, chaotic behavior of a large number of elements can hardly be distinguished from simple randomness. In terms of dynamical richness, it is in between these two extremes where we may expect to find the emergence of complex organization and coherent dynamical patterns [16].

Systems that are strongly ordered, as synchronized systems of oscillators, may only respond slightly to perturbations, returning to there stable order state as the perturbation ceases. In contrast, a chaotic system is unpredictable, and even the smallest perturbation would lead to uncontrolled divergence from any desired trajectory. On that account, the ambition of allowing for change and adaptability requires that the system should not be in a stable ordered state, whereas the capability of controlling the system depends on it not being in a fully chaotic state. It is this logic that leads us to go beyond synchronization and attempt to explore what can be found between the realms of order and disorder.

In this thesis we investigate several possible kinds of dynamical behavior observable in systems of interacting phase oscillators. Our intention is to clarify some of the aspects of the complex behavior encountered in the transition between synchronization and chaos, between order and disorder. In particular, the emphasis will be placed on the control of disordered states, and the different kinds of ordered and coherent dynamical states that can be thereof induced.

In the first chapter, a review is given of the theoretical background and concepts that will be used in this thesis. Mathematical tools are defined and a theoretical framework is presented within which the work is developed. Additionally, a brief review of the state of the research in this area is provided, and previous relevant works are recounted.

In the second chapter we consider a system of globally coupled elements in which a parameter representing a shift in the interactions allows us to regulate the behavior and induce a transition between synchronization and desynchronization. In the latter case, we consider the action of external global noise as a way to induce order in the system and study how the manipulation of the parameters may enable us to affect such states.

The third and fourth chapters may be considered as a conceptual unit. The former concentrates on the extension of the globally coupled case to complex networks and possible transitions between different dynamical states. In particular, properties of the high-dimensional network chaos and their dependence on the system parameters are considered. In the latter, we study the possibility of using a global feedback

mechanism as a method to control the high-dimensional chaos and induce coherent patterns of activity in the system.

Chapter 1

Theoretical background

This thesis focuses on some of the possible dynamical patterns that may emerge from the interaction of oscillatory elements. Models of phase oscillators have become a general framework in the modern research of synchronization phenomena [17, 18, 19]. These models find their roots within the theory of dynamical systems, and they are a very useful tool for the understanding of complex dynamics in large populations of periodic elements.

The subject of this work is networks of interacting oscillators and the possible coherent dynamical patterns that can be encountered between order and disorder. To investigate this, we take inspiration in the progress made on the control of pattern formation in oscillatory media.

In this chapter, relevant concepts of the theory of dynamical systems are presented, and the process of reduction to phase models is introduced. Basic properties of networks are discussed, and a brief review of previous work on synchronization phenomena in phase models is outlined, as well as the main aspects of control of turbulence and pattern formation in oscillatory extended systems.

1.1 Oscillations in nonlinear systems

The second law of thermodynamics announces that closed systems must irreversibly evolve towards a disordered, inert state. This inevitable descent towards thermodynamic equilibrium usually occurs through dissipation of energy through some form of friction. From this it follows that dynamics may be maintained in a system if friction is eliminated.

Such is the case of a frictionless linear pendulum. The kinetic energy conferred to a pendulum is periodically transformed to potential energy and back, resulting in perpetual oscillatory dynamics. Oscillatory dynamics takes place with a certain

amplitude given by the initial energy, and a perturbation sets the system to a different orbit with a different amplitude. Such systems are called *conservative*, in that energy is conserved in the evolution.

But for many systems, exchange of energy and matter with the environment is a fundamental aspect of their nature. In this case, the second law of thermodynamics is inapplicable, and oscillatory dynamics need not die out. In such systems, the flow of energy through the system may give rise to ordered self-organized oscillations which are stable against perturbations. Stable oscillatory dynamics appear as the result of supply of energy, rather than because of its conservation. As such, as long as energy is supplied to the system (for example, in the form of heat, chemical reactants, light or mechanical energy) at the rate at which it is dissipated, activity may be maintained and the system is found in a robust persistent dynamical state. For this reason, such systems are often called *active*. This kind of activity can only arise in nonlinear systems.

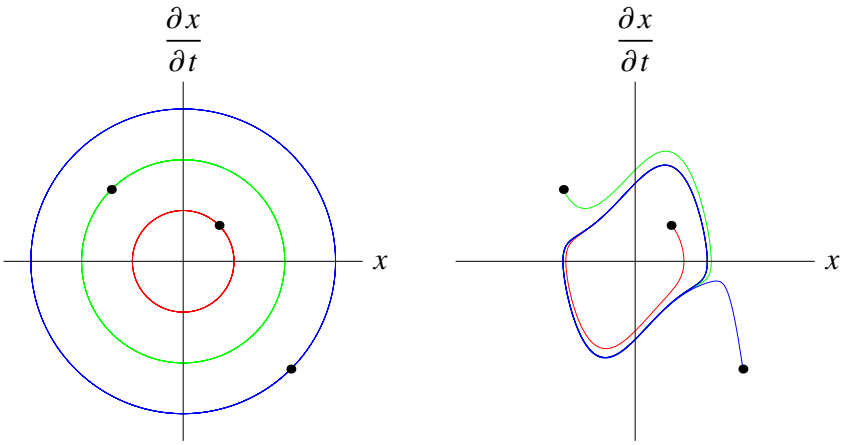

Figure 1.1: Comparison between conservative and dissipative systems. The trajectories in the phase space for different initial conditions are plotted for (left) a frictionless pendulum, and (right) a Van der Pol oscillator.

Let us compare these two different situations in two different systems, shown in Fig. 1.1. In the first panel, the dynamics of a linear frictionless pendulum is represented by plotting its velocity versus its position. Each value of the initial energy conferred to the pendulum defines a specific orbit, which is maintained as long as no other sources of energy or perturbations are present. Each of these orbits are closed, and periodic oscillations persists for all times.

The situation is entirely different in the case of a nonlinear active oscillator, such as the Van der Pol oscillator, shown in the right panel of Fig. 1.1. Starting from any initial condition, this system goes to a unique cyclic trajectory that describes oscillations with a well defined amplitude. If the system is perturbed, it will eventually return to this closed trajectory, and oscillations persist robustly. Such oscillatory behavior corresponds to an *attractor*. The frequency and amplitude of these oscillations, which are properties of the attractor, depend not on the initial conditions,

but on the parameters that characterize the rate at which energy is supplied and dissipated.

The study of the effects of nonlinearities is a central concern of the theory of dynamical systems. Below we describe some formal aspects and concepts, and introduce some of the tools utilized to understand the dynamics of oscillatory systems within this context.

1.2 Dynamical Systems

A complete mathematical description of a system requires that there is a set of variables $\{x_i\}$ that uniquely determine the *state* of the system at any given time. Each state can thus be represented by a vector $\mathbf{x} = \{x_1, x_2, \ldots, x_K\}$, where K is the number of independent variables, and therefore, the dimension of the system. For the systems plotted in Fig. 1.1, the phase space is two-dimensional, with $x_1 \equiv x$ and $x_2 \equiv \frac{\partial x}{\partial t}$. The set of all possible states is therefore a K-dimensional *state space*.

The evolution of a deterministic system is generally described by a set of ordinary differential equation of the form

$$\frac{\partial}{\partial t}\mathbf{x} = \mathbf{F}\left(\mathbf{x}, \mathbf{p}, \mathbf{h}(t)\right) , \tag{1.1}$$

where $\mathbf{p}$ represents a set of parameters that regulate adjustable properties of the system, and $\mathbf{h}(t)$ accounts for external factors that may affect the dynamics of the system and change in time independently of its state. If these factors are absent, that is, if $\mathbf{h}(t) \equiv \textit{constant}$, the system is called *autonomous*, which stresses the fact that its dynamics only depend on the system's own state. This is not to say that the system is closed. Indeed, the components of the vector of parameters $\mathbf{p}$ may stand for a constant input and output of energy and matter. Nevertheless, the fact that these parameters do not depend on time implies that the characteristics of the environment are maintained constant.

To find a solution to Eq. (1.1) we must specify a state of the system at a given time, for example, $t = 0$. $\mathbf{x}(0)$ is thus an initial condition which defines a unique *trajectory* in the phase space consisting of the points $\mathbf{x}(t)$ for all values of t.

1.2.1 Attractors

The behavior of a dynamical system is often characterized by the existence of *invariant sets*. These are sets of points in the phase space such that, if we take an initial condition within the set, then the trajectory will remain inside the set for all times[1]. A set $\mathcal{S}$ is said to be invariant if, for any point $\mathbf{x}(0) \in \mathcal{S}$, then $\mathbf{x}(t) \in \mathcal{S}$ for all t, where $\mathbf{x}(t)$ is a solution to Eq. (1.1).

A special kind of invariant set is one for which all trajectories in a finite neighborhood of it asymptotically approach the set. Such sets are called *attractors*. An attractor is an invariant set $\mathcal{A}$ to which all trajectories with initial conditions in a vicinity of $\mathcal{A}$ converge in the infinite time limit. The set of all initial conditions for

[1] This is sometimes referred to as *forward* or *positive* invariant.

which the trajectory converges to $\mathcal{A}$ is referred to as $\mathcal{A}$'s *basin of attraction*. If a perturbation throws the system out of the attractor but leaves it in its basin of attraction, then the system will return to the attractor after a certain time. Therefore, an attractor, as an invariant set, is always *stable*.

A less restrictive criterium is that of *neutral stability*. A state or set of states is neutrally stable when small perturbations from them leave the system in a vicinity of the initial state for all times, although the original state is not reached again. This is the case of a ball on a flat horizontal patch of grass: the ball rests in a point, but when it is slightly perturbed, it will rest in another point without diverging. In this example, all points in the patch are neutrally stable.

Invariant sets may also be unstable. In this case, the invariant set is not surrounded by a basin of attraction, and any perturbation that brings the system out of the attractor will cause the trajectory to separate from it. As such, unstable invariant sets may form "barriers" that the system will never cross on its own, and the dynamics of the system may be radically different depending on whether it is initialized on one or the other side of a given unstable invariant set.

A dynamical system like (1.1) may have a variety of invariant sets. They may be manifolds of different dimensions, entire regions of the phase space or other kinds of sets. Further more, their number, characteristics and stability may depend on the particular choices for the values of parameters $\mathbf{p}$. When the stability or the number of invariant sets change by varying the value of a parameter, it is referred to as a *bifurcation*, and the particular value of the parameter at which this transformation takes place is called a *critical value*.

Different kinds of invariant sets can be found in dynamical systems. Below we briefly describe the four main categories in which they can be grouped.

Fixed Points

The simplest case of an invariant set is that of a *fixed point*. A fixed point is a specific point in state space for which the dynamics is frozen. Such a point is defined by the condition

$$\mathbf{F}\left(\mathbf{x}_0, \mathbf{p}\right) = 0\,, \tag{1.2}$$

so that the system is in a stationary state in which

$$\mathbf{x}(t) \equiv \mathbf{x}_0 = constant. \tag{1.3}$$

If the system is initially set to the state $\mathbf{x}_0$, it will remain in that state for all times. Whether this state is actually reached by the system from other initial conditions depends on the stability of the fixed point. A stable fixed point is one for which perturbations are damped, and the system's evolution restores it to this state. If it is instead unstable, perturbations will grow in time, and the system will never return to this state.

A perturbation is a small displacement in the coordinates by $\delta\mathbf{x} = (\delta x_1, \delta x_2, \ldots, \delta x_K)$. If $\mathbf{x}(t)$ is a solution to Eq. (1.1) Then the evolution of the perturbed system is given by

$$\frac{\partial}{\partial t}\left[\mathbf{x} + \delta\mathbf{x}\right] = \mathbf{F}\left(\mathbf{x} + \delta\mathbf{x}, \mathbf{p}\right)\,. \tag{1.4}$$

Linearizing, one obtains

$$\frac{\partial}{\partial t}\mathbf{x} + \frac{\partial}{\partial t}\delta\mathbf{x} = \mathbf{F}\left(\mathbf{x}, \mathbf{p}\right) + \mathbb{J}\left[\mathbf{F}\left(\mathbf{x}, \mathbf{p}\right)\right] \cdot \delta\mathbf{x}\,, \tag{1.5}$$

where $\mathbb{J}$ is the Jacobian matrix whose components are

$$J_{ij}\left[\mathbf{F}(\mathbf{x})\right] = \frac{\partial F_i(\mathbf{x})}{\partial x_j}\,. \tag{1.6}$$

The first terms in both sides of Eq. (1.5) cancel out according to Eq. (1.1). Thus, we obtain an evolution equation for the perturbation that reads

$$\frac{\partial}{\partial t}\delta\mathbf{x} \approx \mathbb{J}\left[\mathbf{F}\left(\mathbf{x}(t), \mathbf{p}\right)\right] \cdot \delta\mathbf{x}\,. \tag{1.7}$$

In the case that $\mathbf{x}(t) = \mathbf{x}_0$ is a fixed point, then $\mathbb{J}\left[\mathbf{F}\left(\mathbf{x}_0, \mathbf{p}\right)\right]$ is a constant matrix, and the solutions to Eq. (1.7) have the form

$$\delta\mathbf{x}(t) \approx \delta\mathbf{x}(0) \exp\left(\mathbb{J}\left[\mathbf{F}\left(\mathbf{x}_0, \mathbf{p}\right)\right] \times t\right)\,. \tag{1.8}$$

If the initial perturbation is parallel to one of the eigenvectors e_k of the matrix $\mathbb{J}\left[F\left(\mathbf{x}_0, \mathbf{p}\right)\right]$, then the evolution of this perturbation would be

$$\delta\mathbf{x}(t) \approx \delta\mathbf{x}(0) \exp(\kappa_k t)\,, \tag{1.9}$$

where κ_k is the eigenvalue corresponding to eigenvector e_k. If the eigenvectors form a base, any perturbation can be decomposed into its projections on this base. The evolution in a vicinity of the fixed point is thus determined by the eigenvalues $\{\kappa_i\}$ of the Jacobian matrix evaluated at the fixed point, and the dynamics is exponential.

If all eigenvalues are real, the fixed point is referred as a *node*. Each eigenvector defines a direction, and the sign of the associated eigenvalue decides whether this direction is stable or unstable, i.e., whether perturbations along this direction will grow or shrink. If all eigenvalues are negative, then the magnitude of any small perturbation from $\mathbf{x}_0$ decreases in time, and the system is restored to the fixed point. Therefore, the node is in this case stable. If, on the other hand, at least one of the eigenvalues is positive, any perturbations with a non-zero projection to the eigenvector corresponding to this eigenvalue will grow in time, and the node is unstable. A depiction of these situations in the two-dimensional case is presented in Fig. 1.2.

It is also possible that some of the eigenvalues form pairs of complex conjugates. In terms of Eq. (1.9), the presence of complex eigenvalues signifies that, apart from approaching or leaving the fixed point, the trajectory will rotate around it with a frequency equal to the magnitude of the imaginary part of the eigenvalue. This kind of fixed point is referred to as a *focal point*. Provided that all other eigenvalues are negative, the real part of the pair of complex eigenvalues decides the stability of the focus. If the real part is negative, then the focal point is stable, and the trajectory wraps around it in an inwards-directed spiral. In the case of a positive real part, the spiral is directed outwards, and the trajectory goes away from the focal point. Thus, such a focal point is unstable.

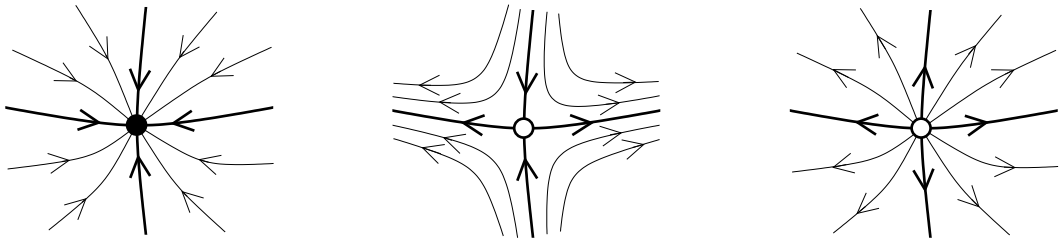

Figure 1.2: Different kinds of nodal fixed points in a two-dimensional dynamical system. (a) Both eigenvalues of the Jacobian are negative and the node is stable. (b) One eigenvalue is positive and the trajectories diverge in the direction of the corresponding unstable manifold. (c) Both eigenvalues are positive and trajectories diverge in all directions.

It is clear that not only the position but also the stability of a given fixed point may depend on the values of the parameters $p_1, p_2, \ldots, p_M$. By manipulating one or more of these parameters we may change the stability of the focal point. This is, for example, the kind of bifurcation that takes place in the case of the system

$$\dot{x}_1 = ax_1 + x_2 \ , \qquad \dot{x}_2 = -x_1 + ax_2 \ , \tag{1.10}$$

where $\dot{x}_j \equiv \frac{\partial x_j}{\partial t}$. For this system there is only one fixed point at the origin, which is stable if $a < 0$ and unstable if $a > 0$. The system has thus a bifurcation at $a = 0$ where the stability of the fixed point is exchanged. At the critical point $a = 0$, the fixed point is neutrally stable and the system is conservative. For all initial conditions, the trajectory in the phase space will rotate around the focal point without collapsing to it or going away, as happened in the case of the frictionless pendulum in Fig. 1.1a. The amplitude of this rotation is given by the initial conditions, and it is maintained in time. In Fig. 1.3, the different kinds of typical behavior are shown for different initial conditions.

Nonlinearity, limit cycles and chaos

The existence of a fixed point is tied to condition (1.2). When $\mathbf{F}$ is a linear function of $\mathbf{x}$, then (1.2) is a set of K linear equations with K unknowns. As such, it either has an infinite number of solutions (meaning that all states are fixed points), it has none or it has a single fixed point. In this latter case, Eq. (1.7) is exact, and the evolution of a perturbation necessarily follows an exponential law. Thus, unless the system is in a critical situation of neutral stability, it can only collapse to a single stable state, or its trajectories will grow indefinitely.

Quantities that grow to infinity are usually not physically meaningful. Therefore, it is very often necessary to include nonlinear contributions. Nonlinearities can

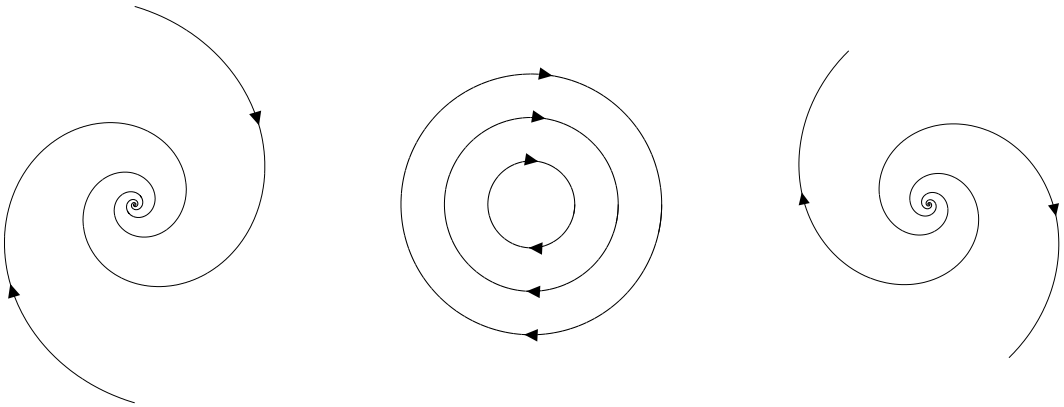

$a < 0$ $a = 0$ $a > 0$

(a) **(b)** **(c)**

Figure 1.3: Change of stability of the focal fixed point in Eq. (1.10) when changing parameter a. (a) The fixed point is stable for negative values of a and the orbit spiral towards it. (b) At $\alpha = 0$ all orbits are circular, and the fixed point is neutrally stable. (c) When $a > 0$ it is unstable, and all orbits get away from it in reversed-rotating spirals.

drastically reduce the tractability of the system, but the presence of nonlinear terms also allows for a greater richness in behavior.

A simple but important extension is obtained by introducing nonlinear terms in Eqs. (1.10) in the form

$$\begin{aligned} \dot{x}_1 &= a x_1 + x_2 - x_1(x_1^2 + x_2^2)\,, \\ \dot{x}_2 &= -x_1 + a x_2 - x_2(x_1^2 + x_2^2)\,. \end{aligned} \tag{1.11}$$

This system also has a single fixed point at the origin, and the analysis of its stability yields the same results as for system (1.10). Nevertheless, the linear expansion (1.7) ceases to be valid far away from the fixed point. If we write these equations in polar coordinates, the equations for the radial and the angular variable can be decoupled. The angular variable increases at constant rate, and the equation for the radial coordinate $r = \sqrt{x_1^2 + x_2^2}$ is

$$\dot{r} = a r - r^3\,. \tag{1.12}$$

When $a < 0$, Eq. (1.12) has only one stable fixed point at $r = 0$. However, if $a > 0$ this equation has another fixed point $r = \sqrt{a}$, which is stable, and $r = 0$ is instead unstable. This implies that the dynamics of the system will converge to a circle of radius $r = \sqrt{a}$, starting from initial conditions both inside and outside the circle. This circle is therefore an attractor, and it is a closed trajectory along which the system evolves perpetually with a constant period. Since all trajectories converge to it in the infinite time limit, it is called a *limit cycle*. The bifurcation here depicted is the well-known *Andronov-Hopf bifurcation*[2]. An example of different trajectories

[2]This type of bifurcation is often further classified into *subcritical* and *supercritical*. The considered example belongs to the latter category.

for both $a < 0$ and $a > 0$ can be seen in Fig. 1.4.

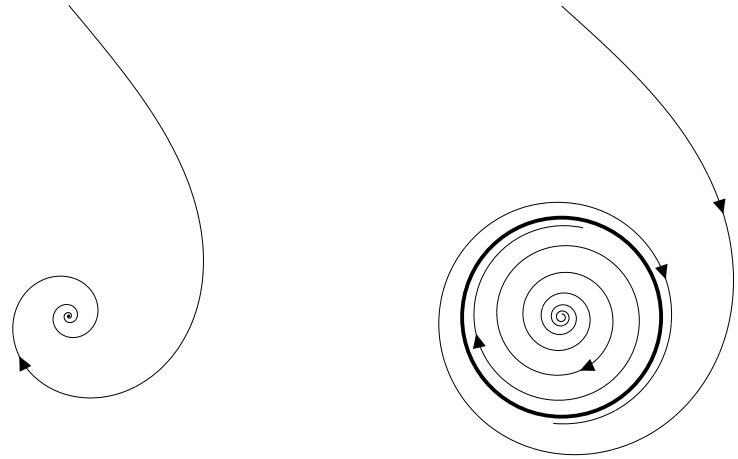

Figure 1.4: Change of stability of a focal point with the appearance of a stable limit cycle in system (1.11). (a) The fixed point is stable for negative values of a and all orbits spiral towards it. (b) When $a > 0$ the origin is unstable, but all trajectories go towards a stable circular limit cycle with radius $\sqrt{a}$.

The motion along a limit cycle has a specific frequency for a given set of parameter values. In systems with at least three variables, several different bifurcations may lead to superimposed rotations with different frequencies, all of them present simultaneously. For example, the system might move on the surface of a torus, wrapping around it and rotating around the symmetry axis with different frequencies. If the ratio of these frequencies were an irrational number, the trajectory would not be a closed curve, as it would never pass through any point twice. This kind of behavior is known as *quasiperiodic*.

In a quasiperiodic attractor, the distance between two orbits that have started from close initial conditions remains —at least on the average— constant. However, in systems of three or more dimensions, there is a fourth kind of attractor in which close trajectories always separate while remaining in a confined region of the phase space. Such attractors are called *chaotic*. This separation of close trajectories implies an extreme sensitivity to initial conditions. Indeed, if close trajectories separate, two trajectories starting from very similar initial conditions will eventually be far away from each other.[3]

When attempting to predict the evolution of a system, perhaps through numerical computation, we need to consider that a certain error is necessarily made in determining its initial state. For a system in a chaotic attractor, no matter how

[3]Since the Jacobian matrix in Eq. (1.7) is not constant in this case, Eq. (1.9) is not applicable. However, it is usually accepted that the separation of close trajectories in chaotic systems is approximately exponential [20].

small this error is, rapid separation of close trajectories implies that this error will grow with every time iteration, eventually rendering the prediction invalid, even if the computation could be carried out with infinite precision.

A common property of chaotic attractors is that their geometry in the phase space is often very complex. This is clearly seen in the embedding dimension of the attractor. In the case of fixed points and limit cycles, there is no question of the dimension of such attractors: as any single point, a fixed point has dimension 0; and a limit cycle (a closed curve) has dimension 1. Quasiperiodic attractors may be of any higher dimension, depending on how many different rotation modes they include. If, for example, the system moves on the surface of a torus, the dimension of the attractor is 2.

When it comes to chaotic attractors, it is usually found that their geometry is more intricate, and standard definitions of dimension —like the box-counting dimension[4] or the Hausdorff dimension— yield non-integer values [21, 22]. In the terminology of Mandelbrot, such kinds of objects are called *fractals*. Below in Sec. 1.2.2 we introduce the particular measure of embedding dimension that will be used in this work.

1.2.2 Lyapunov exponents

The distinctive property of systems with chaotic attractors is their sensitivity to initial conditions. If we consider a trajectory $\mathbf{x}(t)$ in the attractor, then this sensitivity implies that another trajectory with initial conditions $\mathbf{x}(0) + \delta\mathbf{x}$, no matter how small $\delta\mathbf{x}$ is, will quickly become separated from $\mathbf{x}(t)$. For small displacements, this separation is approximately exponential in time [20].

Of course, the rate of separation may change from point to point in the trajectory, or may even become negative. The sensitivity to the initial conditions is therefore a property that should take into account all points of the trajectory. This is characterized by the quantity

$$\lambda_1(\mathbf{x}(0), \delta\mathbf{x}(0)) = \lim_{t\to\infty} \frac{1}{t} \ln\left(\frac{|\delta\mathbf{x}(t)|}{|\delta\mathbf{x}(0)|}\right), \tag{1.13}$$

which is called the maximal Lyapunov exponent. Sensitivity to initial conditions requires that this quantity be positive. Since $\delta\mathbf{x}(0)$ is infinitesimal, then so will be $\delta\mathbf{x}(t)$ for all times, and Oseledec's multiplicative ergodic theorem guarantees that the limit exists under very general conditions. In principle, this limit will depend on the initial condition $\mathbf{x}(0)$ and initial perturbation $\delta\mathbf{x}(0)$. Nevertheless, roughly speaking, we can imagine that the trajectory will cover the entirety of the attractor in the infinite-time limit. Therefore, we can expect that the value λ_1 will be the same for all initial conditions in the attractor.

As we have seen before, the stability properties of a fixed point are determined by the Jacobian matrix of the system, more specifically by the eigenvalues of the Jacobian of the equations of motion evaluated at the fixed point. However, other attractors for which the dynamics of the system persist may not be analyzed in this

[4] Also known as the MinkowskiBouligand dimension.

way. Therefore, other characteristics should be analyzed to determine the stability and other properties of an attractor.

Different criterions for stability exist. In general, the strongest criterion is that of *asymptotical stability* which roughly means that all trajectories in a close (finite) neighborhood of an attractor will converge to it in the infinite-time limit. If we take all points in the K-dimensional volume of this neighborhood as initial conditions for the system and let them evolve independently, then after infinite time this volume will be collapsed to the volume of the attractor, which is necessarily smaller then the initial volume of the neighborhood. The existence of an attractor therefore requires that the volume in its vicinity is compressed by the evolution.

At any point $\mathbf{x}_0$ in the phase space, we may in the same way choose a K-dimensional sphere with center at this point and infinitesimal radius δr, so that its volume is $V_0 = \pi(\delta r)^K$ and all points in the sphere may be considered to be initial conditions for different trajectories. After an infinitesimal time of evolution δt, the sphere will be deformed by the evolution. According to Eq. (1.7) the evolution of this sphere will be governed by the Jacobian matrix of the system. If we assume that $\mathbb{J}\left[\mathbf{F}\left(\mathbf{x}_0(0)\right)\right] \approx \mathbb{J}\left[\mathbf{F}\left(\mathbf{x}_0(\delta t)\right)\right]$, then the sphere will stretch and compress approximately along the directions of the eigenvectors e_k of the Jacobian matrix, according to the associated eigenvalues κ_k. In this infinitesimal evolution time, the sphere with radius δr will become an ellipsoid with K principal radii $\delta r_1, \delta r_2, \ldots, \delta r_K$, where the ordering is taken according to decreasing size. It will therefore be that $\delta r_j \approx \delta r \exp\left(\kappa_j \delta t\right)$, and then the volume after the infinitesimal evolution time will be

$$\begin{aligned} V_0(\delta t) &\approx \pi \prod_{i=1}^{K} \delta r \exp(\kappa_i \delta t) \\ &\approx V_0(0) \exp\left[\delta t \sum_{i=1}^{K} \kappa_i\right] . \end{aligned} \tag{1.14}$$

If the sum of the eigenvalues is negative, then the volume in the phase space in the vicinity of $\mathbf{x}_0$ will shrink. A schematic representation of this is shown in Fig. 1.5.

The eigenvalues of the Jacobian κ_i depend on the point at which the Jacobian is calculated. Consequently, the rate of compression or expansion of a volume in the phase space is different at each point of a given trajectory, and the directions along which it stretches and contracts change. To construct properties that characterize the entire attractor rather than a given point, we let such an infinitesimal K-dimensional sphere of infinitesimal radius δr and center at $\mathbf{x}_0(0)$ evolve for a long period of time t . The sphere will in general deform to an K-dimensional ellipsoid, whose center is at $\mathbf{x}_0(t)$ and whose principal axes can be identified as $u_1(t), u_2(t), \ldots, u_K(t)$, where the order is such that the principal radii $\delta r_i(t)$ associated with each axis u_i are in decreasing order, that is $\delta r_1(t) > \delta r_2(t) > \ldots > \delta r_K(t)$.

If $\mathbf{x}_0(0)$ is a point inside the attractor, we can consider the limits

$$\lambda_i = \lim_{t\to\infty} \frac{1}{t} \ln\left(\frac{|\delta r_i(t)|}{|\delta r|}\right) , \tag{1.15}$$

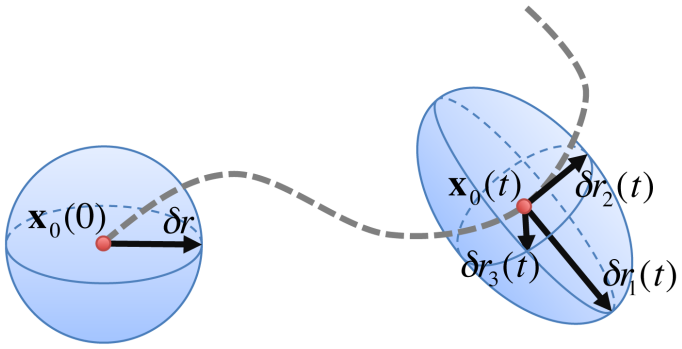

Figure 1.5: Evolution of a sphere of infinitesimal radius δr in the phase space. After a small time t, the sphere is deformed to an ellipsoid with radii $\delta r_j(t)$ in the orthogonal directions.

which, under very general conditions, exist and are independent of the center of the sphere of initial conditions. The K quantities λ_i constitute the full spectrum of Lyapunov exponents. They determine the rates of compression or expansion of volume in the phase space in different directions along the trajectories inside the attractor. For λ_1, this definition is equivalent to 1.13. Therefore, λ_1 measures the average rate of expansion or compression along the direction of maximum stretching (or minimum shrinking) at each point in the attractor. Since the principal axes of an ellipsoid are orthogonal, λ_2 determines the average maximal rate growth or minimal rate of shrinking in the subspace orthogonal to the direction of maximum growth or minimal shrinking. In this sense, all Lyapunov exponents measure the rates of expansion and contraction in a recursive series of nested orthogonal subspaces.

The Lyapunov exponents provide a convenient way of characterizing the attractor, and thus the dynamics of a system. The fact that an attractor exists requires that the sum of all Lyapunov exponents be negative, since the contrary would imply that the volume in the phase space grows unboundedly. The presence of an attractive fixed point requires furthermore that all of them be negative, since any volume within the basin of attraction should shrink in all directions until collapsing to a point.

If the maximal exponent were to be zero and all other negative, this would mean that all trajectories collapse to a line, on which they remain, in the average, at constant distance from each other. This is what is encountered, when a stable limit cycle is present. Similarly, if the k largest exponents are zero and the rest are negative, we can infer that the trajectories will collapse to a k-dimensional quasiperiodic attractor. However, if the system is in a neutrally stable state, any trajectory in its close vicinity will remain close but always at a finite distance. Therefore, the maximal Lyapunov exponent would also be zero in this situation.

A chaotic attractor is characterized by a positive (non-zero) maximal Lyapunov exponent λ_1. However, as we have seen, the presence of an attractor requires that the mean value of the Lyapunov spectrum be negative. The case in which the sum of Lyapunov exponents is negative, but more than one of them is positive is sometimes

referred to as *hyperchaos*.

Exact determination of Lyapunov exponents in numerical simulations is impossible, and therefore only estimations can be made. For numerical calculation, the main problem lies in the assumption that a single trajectory should cover all points of the attractor. For many attractors, in particular chaotic attractors, this assumption may be far from being true for any finite time. Nonetheless, it can be shown that for well behaving systems, convergence to asymptotic values occurs rather quickly, so that a suitable estimation can be reached in reasonable computation times.

Numerical calculation

Computing the trajectories for infinitely many initial conditions in a sphere of infinitesimal radius for an infinitely long time is obviously impossible in a numerical integration. Approximate numerical methods for the calculation of the Lyapunov exponents assume that the behavior of the trajectories for all initial conditions within the sphere can be accounted for with a finite number of them. A standard such method is the one introduced by Benettin *et al.* [23] and Shimada and Nagashima [24].

In numerical integrations of the equations of motion, time is divided in in discrete increments Δt. Moreover, since infinitesimal perturbations cannot be accounted for with a limited numerical precision, the evolution of perturbations needs to be analyzed in the *tangent space* of a trajectory, that is, by tracking the evolution of finite perturbation vectors according to the linearized system, where the linearization takes place at each point of the non-linearized, unperturbed trajectory. The perturbation vectors evolve according to Eq. (1.7). If $\mathbf{x}_0(t)$ represents the trajectory whose initial condition is $\mathbf{x}_0(0)$, then each perturbation vector $\delta\mathbf{x}_j$, after an integration time-step, will be

$$\delta\mathbf{x}_j(t+\Delta t) \approx \Delta t \times \mathbb{J}\left[\mathbf{F}\left(\mathbf{x}_0(t)\right)\right] \cdot \delta\mathbf{x}_j(t) + \delta\mathbf{x}_j(t)\,. \tag{1.16}$$

Recursively, the evolution of such a perturbation can be tracked over long periods of time for each perturbation vector as

$$\delta\mathbf{x}_j(M\Delta t) \approx \left[\prod_{m=0}^{M} \Delta t \times \mathbb{J}\left[\mathbf{F}\left(\mathbf{x}_0(m\Delta t)\right)\right] + \mathbf{I}\right] \cdot \delta\mathbf{x}_j(0)\,, \tag{1.17}$$

where $\mathbb{I}$ is the identity matrix. If K perturbations are set to evolve simultaneously according to 1.17, they will all rapidly align with the direction of maximum elongation beyond numerical precision. To avoid this, a process of orthonormalization, such as the Gram-Schmidt method, must be applied to the set of perturbation vectors after a certain number of iterations. This orthonormalization must follow a decreasing order in the magnitude of the perturbation to preserve the growth or shrinking of volume in the phase space along perpendicular direction. The first vector of the orthonormal base will therefore coincide in its direction with the largest of the perturbation vectors at the end of the evolution time. After such a process has been applied, an approximate value for the Lyapunov exponents can be calculated from the projection of the perturbation vectors to the orthonormal base. More in-

formation on the method to calculate the Lyapunov exponents is provided in Ref. [25].

Kaplan-Yorke dimension

The existence of an attractor implies that any expansion along certain directions in the phase space should be compensated by contraction along other directions. Thus, the dimension of an attractor may be characterized by the number of such orthogonal directions along which the expansion and compression balance out. This is the idea behind the definition of the Kaplan-Yorke measure of embedding dimension of an attractor [26], given by

$$D_{KY} = q + \frac{\sum_{i=1}^{q} \lambda_i}{|\lambda_{q+1}|}\,, \tag{1.18}$$

where q is an integer such that

$$\sum_{i=1}^{q} \lambda_i \geqslant 0, \qquad \sum_{i=1}^{q+1} \lambda_i < 0\,. \tag{1.19}$$

If $\lambda_1 < 0$, then the Kaplan-Yorke dimension is zero, as corresponds to a fixed point. Generally, D_{KY} specifies the number of directions in the attractor necessary to balance out expansion and compression. Note however that the definition (1.18) may yield non-integer values. As was discussed before, this is what occurs for chaotic attractors, since the geometry of such object is in general fractal.

There are several different measures of embedding dimension. Whether the Kaplan-Yorke dimension coincides with other methods has never been mathematically proved, and the debate is ongoing. Still, numerical calculations for different systems give satisfactory results, and the Kaplan-Yorke dimension is a broadly used measure to determine the embedding dimension of attractors in dynamical systems.

1.3 Oscillators

Dynamical systems may have any number of degrees of freedom. Thus, a limit cycle may be embedded in a phase space of any dimension, as a result of highly nonlinear coupling between variables. The analytic treatment of such systems is rarely possible.

Even for tractable cases, taking into account interactions between a large number of elements in limit-cycle oscillations may be a futile task. However, the problem can be greatly simplified if only weak interactions are considered, such that deviations from the limit cycle are small. In this case, the number of effective degrees of freedom can be greatly reduced. Within this framework, general models can be constructed in which the interactions of oscillatory elements can be studied. Below we present essential ideas of the reduction method.

1.3.1 Phase reduction

The system 1.12 has a stable limit cycle with constant radius $r = \sqrt{a}$, whereas the angular variable $\theta(t)$ evolves according to equation

$$\dot{\theta} = t\,. \tag{1.20}$$

The evolution in state space consists of rotations at constant angular velocity. For a fixed value of the parameter a, the trajectory in the limit cycle is fully described by the angular variable.

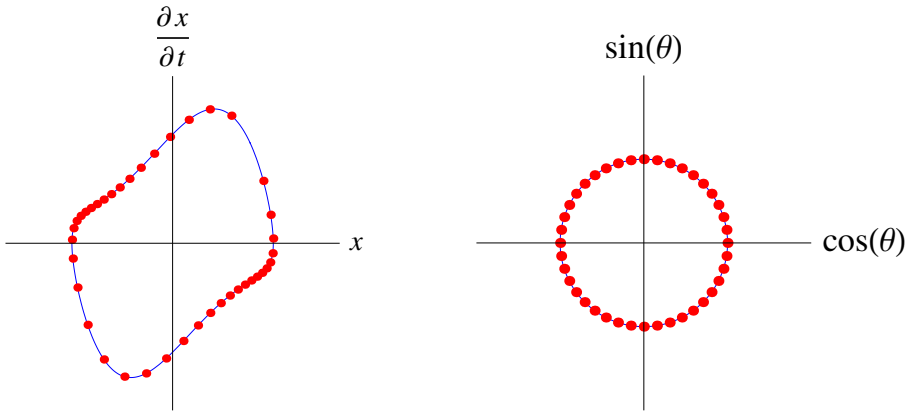

Figure 1.6: Mapping of a limit cycle in a dynamical system (Van der Pol oscillator) to the unit circle. Subsequent dots in the left panel are visited in equivalent time intervals. Subsequent dots in the right panel correspond to $\exp(i\theta(t))$ for equivalent phase intervals, so that $\dot{\theta} = 2\pi/T$.

In most systems of interest, a periodic attractor will be much more complicated than the attractor of system (1.11), involving many variables that change at different rates. Nevertheless, no matter how complicated a limit cycle may be, it will always be a closed curve, and therefore can be mapped to a circle. Hence, a system in a limit cycle can always be described by a single variable called the *phase* of the oscillation, such that it increases linearly in time from 0 to 2π, and is bounded to this range[5]. Thus, the phase describes the progress of the system along the periodic attractor.

The introduction of the phase variables implies the need of finding a mapping that projects the stable limit cycle to a circle, given by $\mathbf{x} \to \theta(\mathbf{x})$. Furthermore, each point in the limit cycle should be mapped to a point on the circle in such a way that any pairs of points on the limit cycle visited with a constant time difference should be mapped to a point on the circle with a constant phase difference. This leads to the condition,

$$\frac{\partial\theta(\mathbf{x}(t))}{\partial t} = constant = \frac{2\pi}{T}\,, \tag{1.21}$$

[5]The phase variable operates under a modular arithmetic with modulo 2π. Consistently, all functions involved are 2π-periodic.

where T is the period of the limit cycle. In Fig. 1.6, such a mapping is shown for the Van der Pol oscillator.

When two or more systems involved in periodic oscillations interact, it is generally the case that each of them will be pushed off of the limit cycle on occasion. If the interactions are weak enough, these deviations from the limit cycle will be small, and the system will not leave the basin of attraction of the limit cycle. For this reason, it is important that the definition of a phase variable not be restricted to the limit cycle, but be also valid in its vicinity.

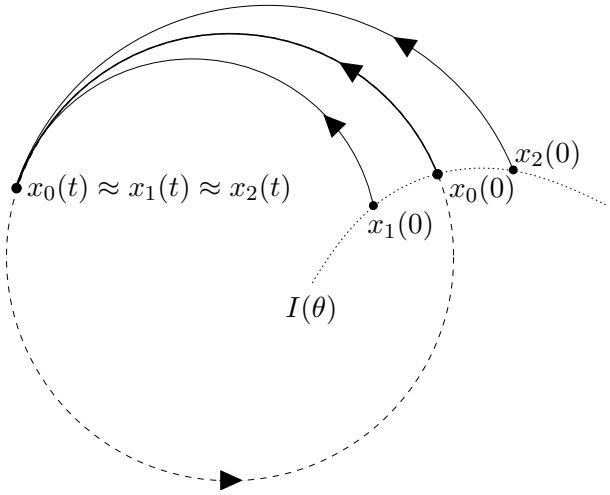

Figure 1.7: Schematic representation of an isochronous surface in the vicinity of a limit cycle. Two states are assigned the same phase value if the distance between them vanishes in the infinite time limit.

In general, every point in the basin of attraction may be identified with a given phase value according to where it will land on the limit cycle after infinite time has passed. If $\mathbf{x}_0(0)$ is a point on the limit cycle, then $\mathbf{x}_0(t)$ will be on the limit cycle for any time t, and $\theta(\mathbf{x}_0(t))$ is the phase of each point in the limit cycle, defined up to a constant value in $[0, 2\pi)$. We can therefore also say of all points $\mathbf{x}(t)$ in the basin of attraction, such that

$$\lim_{t\to\infty} |\mathbf{x}_0(t) - \mathbf{x}(t)| = 0\,, \tag{1.22}$$

that $\theta(\mathbf{x}_0(t)) \equiv \theta(\mathbf{x}(t))$. Each point in the limit cycle thus defines an *isochronous surface* $I(\theta)$ of states that will coincide on the limit cycle after infinite time, and all points on this surface are assigned the same phase value. Small perturbations from the periodic attractor may thus be accounted for as changes in the phase value of the trajectory, according to the isochronous surface to which the perturbed state belongs. Therefore, we can reduce the effective degrees of freedom of any K-dimensional system in the vicinity of a stable limit cycle to a 1-dimensional description of phase dynamics. This mathematical process is usually referred to as *phase reduction*.

This kind of formalism is very useful, in that it allows us to describe an enormous class of systems by a generic model involving extremely simple mathematical objects called *phase oscillators*, whose dynamics is given by a single variable. Conversely,

results found for such simple systems can be transferred to the dynamics of complex oscillators whose perturbations are small enough to allow such a phase description.

1.3.2 The Kuramoto model

Within the framework of phase-reduced systems, the interactions between different oscillatory systems are greatly simplified. If a set of N oscillatory systems of the form 1.1 is considered, then the equation for the i-th element will generally have the form

$$\frac{\partial}{\partial t}\mathbf{x}^i = \mathbf{F}^i\left(\mathbf{x}^i\right) , \tag{1.23}$$

where $\mathbf{x}^i \in \mathbf{R}^K$. If these systems interact with each other weakly, their equations become

$$\frac{\partial}{\partial t}\mathbf{x}^i = \mathbf{F}^i\left(\mathbf{x}^i\right) + \epsilon\mathbf{G}^i\left(\mathbf{x}^1, \mathbf{x}^2, \ldots, \mathbf{x}^N\right) , \tag{1.24}$$

with the small parameter $\epsilon \ll 1$ indicates the weak intensity of the interaction. Assuming that each of these systems has a stable limit-cycle attractor of period T^i for $\epsilon = 0$, the phase reduction formalism tells us that there is a continuous mapping that projects the solutions of Eqs. (1.24) to the N-torus, where the solutions are described by

$$\frac{\partial}{\partial t}\theta_i = \Omega_i + \epsilon H_i\left(\theta_1, \theta_2, \ldots, \theta_N, \epsilon\right) , \tag{1.25}$$

where $\Omega_i = 2\pi/T^i$. It can be shown that if the frequencies of the different interacting systems are similar, this mapping can be chosen in such a way that the coupling function takes the form

$$\frac{\partial}{\partial t}\theta_i = \Omega_i + \epsilon h_i\left(\theta_1 - \theta_i, \theta_2 - \theta_i, \ldots, \theta_N - \theta_i, \epsilon\right) + O(\epsilon^2) , \tag{1.26}$$

where $h_i(\theta)$ are 2π-periodic functions.

Y. Kuramoto [5] used a perturbation method of time-averaging to derive a simpler expression. By making variable change in the form $\theta_i = \Omega t + \phi_i$, the system can be analyzed in terms of how it deviates from collective oscillations. The variables ϕ_i are sometimes called *phase deviation* variables. With this method, Y. Kuramoto showed that the phase reduced system for weakly coupled, nearly identical limit-cycle oscillators generally is

$$\frac{\partial}{\partial t}\phi_i = \omega_i + \epsilon\sum_{j=1}^{N}\Gamma_{ij}(\phi_i - \phi_j) , \tag{1.27}$$

where the interaction between each element and the environment is given as a superposition of its pair-wise interactions with each other element in the ensemble.

Functions Γ_{ij} can be further expanded in Fourier series, of which commonly only the first order terms are retained. With this approximation, the general model becomes

$$\frac{\partial}{\partial t}\phi_i = \omega_i + \sum_{j=1}^{N} K_{ij}\sin(\phi_j - \phi_i + \alpha_{ij}) \tag{1.28}$$

where α_{ij} is a natural phase shift in the interaction, and K_{ij} characterizes the intensity of the interaction between different pairs of elements. The presence of the phase shifts α_{ij} makes the analytic treatment of this model complicated, and they are often omitted. The role of phase shifts as a factor that introduces frustration in the system has been discussed by Daido [27], who considered the special case in which the phase shifts are either 0 or π. Then, interactions may be attractive or repulsive, and frustration may lead to interesting dynamics [28]. However, these phase shifts may be of great importance for reasons that we see below.

As a simple case, Y. Kuramoto considered the situation in which all interactions between the elements are equally weighted. This allows the system to be studied within a mean-field approach. This leads to the system commonly known as the Kuramoto model, given by

$$\frac{\partial}{\partial t}\phi_i = \omega_i + \frac{\mu}{N}\sum_{j=1}^{N}\sin(\phi_j - \phi_i) \tag{1.29}$$

The Kuramoto model as given by Eq. (1.29) is the cornerstone for studies of synchronization phenomena. Many variations and extensions of this model have been investigated, and its mathematical implications have been explored extensively [29].

1.3.3 Phase shifts as time delays

The model (1.24) describes oscillatory elements coupled in such a way that the state of each element affects all others at a given time. An extension to this model is needed when the interactions take place through the transmission of information between elements, so that a certain time delay exists in the coupling function.

As a simple case, let us consider the situation when all the time delays are the same. The equations are

$$\frac{\partial}{\partial t}\mathbf{x}^i(t) = \mathbf{F}^i\left(\mathbf{x}^i(t)\right) + \epsilon\mathbf{G}^i\left(\mathbf{x}^1(t-\tau), \mathbf{x}^2(t-\tau), \ldots, \mathbf{x}^N(t-\tau)\right) \tag{1.30}$$

It has been proven by Izhikevich and Hoppensteadt [30, 31] that if the phase shift is small enough —namely, if $\tau \ll \epsilon^{-1}$— then a phase reduction can be performed such that in the phase model the time delay is no longer explicit, but only a phase shift appears in the equation. The general form of such phase model would be

$$\frac{\partial}{\partial t}\theta_i = \Omega_i + \epsilon h_i\left(\theta_1 - \theta_i - \alpha, \theta_2 - \theta_i - \alpha, \ldots, \theta_N - \theta_i - \alpha\right) + O(\epsilon^2) \tag{1.31}$$

where $\alpha = \tau\Omega \mod 2\pi$ and the functions h_i are the same as in 1.26. The presence of time delays in the original system is thus translated to the phase model in the form of phase shifts. As we mentioned before, phase shifts are often discarded in the studies of the Kuramoto model. We now see that considering these phase shifts not only addresses a more general problem, but also allows to take into account the effect of time delays in the interactions. Phase shifts can also appear when higher harmonics in the functions $\Gamma_{ij}(\phi)$ are considered, which can lead to very interesting dynamics [32, 33, 34, 35, 36]. The presence of phase shifts in the interactions between pairs of elements plays a leading role throughout this work.

1.4 Networks

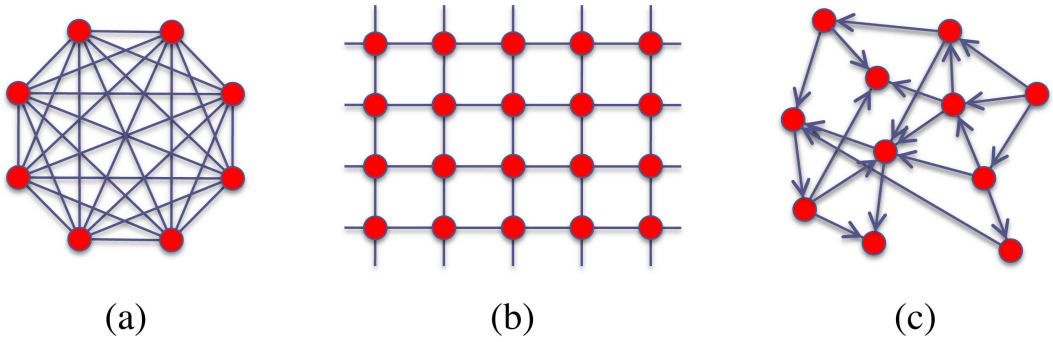

Figure 1.8: Different paradigms for networks. (a) All-to-all or global coupling, (b) lattices and (c) directed networks.

In systems of interacting elements, the interactions between them may take diverse forms. The specific set of interactions can be a fundamental property of a system, on which its functioning or stability may be entirely dependent. In Fig. 1.8, three different examples of interaction orgnization are shown.

Fig. 1.8a correspond to *global* or *all-to-all* coupling. Here, each element interacts with all others in the same uniform and reciprocal way. This may be a valid approximation to a situation in which interactions have no dependence on the spatial distance between the elements, as occurs when the coupling takes place through a fast-diffusing chemical agent. In such cases, it is usually possible to analyze the system within a mean-field approach.

The case in Fig. 1.8b corresponds to a *lattice*. Each element occupies a point in a regular grid and interacts reciprocally and uniformly with its neighboring elements. The number of elements with which each element interacts is directly proportional to the dimension of the system. This is a typical representation of systems for which the spatial distribution of the elements is the decisive factor in determining the pattern of interaction (for example, where interactions are a function of the physical distance between the elements). In this approach, each connection has the same associated distance in Euclidean space. The continuous limit can be reached when this distance goes to zero as the number of elements is increased.

A more general case is that in which the interactions take place only between certain prescribed pairs of elements. The resulting networks may be highly heterogeneous and may have complex topological properties. A diagram of such a network is shown in Fig. 1.8c. This situation can be found when interactions depend not only on the distance between elements, but also on several other factors, as it happens with networks of trains traveling between stations, logistic and distribution networks, streets connecting intersections or dendrites and axons connecting neurons. The connections may be established through a growth process, as in the case of the links between webpages in the World Wide Web or the growth of tubular hyphae in mycelial fungi [37]; or result from specific requirements, as happens with conveyor

belts between machines in a factory and in logistic netwroks [38, 39]. The structure of networks can moreover result from a predominantly random process. This may be the case, for example, in social networks, where the factors that lead a person to interact with another one may be largely accidental [40].

Another important aspect of networks is that they may exhibit non-reciprocal interactions, as is indeed the case in all the examples given above. This is a property that may not be particularily relevant for physical systems, but can be crucial for technological and biological applications.

It is important to point out that the diagrams presented in Fig. 1.8 are arbitrary graphical representations of three given networks. The particular *layout*, that is, the location of each point in the drawing, is chosen for each of them as to facilitate understanding. However it must be kept in mind that the connections the between elements are an abstract concept. Any deformation to these schematic representations consisting of moving the points by keeping them linked to the same neighbors correspond to the same network.

1.4.1 Aspects of Network Theory

Networks constitute a broad category that incorporates all patterns of interaction whose description accepts a scalar representation of the pair-wise interactions. The mathematical abstraction of a network is a *graph*, although in modern literature both terms have become practically interchangeable [42]. In essence, a network is simply a set of *nodes*[6] or *vertices*, which represent the elements of the system, and a set of *edges* or *links*, ordered pairs which correspond to each one of the interactions. A simple way to represent a network is by its *adjacency matrix* A, whose elements are $a_{ij} = 1$ if there is a directed link from node i to node j, and $a_{ij} = 0$ otherwise[7]. If this interaction is reciprocal between all pairs of elements, that is, if A is a symmetric matrix, the network is referred to as being *undirected*. However, for many interesting systems it is a defining aspect that the interactions are not reciprocal. Instead, interactions are unidirectional, i.e., carry information or material flow only in one direction. In this work, we generally concentrate on *directed* networks, of which global coupling is the limiting case with all connections present.

A *weakly connected* network is one which cannot be divided in two networks without removing any edges. This means that a weakly connected network is one single structure. A more stringent condition is that of *strong connectedness*: In this case, any node may be reached from any other by transiting the links according to their direction. For undirected networks, these two conditions coincide.

If a network is strongly connected, it means that from a given node i, any other given node j may be reached by following the directions of the edges. This establishes an ordered set or sequence of nodes that are transited together with the edges between them. This sequence is know as a *path* from i to j, and the number

[6] This terminology is widely used in the literature. Nevertheless, the meaning of the word "nodes" in this section is completely unrelated to the meaning given in Sec. 1.2.1.

[7] This is the case for *unweighted* networks. Weighted networks allow for a specific non-binary quantity to characterize the intensity of each interaction. Such case will not be considered in the present work.

of edges transited is the path's *length*. Of course, in a network there may be several different paths leading from i to j. However, the shortest of these paths is the most relevant[8], and throughout this thesis, we will refer to the shortest path when ambiguity may arise. It is clear that, in a directed network, the shortest path from i to j need not have the same length as that from j to i.

For any pair of elements in a strongly connected network, the length of the shortest path between them can be determined. The maximum of these lengths amongst all ordered pairs of elements in a network is called the *diameter*. The diameter of a network is an important quantitative property, in that it introduces a sense of "maximum distance" between elements. The definition of diameter can also be extended to weakly connected networks, by considering only the maximum lengths amongst the shortest paths between pairs of elements for which a path between them exists. A quantity similar to the diameter that can be calculated to describe the properties of a network is its *average path length*, defined as the mean value of the length of the shortest paths between all possible pairs of nodes in the network. the

A characteristic aspect of networks is their heterogeneity with respect to nodes nodes. In principle, each node may have a different amount of incoming and outgoing connections. The number of edges that a given node i has is said to be its *degree* k_i. For directed networks, a distinction should be made between the *indegree*, or the number of edges that are directed to the node, and the *outdegree*, or the number of edges that connect the node to other nodes in the network. Therefore, we have

$$k_j^{in} = \sum_{i=1}^{N} A_{ij} \qquad k_j^{out} = \sum_{i=1}^{N} A_{ji}\,. \tag{1.32}$$

Since an edge may only connect one node to another, the sum of the indegrees of all nodes should be equal to the sum of their outdegrees, which equals the total number of edges. If the number of nodes is N and the number of edges is M, then it is clear that the the mean value of the degree is

$$\langle k^{in} \rangle = \langle k^{out} \rangle = \frac{1}{N} \sum_{i=1}^{N} \sum_{j=1}^{N} A_{ij} = \frac{M}{N}\,. \tag{1.33}$$

The distribution of degree values in the network has for a long time been considered a defining feature of a network. It has been found that networks encountered in many natural systems and systems subject to evolutionary processes have degree distributions that follow power-laws and fat-tailed distributions. The distribution of degrees in the network may play a very relevant role in the propagation of information and its robustness [43, 44].

1.4.2 Random networks

In 1959, Paul Erdős and Albért Rényi made a statistical analysis of the expected properties of a graph chosen randomly from the set of all possible graphs with N

[8] There still may be more than one with the same minimal length.

nodes and M edges [45, 46]. This gave rise to the theory of random graphs, but also brought the idea of not only analyzing the statistical properties of an *ensemble* of graphs, but of *constructing* a graph according to a random process. They subsequently proposed a model in which a set of N nodes is connected in such a way that each pair of elements would have an edge between them according to a certain probability ρ.

Since each element can have at most $N-1$ neighbors, and each of the edges to these neighbors exists with a probability ρ, the probability that any given node has k edges to other nodes is

$$P_{ER}(k) = \binom{N-1}{k} \rho^k (1-\rho)^{N-1-k} \,. \tag{1.34}$$

This degree distribution is the same for incoming and outgoing edges, and its mean value is simply $(N-1)\rho$. Since there is no correlation between the degrees of different nodes, such networks are said to have *random structure*. Other network models are known to have more complex topological properties.

Erdős and Rényi derived a general description of statistical properties of networks constructed in this way. This work awoke the interest of many mathematicians who studied random graphs for decades, but the repercussions of these findings did not have a great impact on other disciplines for almost forty years. In 1998 Watts and Strogatz introduced their famous model, which consisted of a random process to generate networks with properties that emulated statistical aspects of real social networks [40]. This model inspired a myriad of investigations in diverse areas of science, where network models play a central role.

The design of random processes for constructing networks with specific properties have permitted the development of models that emulate statistical aspects of real-world systems. This was particularly prolific in the areas of social networks, economic systems, and artificial networks like the internet or power grids. As studies continued to demonstrate that dynamical properties of different systems may show an important dependence on the network topology, the need for more refined models, as well as better measurements that captured the meaningful properties of networks, lead to intense research in these fields [47].

Several models to generate networks that emulate the patterns of interactions in systems of interest have been developed. Many of them rely on probabilistic methods that are designed to describe the process of growth of a network, such as the Barabasi-Albert preferential attachment growth model [48]. In this particular model, the network is constructed as if nodes were aggregating to the system one by one, connecting to already present nodes with a probability that is a function of the number of edges they already have.

Robust properties of natural systems (whose millions of years of evolution may be seen as an optimization process) are sometimes believed to be codified in their network structure [49]. Attempts to characterize these aspects have led to the introduction of increasingly sophisticated measures, such as assortativity, betweenness, degree centrality or modularity.

Progress in network research has been extensively reviewed [43, 44, 50, 51]. Since this work concentrates on general aspects of synchronization phenomena, we prefer to

work with the simplest network models, obtained by connecting any pair of elements in an uncorrelated way. Such random networks are of the Erdős-Rényi type, and only they will be considered in this work.

1.5 Synchronization

The phenomenon of synchronization has intrigued scientists for centuries, probably since the discovery of C. Huygens in 1665 that two almost identical pendulums hanging from the same beam tended to oscillate with the same frequency and in opposite directions. He called this a strange "kind of sympathy" between the pendulums, and he further observed that if this oscillation state was perturbed, the *counter-phase* oscillations were restored within a half hour. Huygens deduced that this remarkable behavior arose from imperceptible movements and deformations of the beam, which however small, over time lead the two oscillators to a stable state of synchrony [52].

In spite of its early start, a solid foundation for a theory of synchronization in populations of interacting units was not established for centuries. It was first Arthur T. Winfree who, already in his early publications put forth central ideas that would be the catalyzer for many forthcoming works [56]. After Winfree's death, Strogatz [54] wrote: "Winfree's first paper [53] concerned the mutual synchronization of biological oscillators. How is it that thousands of neurons or fireflies or crickets can suddenly fall into step with one another, all firing or flashing or chirping at the same time, without any leader or signal from the environment? Norbert Wiener had posed this problem in his book *Cybernetics* [55], but he did not make significant mathematical progress on it, nor did anyone else until Winfree came along."

Winfree formulated the problem in terms of large populations of interacting elements, which would be mathematically intractable. However, he understood that the problem would be greatly simplified if the elements were nearly identical, and the interactions between them were weak enough. He proposed a model in which he assumed that each element was coupled to a global field generated by all elements, with equations of the form

$$\dot{\phi}_i = \omega_i + \left(\sum_{j=1}^{N} X(\phi_j) \right) Z(\phi_i)\,, \tag{1.35}$$

similar to the mean-field approximation in statistical physics [56]. With some numerical simulations and analytical approximations, he found a temporal analog to a phase transition leading to the spontaneous formation of clusters of oscillators that freeze in synchrony.

Y. Kuramoto took up these ideas, and formulated them in more sound mathematical terms [5, 57, 58]. With the use of the perturbative method of averaging, he showed that Eq. (1.27) is a universal expression for weakly coupled, nearly identical oscillators, where the functions Γ_{ij} can be calculated from the original equations of motion of the oscillators.

Even though this kind of phase reduction approach is a great simplification, the analysis of large populations of weakly interacting, nearly identical oscillators

is generally too complex for analytical treatment. Kuramoto, as Winfree, acknowledged that the mean-field case would be the most tractable, and therefore proposed the simplest non-trivial case of equally weighted, uniform interactions, in which the functions Γ_{ij} are given by the first Fourier component. With this assumptions, he derived a mean-fieald theory to describe the emergence of synchronization in large populations of phase oscillators [5].

1.5.1 Synchronization in the Kuramoto model

The evolution equations of the Kuramoto model (1.29) may be further simplified by introducing the global order parameter

$$Z \equiv R\exp(i\Phi) = \frac{1}{N}\sum_{j=1}^{N}\exp(i\phi_i)\,. \tag{1.36}$$

This order parameter has a clear geometrical interpretation. Let us imagine oscillators swarming on the unit circle, where node j is represented by $\exp(i\theta_j)$. As illustrated in Fig. 1.9, the order parameter characterizes the rotation asymmetry in the distribution of phases.. The modulus R determines how concentrated the phases of all elements are, and is therefore known as *phase coherence*. Φ measures the global phase of coherent rotations.

R measures the coherence of the elements, and is therefore a measure of the spontaneous emergence of order in the system. However, other kinds of ordered states can also be present in the system, which would yield $R = 0$. For example, clustered states are highly ordered states that cannot be detected by parameter Z.

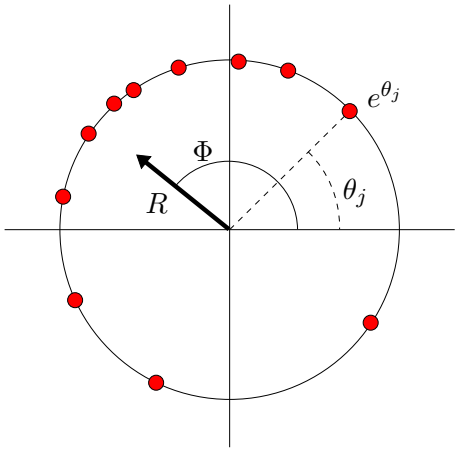

Figure 1.9: Geometrical interpretation of the global order parameter $Z \equiv R\exp(i\Phi) = \frac{1}{N}\sum_{j=1}^{N}\exp(i\phi_i)$.

In terms of these quantities, the Kuramoto model can be rewritten as

$$\dot{\phi}_i = \omega_i + KR\sin(\Phi - \phi_i)\,, \tag{1.37}$$

where all equations are effectively uncoupled, and all elements only interact with the global field which is generated collectively. This result corresponds to the model

proposed by Winfree, but in the analysis by Kuramoto they emerge naturally as a consequence of pairwise interactions between the elements.

Eq. (1.37) has the form of a mean-field coupling by which each oscillator is affected by the global signal from all elements in the system. This constitutes a positive feedback: if an asymmetry in the distribution of phases is present and a non-zero magnitude of the Kuramoto parameter arises, the interactions will foster its growth, which in turn will make the interactions stronger. A sort of circular causality is thus present that leads to the emergence of self-organized global rotations.

In his analytical theory, Y. Kuramoto assumed that the frequencies ω_i are distributed according to a unimodal probability density $g(\omega)$ which is symmetric around the mean value Ω. In this formulation and in the infinite-size limit $N \to \infty$, Kuramoto found the existence of a critical value for the coupling strength K_c such that for $K < K_c$ all elements roam incoherently with different frequencies, and the order parameter is $R = 0$. However, above the critical value $K > K_c$, a finite number of elements become entrained in coherent rotations with the same average velocity, yielding a finite value $R > 0$. Kuramoto found the analytical expression for this critical value to be

$$K_c = \frac{2}{\pi g(\Omega)}\,. \tag{1.38}$$

A schematic representation of the dependence of the order parameter R on the coupling strength is shown in Fig. 1.10.

In the particular case in which all elements are identical, that is, $\omega_i = \Omega$ for all i, the distribution of the frequencies has the form $g(\omega) = \delta(\Omega - \omega)$. From expression (1.38), it can be deduced that the critical value of the coupling strength is $K_c = 0$, and the system synchronizes for any positive value of K. In this case, the dependence shown in Fig. 1.10 would be a Heavyside step function with a phase coherence $R = 1$.

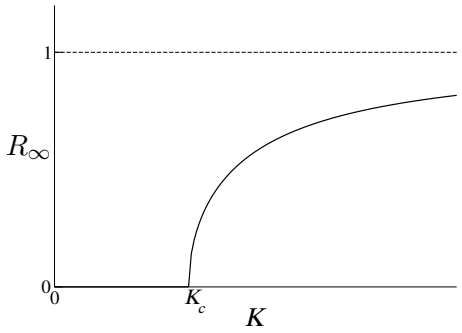

Figure 1.10: General form of the dependence of the average magnitude of the order parameter on the coupling strengh at the onset of synchronization.

1.5.2 Synchronization of globally coupled identical oscillators

The Kuramoto model is a very useful approach to a great variety of systems [59]. In the case of globally coupled identical oscillators, this model is even further simplified,

given that all frequencies are equal, that is $\omega_i = \omega$, and all interaction functions are the same, namely $\Gamma_{ij} = \Gamma$. However, the presence of higher harmonics or phase shifts may introduce effects that cannot be captured with interactions of the form (1.29).

However complicated the function $\Gamma(\phi)$ may be, it can be shown that the synchronized state is stable against small perturbations if

$$\left.\frac{\partial \Gamma(\phi)}{\partial \phi}\right|_{\phi=0} < 0\,, \tag{1.39}$$

and unstable otherwise [42, 18]. If we define a function $F \equiv \Gamma(\phi) - \Gamma(0)$, then by rewriting Eqs. (1.27) with this definition we will see that $\Gamma(0)$ determines the velocity Ω of the synchronized state, and F is an attractive interaction in the vicinity of the synchronized state if condition (1.39) is satisfied.

When condition 1.39 holds, it remains satisfied if we replace $\Gamma \to K\Gamma$ as long as $K > 0$. Manipulating the intensity of the interaction will not destabilize the synchronized solution when elements are identical. Therefore, synchronization is stable without a threshold, that is, for any positive intensity K. A desynchronization transition will therefore take place when this parameter crosses zero.

Such a transition may also be induced by changing parameters other than the intensity. In Chapter 2 we will study the case in which this desynchronization transition takes place when varying the phase shift value while keeping the intensity of the interactions constant.

1.5.3 Synchronization on networks

The remarkable result that a population of interacting oscillators may spontaneously develop synchronous coherent dynamics has attracted attention from different areas of the scientific community, and many attempts have been made to try to extend these results to more specific situations. Here we will discuss two aspects of the model (1.29) and its analytical description that are pertinent to our investigations.

The analytical mean-field description one must assume that the number of elements is infinite. This is necessary to be able to assume the existence of a stationary state in which the phases of all elements have a stationary density, even though they rotate with different velocities, so that R remains constant. This renders the analysis invalid for systems with a finite number of elements, and many attempts have been made to solve this conflict [59]. Nevertheless, numerical simulations have shown that the predictions of this theory are valid even far from the thermodynamic limit [60, 61].

The second aspect of the model that has been extensively addressed is the uniform global coupling. Different interaction schemes have been devised [63], but the most prominent approach has been the consideration of interactions given through a network [42]. The revival of the interest in networks that has taken place within the physical and biological sciences has also put forth the question on how the emergence of synchronization may be affected by the presence of network interactions. To take into account network interactions in the Kuramoto model, we must return to the general form of a phase model for nearly identical elements, given by Eq. (1.27). In

this case, it is clear that $\Gamma_{ij}(\phi_j - \phi_i) \equiv 0$ if $T_{ij} = 0$, that is, if there is not an edge from node i to node j. In the first harmonic apporximation, the Kuramoto model in a network takes the form

$$\frac{\partial}{\partial t}\phi_i = \omega_i + \frac{\mu}{N}\sum_{j=1}^{N} T_{ij}\sin(\phi_j - \phi_i)\,, \tag{1.40}$$

where all network interactions are assumed to have the same intensity μ.

A general mathematical description of the onset of synchronization in the Kuramoto model on networks can be found in Ref. [62]. As a general result, the introduction of network interactions produces a rescaling of the critical coupling intensity given by Eq. (1.38). An estimation of the critical value in the presence of a network is given by

$$\mu_c = K_c\frac{N}{\Lambda}\,, \tag{1.41}$$

where Λ is the largest eigenvalue of the adjacency matrix T [62]. This estimate is in good agreement with numerical simulations for networks with uncorrelated structure, as in the Erdős-Rényi model. However, the results are not valid in cases where there is a strong correlation between the indregee and outdegree of each node, or between the degrees of neighboring nodes, as in the case of scale-free networks [42]. In these cases, the critical value of the coupling intensity at which the onset of synchronization takes place can be largely reduced [64].

A recent review of different results obtained for the onset of synchronization in networks and various applications is given in Ref. [42].

1.5.4 Desynchronization and collective chaos in the globally coupled Kuramoto model

The study of ensembles of coupled oscillators has mostly concentrated on the onset and stability of synchronized oscillations. However, in many situations, as in the case of neurons in the brain, the onset of collective synchronized firing is a decidedly undesirable phenomenon, and schemes to prevent it have direct and important medical applications [2, 3]. Therefore, the destruction of the synchronized state also has aspects worth studying.

In general, in the globally coupled Kuramoto model (1.29), the absence of synchronous oscillations is characterized by a vanishing phase coherence, that is $R = 0$. In this case, as can be seen from Eq. (1.37), the interaction between each element and the global field disappears, and each element is effectively independent from all the rest. Therefore, all elements rotate with their own frequencies, unaffected by the presence of others. As such, changing the coupling strength in the range $0 < K < K_c$ produces no effect in the dynamics of the system in the infinite-size limit.

For a finite number of elements, fluctuations in the order parameter R remain for all times if the frequencies of all elements are not identical. Popovych, Maistrenko and Tass [65] have found a general route to desynchronization where frequency splitting is observed as the coupling strength is reduced towards the critical point.

Below the critical point, a region is found where the dynamics of the system is chaotic, interjected by a series of periodicity windows.

Chaos in this case emerges out of the heterogeneity of the elements. Each element has its own frequency, and the interaction of different elements leads to complex dynamics. Indeed, if all elements had identical frequencies, not only chaos, but any dynamics would actually be absent, and the desynchronization transition would lead to a stationary state in which $R = 0$ for any system size.

In this work we will examine how introducing network interactions between identical oscillators may lead to a different kind of chaos in the desynchronization transition.

1.6 Oscillatory extended systems

A special kind of interaction between oscillatory elements is found in continuous media, such as chemical systems, where the spatial distribution of concentrations plays a decisive role. In particular, when the local dynamics of the concentrations is periodic, one speaks of oscillatory extended systems, or oscillatory media.

A way to represent such systems is to consider a lattice of oscillators, in which the interactions take place between direct neighbors. The equations would be of the form 1.24, where function G includes a summation over neighbors of the nodes,

$$\frac{\partial}{\partial t}\mathbf{x}^i = \mathbf{F}^i\left(\mathbf{x}^i\right) + \epsilon \sum_{j \in \mathcal{N}_i} \mathbf{G}_{ji}\left(\mathbf{x}^j, \mathbf{x}^i\right) , \tag{1.42}$$

where $\mathcal{N}_i$ is the set of neighbor nodes of node i.

In such a lattice, the connections between the nodes have an associated distance d in the physical space. Since this elementary lattice distance is small, a linear approximation can be used, where the interaction would be of the kind

$$\frac{\partial}{\partial t}\mathbf{x}^i = \mathbf{F}^i\left(\mathbf{x}^i\right) + \epsilon \sum_{j \in \mathcal{N}_i} \mathbf{K}\left(\mathbf{x}^j - \mathbf{x}^i\right) . \tag{1.43}$$

Here, it is convenient to represent the system not as a set of individual oscillators, but as a field with different values at different nodes. Then, we substitute the discrete index i with a continuous spatial variable x, where we consider the one-dimensional case for simplicity. The resulting equations are

$$\frac{\partial \mathbf{x}(x,t)}{\partial t} = \mathbf{F}^i\left(\mathbf{x}(x,t)\right) + \epsilon\mathbf{K}\left(\mathbf{x}(x+d,t) - \mathbf{x}(x,t)\right) + \epsilon\mathbf{K}\left(\mathbf{x}(x-d,t) - \mathbf{x}(x,t)\right) . \tag{1.44}$$

The continuous limit may be attained by taking the limit $d \to 0$. For this we redefine the interaction intensity $\epsilon\mathbf{K} \equiv \mathbf{D}d^{-2}$, and decompose the interaction term in Taylor series up to the second degree, i.e.,

$$\frac{\partial}{\partial t}\mathbf{x} = \mathbf{F}^i\left(\mathbf{x}\right) + \frac{\mathbf{D}}{d^2}\left[\mathbf{x} + d\frac{\partial \mathbf{x}}{\partial x} + d^2\frac{\partial^2 \mathbf{x}}{\partial x^2} - \mathbf{x} + \mathbf{x} - d\frac{\partial \mathbf{x}}{\partial x} + d^2\frac{\partial^2 \mathbf{x}}{\partial x^2} - \mathbf{x}\right] . \tag{1.45}$$

Thus, we finally obtain

$$\frac{\partial}{\partial t}\mathbf{x}(x,t) = \mathbf{F}^i\left(\mathbf{x}(x,t)\right) + \mathbf{D}\nabla^2\mathbf{x}(x,t)\,. \tag{1.46}$$

The general Eq. (1.46) represents a *reaction-diffusion* system, in reference to the chemical systems. The first term dictates the local dynamics of the system at each point in space (for example, the dynamics of the concentrations of different reactants), and the second indicates how different chemical agents diffuse through the system. Nevertheless, the applications of such models are not restricted to chemical systems, and they are frequently used in ecology, biology, cardiology, and other scientific fields [66, 67].

1.6.1 The complex Ginzburg-Landau equation

A reaction-diffusion system would correspond to a system of oscillatory dynamics if function F in Eq. (1.46) describes a system with a stable limit cycle attractor. However, a phase reduction cannot be always be performed. In the continuous limit, also the solutions to (1.46) must be continuous in space, and to satisfy this condition, the inclusion of an amplitude variable may be necessary.

For systems in the vicinity of an Andronov-Hopf bifurcation like the one in system (1.12), it can be shown that a general mapping to the complex plane exists, though which the dynamics can be appropriately described by equation

$$\frac{\partial A}{\partial t} = (1+i\omega)A - (1+i\alpha)|A|^2 A\,, \tag{1.47}$$

where A is a complex variable, and ω and α are real-valued parameters. This is known as the *Stuart-Landau* equation, and its solutions approach a stable limit cycle in the complex plane, in which the system rotates with unit amplitude and constant frequency $\omega - \alpha$. The limit cycle solution is therefore $A = \exp[i(\omega-\alpha)t]$.

A reaction-diffusion system like (1.46), for which the local dynamics are oscillatory in the vicinity of an Andronov-Hopf bifurcation, can be generally described by what is known as the complex Ginzburg-Landau equation, which reads

$$\frac{\partial A}{\partial t} = (1+i\omega)A - (1+i\alpha)|A|^2 A + (1+i\beta)\nabla^2 A\,, \tag{1.48}$$

where β is also a real-valued parameter. The intrinsic velocity ω may be removed from the equations by going to a co-rotating frame of reference, i.e. by making a variable change $A \to A\exp(i\omega t)$. Therefore, the behavior of this system effectively depends on two parameters α and β, which characterize the nonlinear frequency shift and the linear dispersion, respectively. The interplay between local oscillatory dynamics and diffusion can give rise to a variety of different kinds of behavior, including plane waves, spiral waves, localized coherent structures and spatio-temporal chaos [68, 69, 70, 72]. Uniform oscillations are stable as long as the condition

$$1 + \alpha\beta > 0 \tag{1.49}$$

is satisfied. When this condition is violated, the instability of the synchronous state leads to spatio-temporal chaos. This transition is known as the *Benjamin-Feir instability*, and it may result in different kinds of turbulence, depending on the parameter values.

In the vicinity of the destabilization of uniform oscillations, a regime of *phase turbulence* develops, where small deviations in the phase and amplitude values occur with respect to the synchronous regime. This is accompanied by the propagation of amplitude *shocks*, or narrow regions with amplitude higher than the average value, that travel along the system. An example of this regime can be seen in Fig. 1.11a, where the amplitude of the oscillations is shown in gray scale for a one-dimensional system as a function of time.

As we move away from the instability line, the system becomes more strongly turbulent, and a regime of *defect turbulence* appears. Defect turbulence is characterized by the presence of a large number of amplitude *defects*, or points in the system where the amplitude vanishes, which is accompanied by a discontinuity in the phase value. These phase singularities are often referred to as phase slips or *kinks*, and they can diffuse and wander along the system, as well as reproduce and propagate. In fully developed defect turbulence, these phase slips occupy a large part of the medium, and dominate the dynamics, as can be seen in Fig. 1.11b.

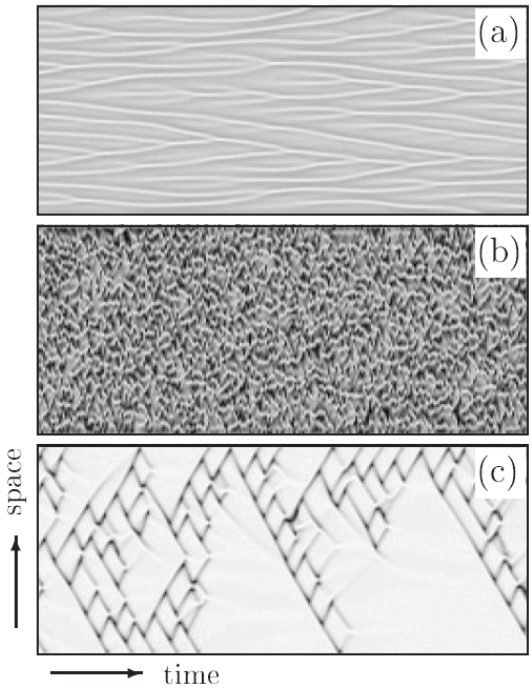

Figure 1.11: Different kinds of turbulence in the one-dimensional complex Ginzburg-Landau equation. (a) Phase turbulence close to the Benjamin-Feir stable region. (b) Fully developed defect turbulence. (c) Cascades of defects propagating on the background of uniform oscillations in the intermittent turbulence regime. This figure has been taken from [72].

The behavior of such phase slips may be very rich, and their dynamics can be quite different for different parameter values [73]. A regime that is of particular interest for our work is that of *intermittent turbulence* in which phase slips persist even into the Benjamin-Feir stable region. In this situation, the repeated occurrence of cascades of phase slips takes place in a background of plane waves or uniform oscillations. This is what is shown in Fig. 1.11c, where it can be seen that phase slips appear, reproduce and propagate, colliding with each other and annihilating, or spontaneously dying out.

1.6.2 Control of turbulence

Different methods to control turbulence in oscillatory reaction-diffusion systems have been proposed. Amongst these, methods that are applied globally to the entire system have proven to be the most interesting, since local access to specific regions of the system may often be unavailable.

A particularly interesting method of control is that of *global feedbacks*. This scheme involves taking signals from the system itself and using them to generate a control signal that acts back on the elements as a common parameter that affects the entire medium. The convenient aspect of such mechanisms is that no control signal needs to be externally designed or attended. Rather, it is the system itself which produces the acting force which exerts control. In this sense, the restoration of synchronization or the formation of patterns induced by global feedback control methods are self-organized processes.

The action of a global feedback can be included in the complex Ginzburg-Landau equation as

$$\frac{\partial A}{\partial t} = (1+i\omega)A - (1+i\alpha)|A|^2 A + (1+i\beta)\nabla^2 A + \mu e^{i\chi}\langle A\rangle\,, \tag{1.50}$$

where $\langle A\rangle = \int_S A(x,t)dx$ represents the average value of A over the entire system. Here, parameter μ controls the intensity of the global feedback, and χ is a phase shift that accounts for a delay in the application of the force.

For an oscillatory system in the turbulent phase, a global feedback like the one introduced in Eq. (1.50) can be shown to induce uniform oscillations [75, 76]. Hence, turbulence can be fully suppressed, and order can be reestablished in the system through such a control mechanism. Perhaps a more interesting aspect is that, for intermediate parameter values between turbulence and the restoration of uniform oscillations, a variety of patterns and coherent structures can be induced by the global feedback. Examples of this are the formation of phase clusters, where the system segregates into well-defined domains with synchronous dynamics; the formation of cellular structures, where an approximately regular array of phase defects and phase clusters is formed, such as honey-comb lattices of small amplitude domains; or the emergence of turbulent "bubbles", a higher-dimensional analog of defect cascades, in which persistent growth and death of defect-like structures occur on a background of uniform oscillations. This type of patterns have been observed to appear in the general model of the complex Ginzburg-Landau equation [76, 75], as well as in experimental and theoretical studies of the catalytic CO oxidation reaction [77, 78].

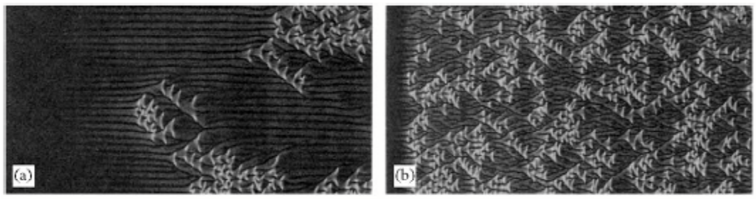

Figure 1.12: Intermittent turbulence induced by a global feedback in the complex Ginzburg-Landau equation. Cascades of phase slips or kinks propagate on the background of uniform oscillations. This figure has been taken from [69].

Global feedback allows one to control the dynamics of such defect cascades or turbulent bubbles. Indeed, the number, frequency and mean life of such cascades can be affected by the feedback parameters, as can be seen in Fig. 1.12. Varying the intensity of the global feedback (and also other parameters, such as the phase shift of the feedback) allow us to control turbulence and induce different levels of activity.

It should also be said a global feedback is an effective way to control the formation of patterns, even if the system is initially in an ordered state. By changing the phase shift value χ in Eq. (1.50), the feedback may have the effect of destroying uniform oscillations, allowing for the emergence of different kinds of patterns. Different routes to turbulence are characterized by the appearance of different coherent structures and different kinds of dynamical behavior [79, 80, 70, 71].

Chapter 2

Globally coupled systems

The emergence of collective global dynamics from simple interactions at the individual level is a common paradigm of self-organization. In such a picture, the properties of the microscopic interactions involving each pair of elements lead to the occurrence of macroscopic order without the regulation of external control.

However, collective behavior need not emerge from specific sets of microscopic interactions. A notable example of such a case is that presented by Teramae and Tanaka [81]. They have analized a system of identical oscillators which are completely independent, i.e., they have no interaction with each other. Instead, they are subject to an external common noise which affects all elements equally. They have found that, under the action of such a noise, starting from any initial condition for all the elements, they will eventually reach a synchronized state, in which the phases of all elements coincide.

This result may not be an astonishing one, if one looks at it from the perspective of a single element. Under a prescribed sequence of perturbations, it is not surprising that the final state will always be the same, independent of the initial condition. Nevertheless, it is not trivial either, and from the perspective of collective behavior it is still a remarkable concept: incoherent random forcing leads a population of fully independent elements to a fully coherent state.

Systems in nature are hardly ever independent of each other. Even disregarding the ever present gravitational force, the concept of *system* becomes superfluous, were there not a certain type of interaction between its composing parts. In fact, in a wide class of systems of different nature, it is often encountered that the elements that compose it interact reciprocally and homogeneously with each other. This can happen for example when interactions take place through a fast diffusing chemical reactant, or when the range of interactions is so large in comparison to the size of the system, that spatial distribution becomes irrelevant. In these cases, we say of the elements that they are globally coupled. This is the case, when interactions between all pairs of elements are of identical form and intensity.

With this kind of coupling, it is usually possible to reformulate the interactions within a mean field approach, in which each element interacts with a global field which is in turn generated by equal contributions from all elements. The nature of the interactions between elements can lead to a variety of different dynamic behaviors and of available equilibrium states.

A trademark phenomenon in systems of globally coupled identical oscillators is the presence of a desynchronization transition [5, 83]. In such a transition, the system evolves to a completely incoherent state, and the field they generate (and interact with) vanishes. In such a situation, the elements become effectively independent as their total interactions cancel each other out.

The presence of global noise may be encountered in very general situations. It may correspond to the case in which fluctuations in the parameters of a system affect the collective dynamics of all elements. The question we would like to address in this chapter is the following: if the elements of a globally coupled system become essentially independent in a desynchronization transition, and the action of a common noise may drive a system of independent elements to synchronization, then what would be the effect of an external common noise? Or to put it differently: can incoherent and uncontrolled perturbations induce order in a system of incoherent globally coupled elements?

To investigate this, we will study a system of globally coupled elements whose interactions are mediated through a phase shift. This phase shift will allow us to induce different types of behavior in the system, in particular a desynchronization transition. Under these circumstances, the action of external forcing and common noise is studied in detail.

2.1 Globally coupled oscillators with a common phase shift

In the following we analyze a system of globally coupled identical oscillators in which the interactions are mediated through a phase shift. The fact that they are identical implies that the natural frequency of all of them is the same, that is, $\omega_i = \omega$. The equations governing the system are

$$\frac{\partial \phi_i}{\partial t} = \omega + \frac{K}{N} \sum_{j=1}^{N} \sin(\phi_j - \phi_i + \alpha)\,, \tag{2.1}$$

where α is a phase shift in the interaction, which is equal for all pairs of elements. This system is clearly a special case of the general model (1.28), in which $K_{ij} = K$ and $\alpha_{ij} = \alpha$ for all $i \neq j$. We will retain α as a control parameter which allows us to affect the nature of the interactions, making them attractive or repulsive in the limits $\alpha = 0$ and $\alpha = \pi$ respectively. We can readily note that condition (1.39) is satisfied for $\alpha = 0$, but is not for $\alpha = \pi$.

It is easily seen that a change of variables of the form $\phi_i \to \phi_i' + \omega t$ will remove the natural frequency ω from the equation for ϕ_i'. This amounts to moving to a frame of

reference that rotates with the natural frequency of the oscillators. This shows that the choice of natural frequency is arbitrary, and we can eliminate it without any loss of generality. Similarly, once the natural freqeuncy has been removed, we can redefine the time units in the way $t \to t'/K$, in which case the left hand side term in Eq. (2.1) will be $\partial\phi_i/\partial t = \partial\phi_i/\partial t' \times \partial t'/\partial t = \dot{\phi}_i K$. Thus, the coupling constant can also be removed from the equations by an appropriate rescaling of time. Thus, Eq. (2.1) can be reduced to

$$\frac{\partial \phi_i}{\partial t} = \frac{1}{N}\sum_{j=1}^{N} \sin(\phi_j - \phi_i + \alpha)\,. \tag{2.2}$$

These equations describe a set of N elements interacting pair-wise with each other, and by changing the parameter α this interaction can be manipulated. Introducing the global parameter given by Eq. (1.36), we find the equality

$$Z(t)e^{-i\phi_i(t)}e^{i\alpha} = \frac{1}{N}\sum_{j=1}^{N} e^{i(\phi_j(t)-\phi_i(t)+\alpha}\,. \tag{2.3}$$

Equating the imaginary parts of both sides of this equation we get

$$R\sin\left(\Phi - \phi_i + \alpha\right) = \frac{1}{N}\sum_{j=1}^{N}\sin\left(\phi_j - \phi_i + \alpha\right)\,, \tag{2.4}$$

which is the right hand side of Eq. (2.2). Here R is the phase coherence, and Φ is the global phase of the system. This means that the pair-wise interaction in a globally coupled system can be reinterpreted as the individual interaction of each element with a global field, which is in turn generated by all elements. The field acts on each element with the same phase shift as the individual interactions. This system may therefore represent an ensemble of oscillators coupled to a delayed global signal. In complex notation, the decoupled equations of motion can be written as

$$\dot{\phi}_i = \frac{1}{2i}\left(Ze^{i\alpha}e^{-i\phi_i} - \text{c. c.}\right)\,, \tag{2.5}$$

where c. c. represents the complex conjugate of $Ze^{i\alpha}e^{-i\phi_i}$. In this equation it is clear that any state in which $Z = 0$ will be a fixed point of the system. On the other hand, it is also clear that if two elements have identical phases at a given moment, they will always be equal, since they are subject to the same forces. Therefore, if $Z = 1$ at any moment, meaning that all phases are identical, they will remain so, and this is therefore also a stationary state. The stability of these states will be analyzed in Sec. 2.2.

In Eqs. (2.5) it also clear that changing α by $-\alpha$ is equivalent to making a variable change $\phi_i \to -\phi_i$ for all i (of course, this would mean $Z \to Z^*$). This implies that the dynamics of the system is symmetric with respect to $\alpha \to -\alpha$, and thus also $\alpha \to 2\pi - \alpha$. Therefore, it is enough for us to concern ourselves with the behavior of the system in the range $\alpha \in [0, \pi]$.

2.1.1 Order parameters

Eq. (2.5) states explicitly the interaction of each element with a global field. This field is in turn generated by all elements collectively. Thus, the quantity Z as defined in Eq. (1.36) can be thought to represent both a dynamic order parameter to measure the level of similitude of the phases or phase coherence in the system, as well as a dynamic global *signal*, which all elements perceive and interact with. It is therefore reasonable to attempt to describe the behavior of the field as a dynamic description of the system.

From Eq. (1.36) we can readily determine that

$$\dot{Z} = \frac{i}{N}\sum_{j=1}^{N} e^{i\phi_j}\dot{\phi}_j\,. \tag{2.6}$$

Inserting Eq. (2.5) in this equation we get

$$\begin{aligned}\dot{Z} &= \frac{i}{N}\sum_{j=1}^{N} e^{i\phi_j}\left\{\frac{1}{2i}\left(Ze^{i\alpha}e^{-i\phi_j} - \text{c. c.}\right)\right\}\,,\\ &= \frac{1}{2}Ze^{i\alpha} - \frac{1}{2N}Z^*e^{-i\alpha}\sum_{j=1}^{N} e^{2i\phi_j}\,.\end{aligned} \tag{2.7}$$

In this way, we obtain an equation for the evolution of the global parameter. However this equation is not closed, and continues to depend on each individual value of the phases through the sum in the last term. We can define a new order parameter to represent this dependence as

$$\eta = \frac{1}{N}\sum_{j=1}^{N} e^{2i\phi_j}\,, \tag{2.8}$$

so that

$$\dot{Z} = \frac{1}{2}Ze^{i\alpha} - \frac{1}{2}Z^*e^{-i\alpha}\eta\,. \tag{2.9}$$

In the same way we can define a whole family of order parameters of the form

$$\begin{aligned}Z = \rho_1 &\equiv \frac{1}{N}\sum_{j=1}^{N} e^{i\phi_j}\,,\\ \eta = \rho_2 &\equiv \frac{1}{N}\sum_{j=1}^{N} e^{2i\phi_i}\,,\\ \rho_3 &\equiv \frac{1}{N}\sum_{j=1}^{N} e^{3i\phi_i}\,,\\ \rho_k &\equiv \frac{1}{N}\sum_{j=1}^{N} e^{k\,i\phi_i}\,.\end{aligned} \tag{2.10}$$

Each of these order parameters is a complex number whose magnitude is smaller or equal to 1. The k-th order parameter will have magnitude 1 when each element

occupies one of k equally distributed clusters (even if some of this clusters are empty). This means, for example, that $\rho_{nk} = 1$ when $\rho_k = 1$ for all $n = 1, 2, 3, \ldots$. All these order parameters are 1 in the synchronized state, when $Z = 1$.[1]

Just as we did with Z we can write an evolution equation for each of these order parameters in the form

$$\dot{\rho}_k = \frac{k}{2}\left[Z\rho_{k-1}e^{i\alpha} - Z^*\rho_{k+1}e^{-i\alpha}\,.\right] \tag{2.11}$$

In particular, the equation for η is

$$\dot{\eta} = Z^2 e^{i\alpha} - Z^*\rho_3\, e^{-i\alpha}\,. \tag{2.12}$$

This formalism allows us to move from a picture in which the system is described by the individual phases of all elements, to a picture in which a family of order parameters describes the configuration of the system as a superposition of clustered states. This family of order parameters is in principle infinite, but for our purposes it suffices to consider only the first three, namely on Z, η and ρ_3 from now on.

The first order parameter ρ_1 coincides with the standard global order parameter Z. The synchronous state $|Z| = 1$ is a fully coherent state, and a state for which $Z \approx 0$ is an incoherent state. In this terminology it is explicit that Z measures a level of global coherence or order in the system, in as much it allows to identify macroscopic rotations performed by the elements collectively.

As a collective phenomenon, phase coherence may be interpreted as a macroscopic variable, in the same sense that pressure is the macroscopic force exerted by an ensemble of particles. Thus, the global order parameter can be interpreted to be a global signal, as could be measured by an external observer without access to the specific distribution of phases.

However, an incoherent state need not be a disordered state. Indeed, many regular distributions of phases may be imagined for which no macroscopic signals are produced. In particular, clustering is a kind of internal organization that fails to be represented by the global order parameter. Thus, we can see that ρ_k with $k \geq 2$ characterize hidden internal levels of order in the system.

2.2 Synchronization and desynchronization

To analyze the stability of the fixed point $Z = 0$, we can study a linearized version of Eq. (2.9). To this effect, we propose a solution of the form

$$Z = C_1 e^{(\gamma+i\omega)t} + C_2 e^{(\gamma-i\omega)t}\,, \tag{2.13}$$

where $|C_1|$ and $|C_2|$ are assumed to be very small, that is $|C_1|, |C_2| \ll 1$, so that $Z \approx 0$. Inserting this solution back in Eq. (2.9) one gets

$$\begin{aligned}(\gamma + i\omega)C_1 e^{(\gamma+i\omega)t} + (\gamma - i\omega)C_2 e^{(\gamma-i\omega)t} = \\ = \frac{1}{2}e^{i\alpha}\left(C_1 e^{(\gamma+i\omega)t} + C_2 e^{(\gamma-i\omega)t}\right) - \frac{1}{2}e^{-i\alpha}\eta\left(C_1^* e^{(\gamma-i\omega)t} + C_2^* e^{(\gamma+i\omega)t}\right).\end{aligned} \tag{2.14}$$

[1] The synchronous case, where all elements are in one cluster coincides with the case with k clusters with $k-1$ of them empty.

In this approximation, η is taken to be a constant parameter. Since $e^{(\gamma+i\omega)t}$ and $e^{(\gamma-i\omega)t}$ are linearly independent, this equation can be separated in the two following equations.

$$\begin{aligned}(\gamma+i\omega)C_1 =& \frac{1}{2}e^{i\alpha}C_1 - \frac{1}{2}e^{-i\alpha}\eta C_2^*\,,\\ (\gamma-i\omega)C_2 =& \frac{1}{2}e^{i\alpha}C_2 - \frac{1}{2}e^{-i\alpha}\eta C_1^*\,.\end{aligned} \tag{2.15}$$

Solving for C_2^* in the lower equation and plugging this in the first one, and introducing the notation $\lambda = (\gamma + i\omega)$, we get

$$\left(\lambda - \frac{1}{2}e^{i\alpha}\right)\left(\lambda - \frac{1}{2}e^{-i\alpha}\right) = \frac{1}{4}|\eta|^2\,, \tag{2.16}$$

which is a quadratic equation on λ. The solution to this equation is

$$\lambda = \gamma + i\omega = \frac{1}{2}\left(\cos\alpha \pm \sqrt{|\eta|^2 - \sin^2\alpha}\right)\,, \tag{2.17}$$

which gives us the exponents for the time dependence of Z in Eq. (2.13). If $\gamma > 0$ it means that $|Z| \gtrsim 0$ will grow in time; therefore, any state with $Z = 0$ will be unstable. Correspondingly, if $\gamma < 0$, all small perturbations of $Z = 0$ will be damped and the system will be restituted to a $Z = 0$ configuration. If the square root in the second term is real, it can at most be equal to $\frac{1}{2}\cos^2\alpha$, which only happens in the special case in which $|\eta|^2 = 1$ exactly. Any other configuration with $|Z| \approx 0$ results in growth of $|Z|$ for $0 < \alpha < \pi/2$, and collapse to the $Z = 0$ surface when $\pi/2 < \alpha < \pi$. The solutions to Eq. (2.17) as a function of $|\eta|$ are plotted in Fig. 2.1 for diferent values of α. Here it can be seen that, in the range $\pi/2 < \alpha < \pi$, γ is negative for all values of $|\eta|$.

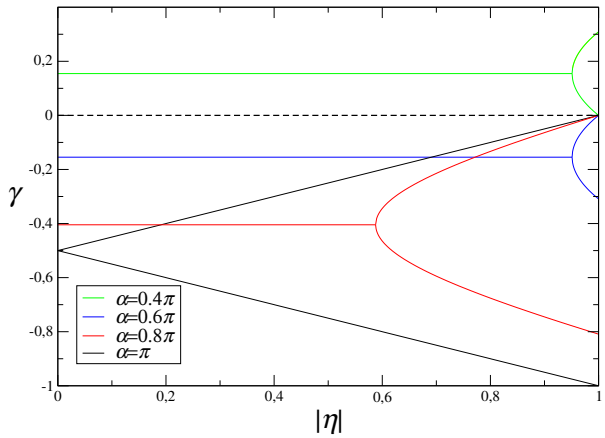

Figure 2.1: Solutions to Eq.2.17 for different values of parameter α.

The solutions for this exponent have two branches for certain values of $|\eta|$. This is reflected in the fact that the relaxation to the fixed point has two modes. A plot of this relaxation for different initial values of $|\eta|$ is shown in Fig. 2.2. Here it can

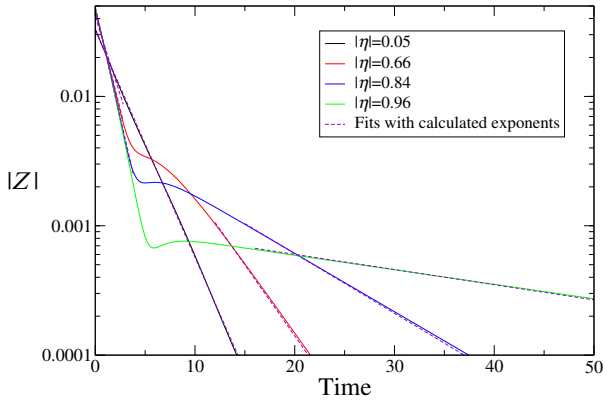

Figure 2.2: Time-volution of the convergence to the incoherent attractor $Z = 0$ for different initial values of $|\eta|$. The dotted lines represent fits whose exponents are calculated with Eq2.17. $\alpha = 0.8\pi$, $N = 100$.

be seen that the relaxation is indeed exponential, where two different modes with two different exponents are present. Furthermore, in dashed line we show fittings produced with the exponents calculated with Eq. (2.17) for the initial value of η. As can be seen, the agreement between the simulations and the theoretical prediction is quite good.

An important thing to point out is that, for all values of α, the positive branch of λ reaches exactly 0 when $|\eta| = 1$, the state in which all elements are distributed in two clusters separated by a phase difference of π. At this point also the negative branch reaches its minimum value. This may indicate that the two-cluster state is neutrally stable against a certain kind of perturbation, while maximally stable against others.

The results of this linear stability analysis show that the incoherent state is unstable in the range $0 < \alpha < \pi/2$, and stable when $\pi/2 < \alpha < \pi$. As should be expected, the only stable state when $0 < \alpha < \pi/2$ is the phase-synchronized state. This can be seen in Fig. 2.3, where the magnitude of the global order parameter is plotted as a function of α in the long-term limit.

Another important set of quantities to elucidate on the stability of different states are the Lyapunov exponents, introduced in Sec. 1.2.2. In Fig. 2.4 we see the largest of them, and the three smallest, calculated as a function of parameter α. It can be seen in Fig. 2.4 that all Lyapunov exponents are negative in the range $\alpha < \pi/2$. However, in the range $\pi/2 < \alpha < \pi$, all but the last two exponents are zero. This means that there are $N - 2$ effective degrees of freedom, determining $N-2$ linearly-independent directions in the phase space along which the system can move without leaving the attractor.

In terms of the Kaplan-Yorke dimension, as defined in Sec. 1.2.2, the fact that all but two exponents are equal to 0 implies that the dimension of the attractor is $N - 2$. In Fig. 2.5 we plot the calculated Kaplan-Yorke dimension, as numerically obtained from simulations. As expected, the dimension jumps from 1 to $N - 2$ at

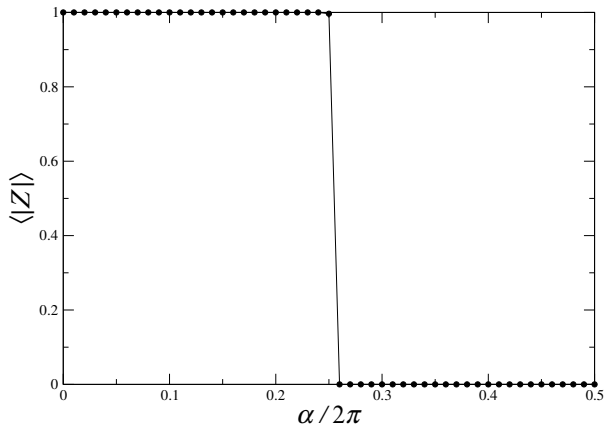

Figure 2.3: Mean magnitude of the global order parameter Z as a function of α in the long-term limit, starting from random initial conditions. $N = 100$.

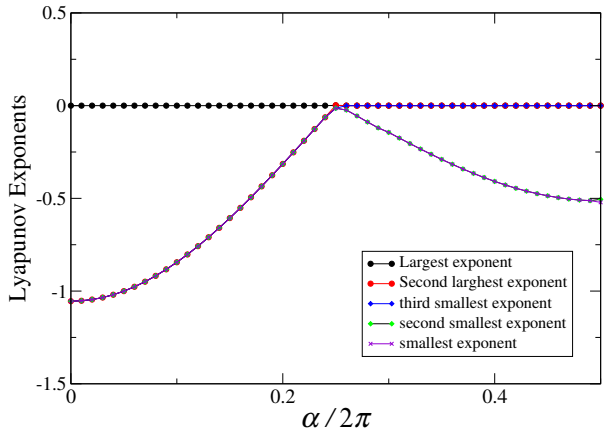

Figure 2.4: The two largest and the three smallest Lyapunov exponents as a function of α. $N = 100$.

$\alpha = \pi/2$. [2]

The condition $|Z| = 1$ necessarily implies that all phases are equal, and since $R = 1$ the only degree of freedom left is that associated with Φ which consists in rigid rotations of a frozen configuration. On the other hand, the condition $Z = 0$ imposes a restriction on the possible configurations of the system, but infinitely many states satisfy it. In fact, $Z = 0$ defines an $(N-2)$-dimensional surface of states that are fixed points of Eqs. (2.5), and all of these fixed points are neutrally stable against perturbations along this surface in the parameter range $\pi/2 < \alpha < \pi$. Perturbations that bring the system away from this surface are damped, as follows from Eq. (2.17). However, the convergence to these states happens at different rates depending on the value of $|\eta|$. In a sense, we can understand that the dynamics of the global parameter depends on the internal organization of the system. States with higher

[2]The dimension $D_{KY} = 1$ corresponds to the rotations of the synchronized state.

values of $|\eta|$ will relax to the incoherent state more slowly. Nevertheless, since all points in the surface are neutrally stable, the state to which the system relaxes may not be the same in which it was before the perturbation.

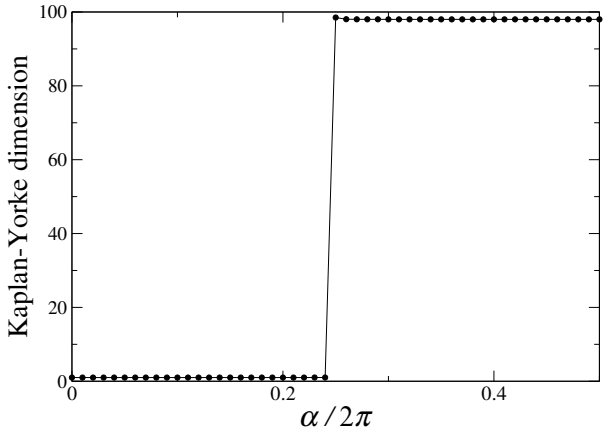

Figure 2.5: Embedding dimension as calculated by the Kaplan-Yorke formula in (1.18) as a function of α. $N = 100$.

Let us consider a situation where the system is persistently moved away from the hypersurface $Z = 0$, for example, by the action of fluctuations or noise. All points on this surface correspond to marginally stable fixed points, and thus, any perturbation that leaves the system on the surface will bring the system to a new marginally stable fixed point. However, transversal perturbations will unfreeze the dynamics of the system, which will evolve towards the stable surface systematically. In this case, the system will effectively drift along the region of the state space where $Z \approx 0$, always keeping close to the surface $Z = 0$ but never exactly on it. A schematic representation of this can be seen in Fig. 2.6. In some regions, the relaxation to the surface will be slower, and we can imagine that the system will spend more time in these regions than in regions where relaxation is faster. In a situation like this, we expect the system to go to states with higher values of $|\eta|$, and therefore naturally organize in a clustered state.

2.3 Forcing and common noise

The system evolves towards an incoherent state in the parameter range $\pi/2 < \alpha < \pi$, but still an infinite number of states can be chosen to satisfy this condition. We now turn our attention to the possible effects on such states of global external forcing as a possible mechanism to control the specific equilibrium state of the system. We begin by considering the simple case of a constant force applied in pulses.

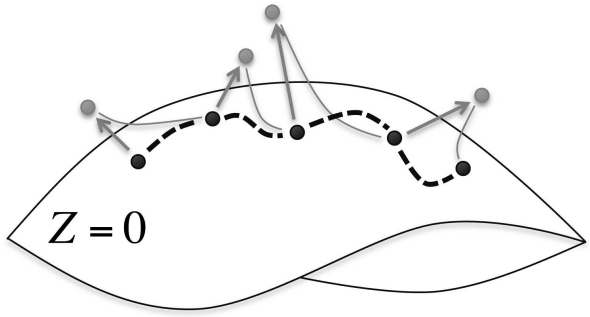

Figure 2.6: Schematic representation of the dynamics in the phase space with persistent perturbations. The system evolves towards the $(N-2)$-dimensional surface of fixed points (black dots). Persistent perturbations "knock" the system away form this surface, letting it evolve back towards it. If the system lands in a different point of the surface, then the presence of small persistent perturbation will effectively amount to making the system drift along the surface (slashed black line).

2.3.1 Constant external forces and pulses

In the following, we will analyze the action of a constant external force on the system. The equations describing this would take the form

$$\dot{\phi}_i = \frac{1}{2i}\left(Ze^{i\alpha}e^{-i\phi_i} - \text{c. c.}\right) + \frac{1}{2i}\left(Fe^{-i\phi_i} - \text{c. c.}\right), \tag{2.18}$$

where F is a complex constant number, such that each element is attracted to the argument of F with an intensity proportional to its modulus. Rewriting, we get

$$\dot{\phi}_i = \frac{1}{2i}\left[\left(Ze^{i\alpha} + F\right)e^{-i\phi_i} - \text{c. c.}\right]. \tag{2.19}$$

In this equation it is clear that, if $|F| < 1$, the new equilibrium state will be one for which $Ze^{i\alpha} + F = 0$. Therefore, the global order parameter will have a magnitude equal to the external force, and the system will reorganize to satisfy this condition.

Clearly, a strong enough force will bring the system to a synchronized state. Eq. (2.19) tells us that this will already happen for $|F| = 1$, and it will naturally also occur for even stronger forcing. On the other hand, the effect of a force with magnitude smaller than one will be to compress the distribution of the phases to accommodate for $Ze^{i\alpha} = -F$. For example, when $\alpha = \pi$, Z coincides with F in the stationary state.

For $|F| < 1$ there are infinite configurations that satisfy this condition. If such a force is applied at a time moment when the system has already attained a stationary state with $Z = 0$, then the system will evolve towards a new state with $|Z| = |F|$. Removing the force after some time will let the system relax back to the $Z = 0$ surface. However, the specific configuration that the system adopts after this may be entirely different to the one before applying the force.

Forcing the system will induce coherence, but it may also induce a level of internal ordering that persists even after the force stops acting on the system. Therefore, we may ask the question of whether levels of internal order are indeed affected by such pulsing perturbations.

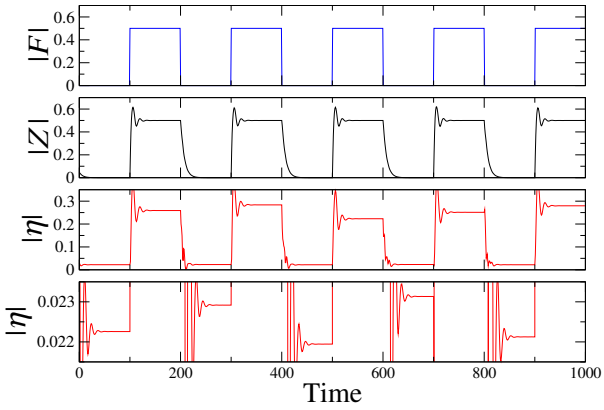

Figure 2.7: Time realization of the first two order parameters under the action of repeated external pulses with constant magnitue and phase. In the last panel, the data from the third panel has been magnified in the vicinity of $|\eta| \approx 0$. $|F| = 0.5$, $\alpha = 0.6\pi$ and $N = 100$.

In Fig. 2.7 we see a numerical integration of the system equations under the action of repeated pulses with constant amplitude and phase. The magnitudes of the first two order parameters Z and η are monitored as the configuration changes under the alternating presence and absence of force. As seen in the second panel, the global parameter follows the magnitude of the forcing, and after brief transients, a state with $|Z| = |F|$ is reached. The second order parameter also follows the time-dependence of the forcing, but the values that it reaches are different for each pulse, meaning that different configurations are attained in each instance. Correspondingly, the stationary value of $|\eta|$ in the absence of forcing changes after each pulse, as can be seen in the last panel, where the scale has been magnified. This means that, even though the global phase coherence in the system repeatedly relaxes to zero, different internal configurations are visited, each with different levels of internal organization.

If after each subsequent pulse the value of $|\eta|$ changes, then it is possible that a systematic change occurs if pulsing is persistent. In figure 2.8, the modulus of parameter η after each pulse is plotted as the number of applied pulses progresses. As can be seen, $|\eta|$ increases systematically (although not monotonically, as clearly seen in the lower panel of Fig. 2.7 and in the early stages of the evolution in Fig2.8), eventually reaching $|\eta| \approx 1$ after a large number of pulses has been applied. The number of pulses necessary for this to happen is very likely to be reduced when the intensity of the pulses is increased.

We can conclude that a series of repeated pulses affects the system by inducing the formation of clustered states. In terms of our discussion in Sec. 2.2, and referring to Fig. 2.6, it is important to note that such pulses act as a perturbation in a direction transversal to the $Z = 0$ surface. After each pulse, the system relaxes back

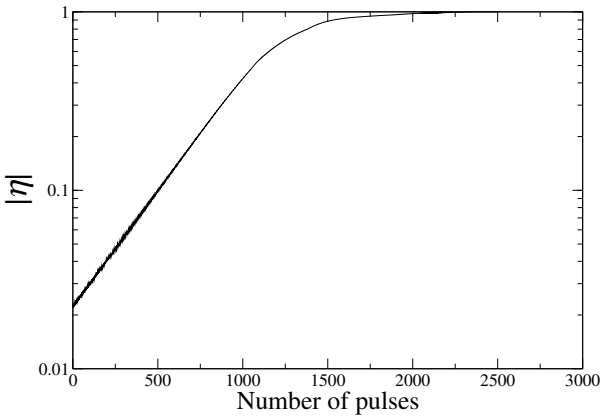

Figure 2.8: Evolution of the second order parameter $|\eta|$ after the application of successive pulses of constant magnitude and phase. $|F| = 0.5$, $\alpha = 0.6\pi$ and $N = 100$.

to the surface, landing at a different point of it, which represents a different configuration with a different level of internal ordering. Repeating this process lets the system evolve from one point in the surface to the next, progressively approaching a clustered state.

2.3.2 Common noise

Inducing order with controlled forcing may be a rather simple task, since a strong enough force will always bring the system to a synchronized state. A more interesting scenario may be that in which the system is subject to random and incoherent forcing [84]. This is the case when common noise is present.

In the beginning of this chapter we mentioned previous studies on populations of independent elements under the action of common noise. The action of such common noise results in synchronization of all elements without a threshold on the noise intensity.

In contrast to the case of independent elements, the synchronized solution is not available to our system in the absence of forcing in the parameter range $\pi/2 < \alpha < \pi$, and the system evolves to any state in the surface $Z = 0$. By introducing a global noise acting as external random forcing we keep the system slightly away from this surface. Since in our interpretation, pulses act as generic perturbations, noise may play a similar role. In this way, we may see whether the system evolves towards a certain region of the phase space.

We introduce a new term in Eqs. (2.5) of the form

$$\dot{\phi}_i = \frac{1}{2i}\left(Ze^{i\alpha}e^{-i\phi_i} - \text{c. c.}\right) + \frac{\sigma}{2i}\left(\xi(t)e^{-i\phi_i} - \text{c. c.}\right), \tag{2.20}$$

where the value of $\xi(t)$ at each time moment is the same for all i, and σ is a real-valued control parameter that determines the intensity of the noise. Both terms have the same form, meaning that each element interacts with the noise field in the

same way it does with the global signal. This is clear if we rewrite these equations in the form

$$\dot{\phi}_i = \frac{1}{2i}\left[\left(Ze^{i\alpha} + \sigma\xi(t)\right)e^{-i\phi_i} - \text{c. c.}\right], \tag{2.21}$$

where the action of the noise is expressed explicitly as fluctuations of the global field. In this sense, the noise acts as a perturbative force on the global coupling.

An external fluctuation of this sort can be thought to represent a wide variety of different external factors that can influence the system as a whole. This could be fluctuating temperatures that affect the periodicity of chemical oscillators, changing light conditions, or even electromagnetic field that acts on charged particles. As the simplest assumption, we will choose to use a white noise of Gaussian distribution, avoiding to temporal correlations that may indeed represent some of these circumstances more realistically, but would introduce unnecessary parameters that would obstruct the analysis.

Therefore, we define $\xi(t)$ as a random complex-valued process whose modulus $|\xi|$ has Gaussian distribution, and its argument $\arg(\xi)$ is uniformly distributed in $[0, 2\pi)$. Its statistical properties are of the form

$$\begin{aligned}\langle\xi\rangle &= 0\,,\\ \langle\xi(t_1)\xi(t_2)\rangle &= 0\,,\\ \langle\xi(t_1)\xi^*(t_2)\rangle &= \delta(t_2 - t_1)\,.\end{aligned} \tag{2.22}$$

Just as with Eq. (2.4), the second term of Eq. (2.20) can be written as a

$$\frac{1}{2i}\left(\sigma\xi(t)e^{-i\phi_i} - \text{c. c.}\right) = \sigma|\xi(t)|\sin\left(\arg\left(\xi(t)\right) - \phi_i\right), \tag{2.23}$$

meaning that all elements are attracted to the instantaneous phase of the noise field, with an intensity proportional to its instantaneous magnitude and to the control parameter σ.

2.3.3 Infinite-noise limit and synchronization

In the extreme case of $\sigma \to \infty$, the dynamics is dominated by the noise term, and the interactions between the elements can be disregarded. In such a case, the situation would be equivalent to that of independent elements under the action of common noise. As said at the beginning of this chapter, a common noise acting on independent identical elements induces phase synchronization. Although only the case of the real noise was considered in Ref. [81], the fact that the noise is complex makes little difference.

In Fig. 2.9 we show the time evolution of the magnitude of the order parameter Z for a realization with noise intensity $\sigma = 100$, for which the initial conditions are set randomly with uniform distribution in the circle. The order parameter grows until reaching unity, indicating that all phases become identical.

The synchronized state should be found for any values of the interaction parameter in the infinite-noise limit, and, as shown by Fig. 2.9, it is also observed for large but finite values of the noise intensity σ. In the absence of interactions (that is, if

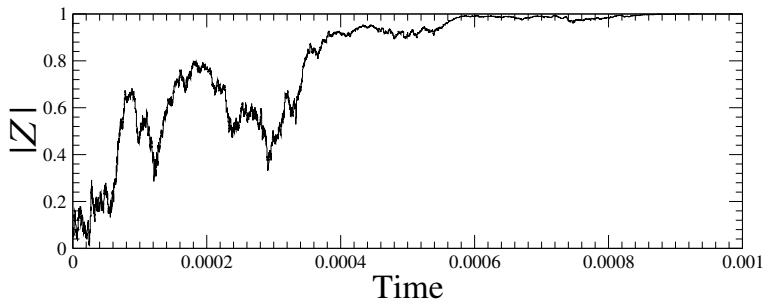

Figure 2.9: Time-realization of $|Z|$ for a very large noise intensity. $\alpha = 0.6\pi$. $N = 100$, $\sigma = 100$

the noise was the only term in Eq. (2.20)), this would happen with no threshold for the noise intensity.

Thus, when for $\alpha > \pi/2$, Eq. (2.20) is composed of two competing terms: the first term will drive the system to an incoherent state , and the second term will drive the system to a fully coherent, synchronized state. The interplay between these two conflicting forces is what we will study next.

2.3.4 Two-cluster state

Since any state with $Z \neq 0$ is unstable in the absence of noise, we can expect this to be the case for small values of σ. However, the system can still move freely along the surface defined by $Z = 0$. Additionally, small but non-zero values of σ will cause the system to remain slightly off of this surface, and allow it to drift along it.

As it turns out, this interplay results in driving the system to a clustered state. In Fig. 2.10 we show the evolution in time of the magnitude of parameters Z and η for a system of $N = 100$ elements and $\alpha = 0.6\pi$. The magnitude of the noise intensity here is $\sigma = 0.01$, and the system is initialized with homogeneously distributed, random phase values. Indeed, $|Z|$ remains close to zero, but $|\eta|$ grows in time, reaching finally values very close to 1. This means that the system never moves away of the $Z = 0$ surface but instead drifts on towards a state where the elements are distributed in two clusters.

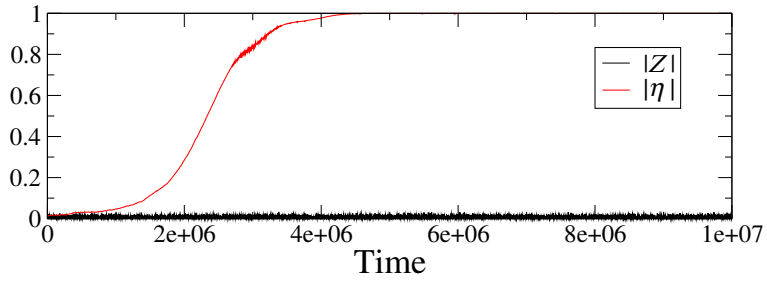

Figure 2.10: Time-realization of $|Z|$ (black) and $|\eta|$ (red) for $\alpha = 0.6\pi$. $N = 100$, $\sigma = 0.01$

The modulus of the order parameter η only reaches its maximum value 1 when all elements are distributed in two clusters which are separated by a phase difference of π, and such that the phases of the elements in each cluster are identical. Furthermore, if the modulus of the global order parameter Z is to be zero, then these clusters must have the same number of elements. As seen in Fig. 2.10, $|\eta|$ reaches a value very close to 1.

To characterize the distribution of the phases in the long-term limit, we monitor the phase distance between elements, which, for elements i and j, we define as

$$d_{i,j} = d_{j,i} \equiv \min\left\{|\phi_i - \phi_j|\,, 2\pi - |\phi_i - \phi_j|\right\}\,, \tag{2.24}$$

where the phases are mapped to the interval $[0, 2\pi]$, that is, $\phi_k \to \phi_k \mod 2\pi$ is applied. This distance goes to zero when the i-th and j-th oscillators have identical phase values.

With this definition of the distance, we may introduce the average distance between close elements as

$$q = \frac{1}{N} \sum_{\substack{i,j=1 \\ d_{i,j}<h}}^{N} d_{i,j}\,. \tag{2.25}$$

The threshold value h determines a vicinity around each element within which the distance is taken into account.

The time evolution of $q(t)$ is shown in Fig. 2.11a, where the threshold value $h = \pi/2$ was chosen. As we can see in the logarithmic scale, this average distance tends to decrease to very low values, eventually reaching 0 for our numerical precision. Although large fluctuations are present, this quantity approximately follows an exponential decay with an exponent 1.9×10^{-4}, which is certainly a function of the noise intensity.

This means that no element is in the vicinity of any other element at a small finite distance, indicating that all elements arrange in clusters within which the phases of all elements are identical. The progressive formation of such clusters can be seen in panels (b) through (d) in Fig. 2.11, where histograms of the distribution of phases (mapped to the $[0, 2\pi]$ interval) are computed for different instants along the evolution. Form an initially uniform distribution, the elements progressively approach each other, eventually forming two clusters that are singular. This point-like clusters are approximately separated by phase difference of π.

The stability of singular clusters can be understood in the infinite-size limit, if one considers a perturbation consisting of pushing one element slightly away from one of the clusters. If two clusters A and B are considered with phases Φ_A and Φ_B respectively, both of which contain the same amount of elements, then the equation of motion for the first cluster will be

$$\dot{\Phi}_A = \frac{1}{2}\left[\sin(\Phi_B - \Phi_A + \alpha) + \sin(\alpha)\right] + \frac{1}{2i}\left(\sigma\xi(t)e^{-i\phi_i} - \text{c. c.}\right)\,, \tag{2.26}$$

and a similar equation will govern the dynamics of the second cluster. If we consider that one element is moved slightly away from the cluster, then in the infinite-size

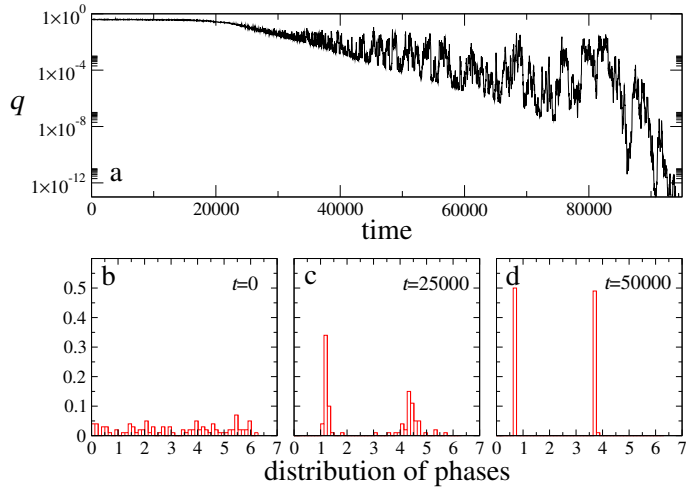

Figure 2.11: (a) Time evolution of the mean distance between close elements $q(t)$. (b-d) Snapshots of the distributions of phases at different times during the evolution. $\alpha = 0.6\pi$, $\sigma = 0.1$ an $N = 100$.

limit, the dynamics of cluster A would not be altered. However, the equation for the phase ψ of this single element would be

$$\dot{\psi} = \frac{1}{2}\left[\sin(\Phi_B - \psi + \alpha) + \sin(\Phi_A - \psi + \alpha)\right] + \frac{1}{2i}\left(\sigma\xi(t)e^{-i\phi_i} - \text{c. c.}\right). \qquad (2.27)$$

The stability of this state against the global coupling requires that $\Phi_B - \Phi_A \approx \pi$. In this case, the first term of these last two equations would vanish, and only the noise term would be present. These equations would then be equivalent to those of two independent oscillators with close phase values under the action of common noise. According to the results presented in Refs. [81, 82], these two elements would synchronize, and then the state with two point-like, evenly populated clusters would be restored. This argument supports the idea that a common noise term may stabilize a state that would otherwise be marginally stable.

In Eq. (2.21) it is clear that the noise term can be considered as a perturbation to the global field to which all elements are coupled. Since this filed is in turn generated by all elements, we can expect fluctuations to the global field Z to be of the order of the noise term. In Fig. 2.12, the average value of the magnitude of the global parameter is plotted as a function of the noise intensity. We can see here that the dependence between these quantities is approximately linear. Since the magnitude of the global parameter is constricted to the range $[0, 1]$, this implies that there is a certain value of the noise intensity above which $|Z| = 1$. This is to be expected, as discussed before, since in the limit of $\sigma \to \infty$, only the synchronized state should be stable.

This implies the presence of a transition on the noise intensity between the two-cluster state in the low-nosie limit and the synchronous state in the large noise limit. To investigate this, we plot in Fig. 2.13 the time-average value of $|Z|$ and $|\eta|$ in the long-term regime for different values of the noise intensity, while α is kept fixed at

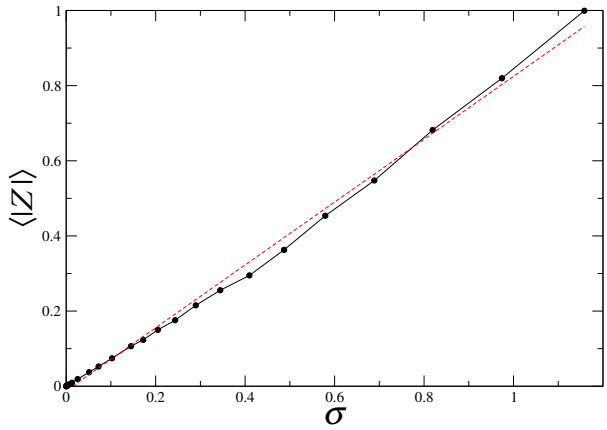

Figure 2.12: Mean magnitude of the global order parameter $|Z|$ (black) as a function of the noise intensity. A straight line (red) is included as a reference. $\alpha = 0.6\pi$, $N = 100$.

a value 0.6π. The system is always initialized in a uniform state with all phases randomly distributed in the circle. As expected, when the noise intensity is large enough ($\sigma \gtrsim 1$) the system goes to the synchronized state with $|Z| = 1$ (and $|\eta| = 1$ as well). However, the convergence to the two-cluster state in the low-noise limit seems to occur with no threshold. This state, as indicated by the vanishing value of the mean distance between close elements q, consists of singular clusters for finite values of σ as well.

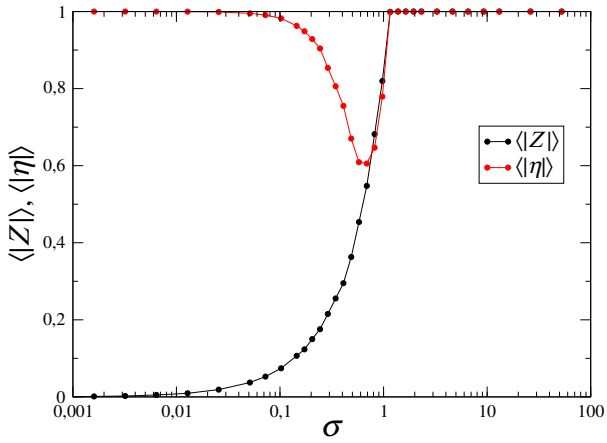

Figure 2.13: Mean value of $|Z|$ and $|\eta|$ as a function of the noise intensity σ. The logarithmic scale is used along the horizontal axis. $N = 100$, $\alpha = 0.6\pi$.

However, as can be seen in Fig. 2.10, even though the mean distance between close elements q does indeed go to zero, $|\eta|$ is not exactly 1, and $|Z|$ is only close to zero, but clearly fluctuates. This means that we can consider all the elements in each cluster as a single element, and the dynamics of the system in the clustered state

should be the same of that of a system with only two oscillators with a repulsive interaction. In this case it is clear that the transition from $Z \approx 0$ for $\sigma \ll 1$ to the synchronous state with $|Z| = 1$ when $\sigma \gg 1$ takes place through fluctuations in the relative positions of the two elements. Indeed, for small noise intensities both elements would remain approximately opposing to each other. In the limit of $\sigma \to 0$ and $t \to \infty$, $|\eta|$ would be exactly 1. Increasing the noise intensities will bring them together, eventually making them collapse in a single point when the noise is strong enough.

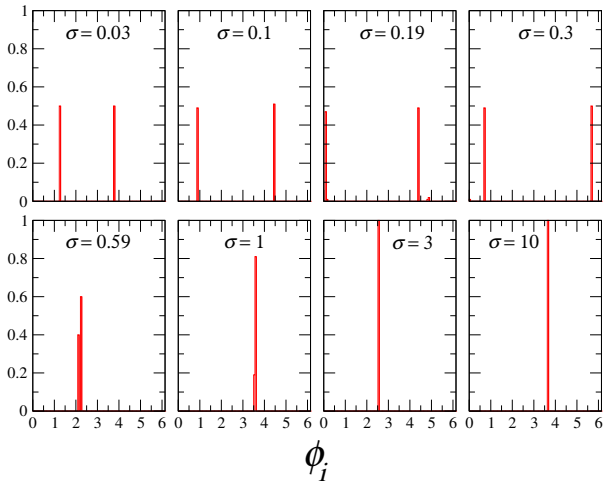

Figure 2.14: Distributions of phases at a single time moment for different noise intensitites σ. All phases are projected to the $[0, \pi]$ interval. $N = 100$, $\alpha = 0.6\pi$.

The transition in a system with many oscillators takes place in the same way. In Fig. 2.14 we show snapshots of the distribution of phases at a given moment in the long-time limit for different values of the noise intensity. It is clear in this figure that even though the relative positions of the clusters change, the spread in phases within each cluster remains very narrow, and presumably vanishing in the infinite time limit. It is also worth noting that for intermediate noise intensities (in this figure, for example, $\sigma = 0.1$ and $\sigma = 0.19$) the elements may distribute in clusters with slightly different numbers of elements. These might be metastable states, in which the system may spend a long time before going to the more strongly stable state with both clusters equal. In the weak noise limit, since any configuration with unevenly distributed clusters would have $Z \neq 0$, these states will be clearly unstable, and the larger cluster would rapidly spread out.

For intermediate values of the noise intensity, both clusters remain well defined, and the angle between them fluctuates around a certain mean value. This mean value decreases as the noise intensity is increased. In Fig. 2.15 we can see how this average distance between the phases of the clusters depends on the noise intensity. The distance here is taken as defined by (2.24), where the phase values of each cluster are taken into account, and the time-averaged value is calculated. Therefore, the mean value of this distance is always smaller than π. In the figure we can see that

the difference between the two clusters is close to π at small noise intensities, and this difference decreases for stronger noises, dropping to 0 for $\sigma > 1$. This denotes the collapse of both clusters into one.

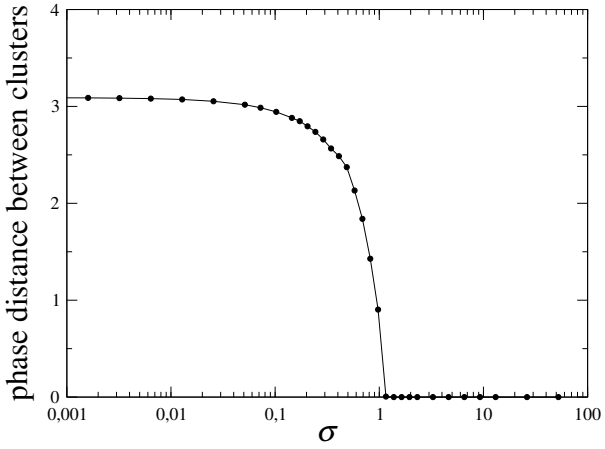

Figure 2.15: Average phase difference between the two clusters in the infinite time limit for different values of σ. $N = 100$, $\alpha = 0.6\pi$.

2.3.5 Three-cluster state

The existence of a stable clustered state when the noise is weak depends on the value of α. Indeed, we have seen that for $\alpha < \pi/2$ the only stable state is the synchronized state, or equivalently, a single-cluster state. In the previous section we have analyzed the behavior for a given value in the range $\alpha > \pi/2$, namely $\alpha = 0.6\pi$, and we have seen that the stable state in the low-noise limit is one with two opposing and equal clusters.

For larger values of α, also the two-cluster state becomes unstable, and a stable three-cluster state appears. This is signaled by a growth in the modulus of parameter ρ_3. In Fig 2.16 we monitor the moduli of the first three order parameters Z, η and ρ_3, starting from uniformly random initial conditions, and we compare the situation at two different values of α. As in the case of $\alpha = 0.6\pi$, in the top panel we see that $|\eta|$ oscillates near the maximum value, while $|Z|$ remains close to zero. $|\rho_3|$ fluctuates broadly around intermediate values.

The situation for $\alpha = 0.8\pi$, plotted in the lower panel of Fig. 2.16, is quite different. Here, the modulus of η remains small, whereas the modulus of ρ_3 steadily grows in time. This indicates that the system gradually approaches a state with 3 clusters with approximately equal spacing. The fact that Z remains close to zero implies that these clusters are similarly populated.[3]

The time-scale involved in the growth of ρ_3 for $\alpha = 0.8\pi$ is orders of magnitude larger than that associated with the growth of η at $\alpha = 0.6\pi$ (in fact, this latter

[3]A wide variety of clustered configurations with different populations in each cluster may yield $Z = 0$. However, those with very dissimilar populations would also yield a value of $|\rho_3|$ far from one. Only small differences in the populations of the clusters may satisfy both conditions simultaneously.

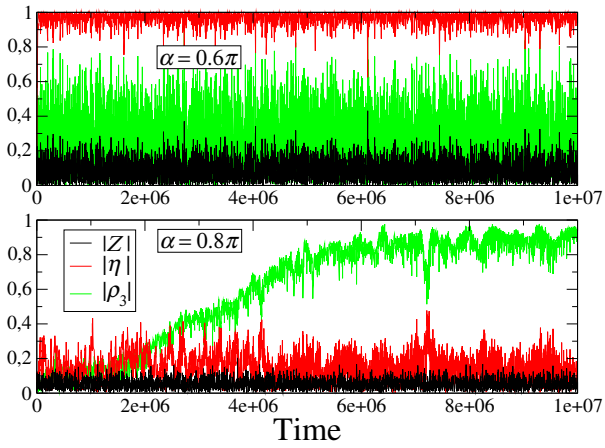

Figure 2.16: Time-realization of $|Z|$ (black), $|\eta|$ (red) and $|\rho_3|$ (green) for $\alpha = 0.6\pi$ and $\alpha = 0.8\pi$. Initial conditions are the same for both realizations, and they are randomly and uniformly distributed. $N = 100$, $\sigma = 0.1$.

is so fast in comparison, that it seems instantaneous in Fig. 2.16). This time-scale depends strongly on the noise intensity. However, very strong noises guarantee synchronization, as it did for other values of α. Therefore, there is an optimal level of noise to attain the three-cluster state, which still sets a very large limit on the minimum simulation times necessary to reach this state. This poses a practical problem in the implementation of the numerical integration of Eqs. (2.20) in which a tradeoff must be evaluated between numerical precision and simulation times. The low-noise limit is thus very hard to investigate in the case of the three-cluster state.

This difference in time-scales can also be observed in Fig. 2.17, where the mean phase distance for close elements $q(t)$, as defined in Eq. (2.24), is ploted as a function of time for a realization with $\alpha = 0.8\pi$ and $\sigma = 0.1$. As can be seen, the distance drops in an approximately exponential fashion, eventually reaching exactly zero for our numerical precision. This means that the clusters in this case are also perfectly defined, point-like clusters. As compared to Fig. 2.11, the decay is much slower, and the times necessary for this distance to vanish are much longer.

As seen for the two-cluster case for $\alpha = 0.6\pi$, the three clusters are well defined in the infinite-time limit but fluctuations in their positions persist for all times, and $|\rho_3|$ will never reach unity. In Fig. 2.18, histograms of the distribution of the magnitude of the three first order parameters are shown in the long-time limit for four different values of α. Here it can be seen that the fluctuations of $|\eta|$ in the cases of the two-cluster state are lower than the fluctuations of $|\rho_3|$ when three clusters are present. What is also quite interesting is that the distributions in the first and second panel, and those in the third and fourth panel are very similar separately, and there are barely any variations in the distributions between different values of α that lead to the same clustered state.

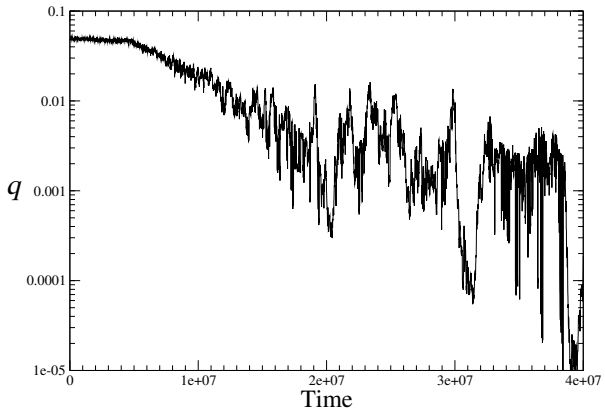

Figure 2.17: Time evolution of the mean distance between close elements $q(t)$. $\alpha = 0.8\pi$, $N = 100$, $\sigma = 0.1$.

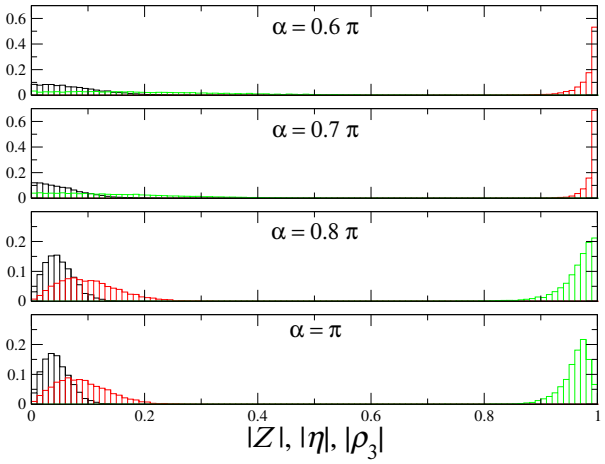

Figure 2.18: Histograms of the values of $|Z|$ (black), $|\eta|$ (red) and $|\rho_3|$ (green) for different values of α. $N = 100$, $\sigma = 0.01$.

2.3.6 Parameter dependences

We have seen that in the range of $\alpha < \pi/2$ the system has a single stable state corresponding to synchronized oscillations. For different values of α in the range $\pi/2 < \alpha < \pi$ we have found that a two-cluster state and a three-cluster state can be found for small noise intensities. Examining the whole interval of possible values of α we find that these states are found in wide ranges of the parameter space.

In Fig. 2.19 we explore the range $0 < \alpha < \pi$ for a constant noise intensity, while we monitor the three first order parameters. The mean values of the modulus of Z, η and ρ_3 are measured in the long-term limit for each value of α, starting from randomly distributed initial conditions for each point. Here it can be seen that a two-cluster state is reached for all values in $\pi/2 < \alpha \lesssim 3\pi/4$, whereas a three-cluster state seems to be the pervasive stable state within $3\pi/4 \lesssim \alpha < \pi$.

Interestingly enough, for any value of α the system goes to a state with either

one single cluster (synchronization), a state with two clusters or a state with three clusters. Presumably, this will also happen for weaker noises in the infinite-time limit. In this sense, it seems that clustering is the natural state of the system in the presence of common noise.

2.3.7 Clusters as single elements

In Sec. 2.3.4 we have considered the case of systems of infinite size to understand the stability of the state with two point-like clusters. This leads us to equations for each cluster that are equivalent to that of a single element. In principle, any clustered state can be treated in the same way, provided that the proper weight is given to the interactions. In particular, the dynamics of any clustered state with k singular clusters with equal populations should be equivalent to that of a system with k elements, and the statistical properties of these systems should be identical.

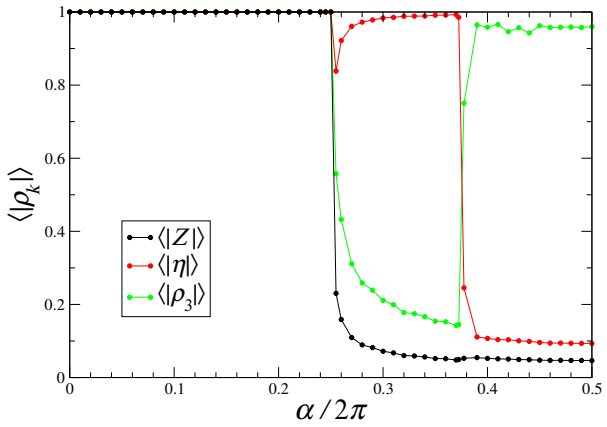

Figure 2.19: Average value of $|Z|$ (black), $|\eta|$ (red) and $|\rho_3|$ (green) as a function of α. $N = 100$, $\sigma = 0.1$.

Thus, the dynamics of a system with hundreds of elements should coincide, in the infinite-time limit, with the dynamics of a system with two elements in the $\pi/2 < \alpha < 3\pi/4$ range, and with three elements in the range $3\pi/4 < \alpha < \pi$.

A system with either two or three elements has a single state which satisfies $Z = 0$, this state will be the only stable one available to the system in the range $\pi/2 < \alpha < \pi$. This suggests that the clustering behavior observed in the simulations so far presented for a system with $N = 100$ elements should already be observed in a system with only $N = 6$ elements, which can be arranged in both two-cluster and three-cluster states maintaining $Z = 0$.

In Fig. 2.20, a plot like the one in Fig. 2.19 was constructed for a system of $N = 6$ oscillators. Here we can see that the clustering behavior in the infinite time limit is the same as observed in the larger system. These results suggest that a system of any large number of elements will behave like a system k elements when it is in a k-cluster state with all clusters equally populated.

These results imply that the behavior of the system should prove to be size independent, provided that the elements in the system can be (at least approximately)

distributed in two and three clusters with equal populations. Furthermore, since our analysis has been mostly performed on a system with $N = 100$ oscillators—which cannot be allocated to three even clusters exactly—but the results are very similar, this behavior proves to be robust even against this restriction. We have also run preliminary simulations with much larger systems, for which the behavior here presented has also been consistently observed.

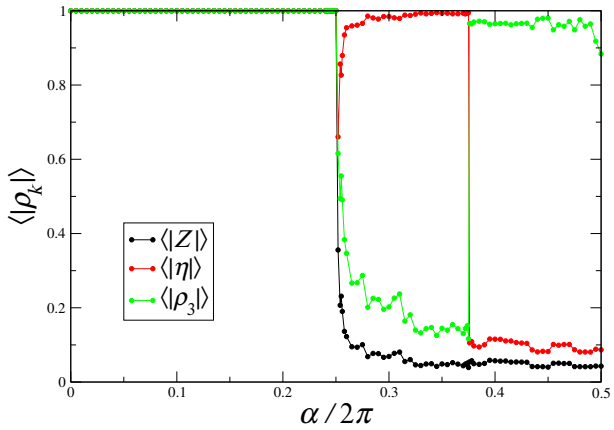

Figure 2.20: Average value of $|Z|$ (black), $|\eta|$ (red) and $|\rho_3|$ (green) as a function of α. $N = 6$, $\sigma = 0.1$.

2.3.8 Uneven cluster distributions

As our stability analysis showed in Sec. 2.2, only incoherent states ($Z = 0$) are stable for $\pi/2 < \alpha < \pi$. When considering two-cluster states, this implies that both clusters should be equally populated and separated by a phase difference of π. However, other two-cluster states may be solutions of the system (2.5), albeit unstable. If we consider a distribution with two clusters, the first one with a fraction p of the population and phase value Φ_A, and the second one with the remaining $1-p$ fraction of the elements and phase value Φ_B, then the equations of motion in the absence of noise would be

$$\begin{aligned} \dot{\Phi}_A &= p \sin(\Phi_B - \Phi_A + \alpha) + (1-p)\sin(\alpha)\,, \\ \dot{\Phi}_B &= (1-p)\sin(\Phi_A - \Phi_B + \alpha) + p\sin(\alpha)\,. \end{aligned} \tag{2.28}$$

A stationary state exists if there is a solution with $\dot{\Phi}_A = \dot{\Phi}_B$. This implies the relationship between the relative populations and the phase difference between the clusters given by

$$p = \frac{\sin(\alpha) - \sin(\Delta + \alpha)}{2\sin(\alpha) - \sin(\Delta + \alpha) - \sin(-\Delta + \alpha)}\,, \tag{2.29}$$

where $\Delta \equiv \Phi_A - \Phi_B$.

This relationship tells us that a given distribution of the population in two clusters has a specific stationary phase distance between them. If the system is initialized

in such a configuration, it will remain frozen for all times. The relationship between these values is plotted in Fig. 2.21. Since p is restricted to the range $[0, 1]$, only values of Δ that correspond to such values are meaningful.

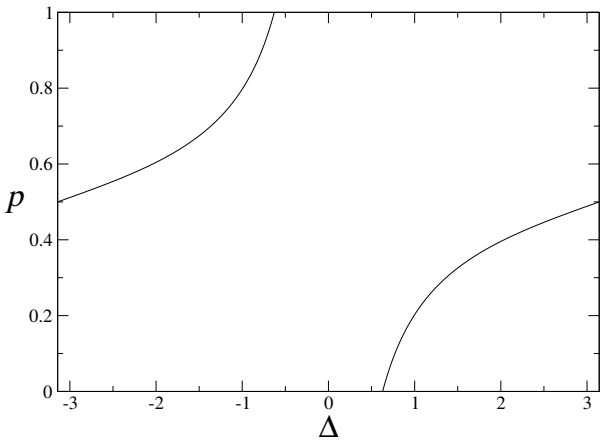

Figure 2.21: Relation between the relative populations of the clusters and the phase difference between clusters. $\alpha = 0.6\pi$

These states are frozen configurations, in that such clustered states persist for all times. However, they are not stable against perturbations, and will never be attained from random initial conditions. The same procedure applied in Refs. [33] and [32] can be followed here to analyze the stability of these clustered states. For these clustered states, the Jacobian matrix for the system (2.2) evaluated on the states determined by condition (2.29) has four different eigenvalues:

$$\begin{aligned}
\lambda_0 =& 0\,,\\
\lambda_1 =& (p-1)\cos(-\Delta+\alpha) - p\cos(\alpha)\,,\\
\lambda_2 =& (p-1)\cos(\alpha) - p\cos(\Delta+\alpha)\,,\\
\lambda_3 =& (p-1)\cos(-\Delta+\alpha) - p\cos(\Delta+\alpha)\,.
\end{aligned} \tag{2.30}$$

λ_0 corresponds to rigid rotations of the whole system, and is correspondingly 0 for all configurations; λ_1 has multiplicity $pN-1$ and corresponds to perturbations to the elements in cluster A; λ_2 has multiplicity $(1-p)N-1$ and corresponds to perturbations to cluster B; and λ_3 has multiplicity 1 and is associated with perturbation to the phase difference between the clusters. The values of the eigenvalues are only meaningful for values of $|\Delta|$ for which p is in the range $[0, 1]$, as seen in Fig. 2.21. We compute the three last of these eigenvalues as a function of the phase difference between the clusters, which are shown in Fig. 2.22.

As can be seen in this figure, λ_2 is positive for all cluster configurations,[4] except for that for which the phase difference between the clusters is π. According to (2.29), this corresponds to the clustered state with two equally populated clusters.

[4]For the choice of range for Δ, cluster B corresponds is the bigger cluster ($p \leq 1/2$).

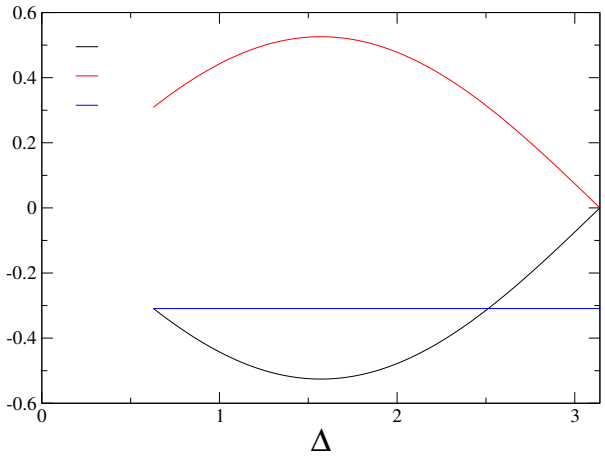

Figure 2.22: Eigenvalues of the Jacobian of the system evaluated on clustered states determined by (2.28). $\alpha = 0.6\pi$

This means that all configurations with uneven clusters are unstable, and only that corresponding to two even clusters separated by a phase distance of π is neutrally stable. For this reason, we can expect that this last state is the only one that can become stabilized by the presence of noise of low intensity.

This analysis is restricted to the consideration that $Z = 0$ must be satisfied, which is a valid approximation in the weak-noise limit. However, for any finite noise intensities, the magnitude of the global order parameter is persistently maintained away from zero, however close. For low noise intensities, the system reacts by adopting a phase distance between the clusters consistent with this value of the noise intensity. However, if the noise is of intermediate intensity (larger than $1/N$), this requirement may be satisfied by adopting different populations in each of the two clusters. In fact, in Fig. 2.14 we have seen that for some noise intensities, this actually occurs in simulations.

In Fig. 2.23 we show the relative difference between the populations of the two clusters as a function of the noise intensity. The absolute value of the difference between the populations is averaged over several realizations. As we have seen before, in the limit of low noise and for a wide range of noise intensities in the lower end, the two clusters are always equally populated. In the higher extreme, only one of the clusters contains all elements. For intermediate values, however, a fraction of the realizations result in an uneven population distribution between the clusters. It is still possible that the range of noise intensities for which uneven cluster distributions are attained in the infinite-time limit expands as the system size is increased. In the infinite system limit, we could expect that a certain range of inequality in the populations is stable for any finite noise intensity.

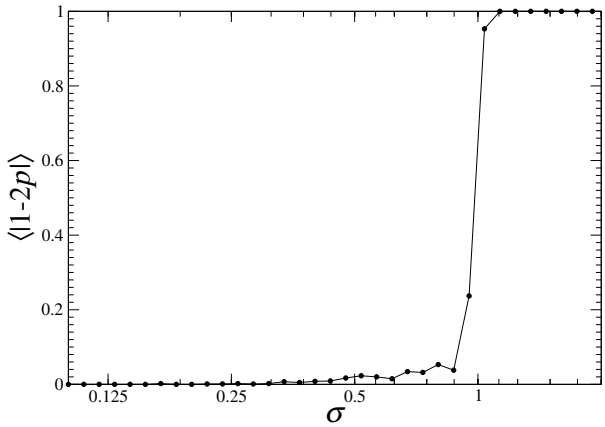

Figure 2.23: Average relative difference in the populations of the two clusters as a function of the noise intensity. The results are averaged over 10 realizations for each point. The sharp increase near $\sigma = 1$ corresponds to an increasing number of realizations that result in full synchronization. $\alpha = 0.6\pi$, $N = 100$

2.4 Heterogenous natural frequencies

So far we have considered all elements to be identical, i.e., they have the same natural frequency. However, in many real-world systems, in particular in biological systems, this condition is rarely satisfied. Even when all oscillatory elements in the system are of the same nature, some variation in their frequencies is to be expected. We therefore want to know how robust the observed results are against structural perturbations and, in particular, against variability in the natural frequencies.

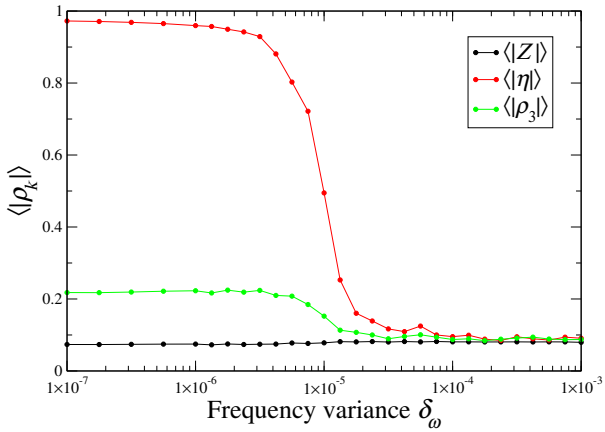

Figure 2.24: Average value of $|Z|$ (black), $|\eta|$ (red) and $|\rho_3|$ (green) as a function of the variance in the natural frequencies δ_ω. The initial conditions for each point are random and uniform. $\alpha = 0.6\pi$. $N = 100$, $\sigma = 0.1$.

If we assign different frequencies to each oscillator, then the synchronized state

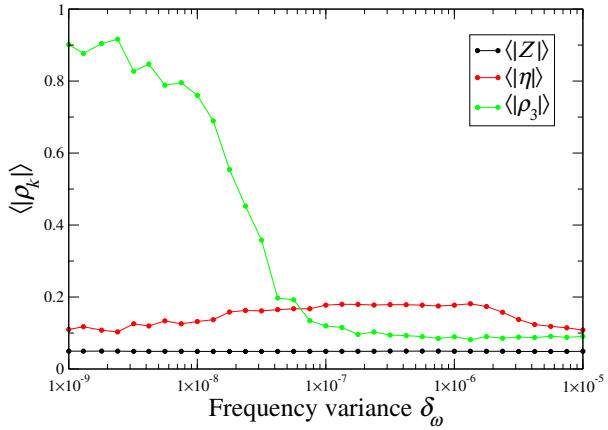

Figure 2.25: Average value of $|Z|$ (black), $|\eta|$ (red) and $|\rho_3|$ (green) as a function of the variance in the natural frequencies δ_ω. The initial conditions for each point are random and uniform. $\alpha = 0.8\pi$. $N = 100$, $\sigma = 0.1$.

might not be stable anymore for $\alpha < \pi/2$ and the incoherent state might not be a fixed point for $\alpha > \pi/2$. Under these conditions, also the 2- and 3-cluster states might be destroyed by heterogeneities in the oscillator population.

We run simulations on a system of $N = 100$ non-identical oscillators whose equations of motion are

$$\dot{\phi}_i = \omega_i + \frac{1}{2i}\left(Ze^{i\alpha}e^{-i\phi_i} - \text{c. c.}\right) + \frac{1}{2i}\left(\xi(t)e^{-i\phi_i} - \text{c. c.}\right), \tag{2.31}$$

where the natural frequencies ω_i have a Gaussian distribution with a mean of 0 and $\langle\omega_i^2\rangle = \delta_\omega$. In Fig. 2.24 we show the dependence of moduli of the first three order parameters when increasing the variance of the distribution of natural frequencies for $\alpha = 0.6\pi$. For this we keep the noise intensity fixed at $\sigma = 0.1$. Here we see that the 2-cluster state persists only until a variance in the natural frequencies of the order of 10^{-5}. For larger values, the oscillators cease to be entrained, with each element performing persistent rotations with different frequencies.

We do the same calculation for $\alpha = 0.8\pi$ where the system shows a 3-cluster stable state for δ_ω. These results are shown in Fig. 2.25. We can see here that the modulus of ρ_3 remains high only for very small values of the variance in the natural frequencies δ_ω. When the variance is close to 10^{-7}, the 3-cluster state seems to be already destroyed. In this sense, the 2-cluster state is much more robust against heterogeneity in the population than the 3-cluster state. These results, both for the 2-cluster and the 3-cluster states, are likely to depend on the noise intensity. The syncronized state for strong noises is however very robust against heterogeneities of the oscillators. In Fig. 2.26 we see that the system continues to synchronize for very large variances.

The variations on the natural frequencies that destroy the clustered state are quite small. However, it is important to stress that this critical value is still finite, and therefore the formation of clusters is preserved up to a certain degree of variabil-

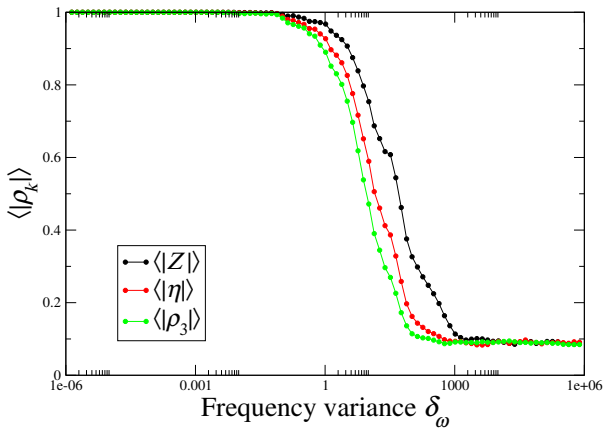

Figure 2.26: Average value of $|Z|$ (black), $|\eta|$ (red) and $|\rho_3|$ (green) as a function of the variance in the natural frequencies δ_ω. The initial conditions for each point are random and uniform. $\alpha = 0.6\pi$. $N = 100$, $\sigma = 10$.

ity. This critical value may be different for systems of different size, with different coupling constants, or oscillators of a different nature. Therefore, it is not to be ruled out that many biological systems may be found to satisfy the conditions for the behavior here described to be observed.

2.5 Final comments

In this chapter we have studied the stationary states of an ensemble of oscillators coupled to a phase-shifted global signal. We have found that this system undergoes a desynchronization transition, after which the final state may be any of an infinite collection of asynchronous states with no coherent oscillations.

The action of a common noise on all elements has been shown to lead to clustered states in such systems. Such clusters are perfectly defined, in that all elements in each cluster have identical phases. In particular, weak common noise drives the system to either a state with two clusters or a state with three clusters, for the conditions used in our simulations.

This result may have important implications for practical applications. In many real systems and experimental situations involving coupled oscillators, fluctuations in common system parameters will always be present, such as variations in temperature, illumination, atmospheric pressure, etc. According to our results, such variations, however small, may over long periods of time induce clustering. Nevertheless, most often it is only the degree of synchronization, as measured by global signals such as the global order parameter Z, that is monitored in experiments. In such cases, the system may seem at first sight to be in a disordered or incoherent state, while highly ordered clustered states may go undetected.

Although realistic fluctuations cannot be always described by Gaussian noise, and some temporal correlations in them may be present, we have no reason to believe

that such correlations would have an important effect. It is actually remarkable that even uncorrelated isotropic fluctuations can induce the kind of order we have observed.

The fact that the clusters are point-like in our system is directly related to the fact that all oscillators are identical. However, in most experimental circumstances, intrinsic variations between elements (or intrinsic noise in their dynamics) cannot be eliminated.In general, heterogeneity in the population would cause the clusters to spread out [85, 86]. Nevertheless, we have seen that the clustered states tolerate a certain degree of heterogeneity in the frequencies of the elements. This tolerance is small, and might be too small for many practical applications. But the robustness of such clustered states would depend on the coupling intensity (which we held fixed here and equal to 1), the noise intensity, the phase shift in the global coupling and even the statistical properties of the noise. Therefore, other parameter values may yield clustered states that are much more robust to variations in the oscillator population. It is possible that this robustness might be high enough for these phenomena to take place in natural and experimental systems.

In our studies we have only used a complex common noise. Furthermore, this noise has been generated by drawing the modulus and the phase from independent distributions. This particular choise of the noise might have an effect on the possible final states, or the times necessary to attain them. Other choices for the noise may lead to a different phase diagram.

Chapter 3

Networks of oscillators with a phase shift

In the previous chapter, we analyzed a system of oscillators in which each element interacts with all other elements in a reciprocal and homogenous way. This type of interaction is a suitable approximation for many systems [5, 56, 87]. However, one often encounters the situation in which each element interacts with a given subset of elements. Furthermore, this interaction is not necessarily reciprocal. Such is the case for systems of such diverse nature as the synaptic network in the brain, telecommunication networks, transport between machinery in a factory, and networks of streets and traffic lights in a city, and many others.

Self-organization has been extensively investigated in the context of chemical reactions, such as the Belousov-Zhabotinsky reaction [88, 89, 90]. This reaction takes place in an aqueous phase, and it involves several reaction steps. After producing many intermediate chemical species, the initial reactants are produced again. As a result, by supplying a constant influx of chemical reactants and removing excess byproducts, the dynamics may be maintained in an oscillatory regime where the concentrations of each species oscillates at a stable frequency.

Many other well-studied reactions have this kind of oscillatory dynamics. When the spatial distribution of the reactant densities becomes a relevant factor, the interplay between the local reaction and the diffusion of the reactants may lead to very complex dynamics. The general behavior of such oscillatory reaction-diffusion systems may be captured under quite general conditions (near the Hopf bifurcation) by the complex Ginzburg-Landau equation, introduced in Sec. 1.6.1. This equation is a general mathematical model describing the evolution of the amplitude and phase of oscillations in time and space for a generic oscillatory reaction-diffusion system. Its validity as a description of such systems has been widely corroborated [91, 77, 78].

Uniform oscillations in a reaction-diffusion system are a stable solution when diffusion happens very fast in comparison to the local dynamics (frequency) of the reaction. In this case, the entire system oscillates with the same amplitude, frequency and phase. But stability analysis shows that this uniform state becomes unstable when the diffusion is slowed down, or the reaction accelerated. In this regime, different kinds of chemical turbulence develop, where the phase and amplitude at different points of the system exhibit spatio-temporal chaotic behavior. This kind of turbulence is widely observed in experimental setups for different kinds of oscillatory reaction-diffusion systems.

A natural way to derive an equation like the complex Ginzburg-Landau equation is to consider a spatially-extended reaction-diffusion system as a set of individual elements whose dynamics are given by the reaction, and place them in a lattice, through which each element interacts with its immediate neighbors. The continuous limit is therefore obtained by decreasing the separation between elements in the lattice and increasing the number of elements while maintaining the dimensions of the system fixed.

Lattices are a very simple way of representing the distribution of elements embedded in euclidean space. However, as explained in Sec. 1.4, a lattice is a kind of network, albeit a very restrictive kind. Indeed, in the set of all networks that can be constructed with a given set of elements and a given number of edges, lattices only represent a negligible fraction. The question arises of how the results obtained for reaction-diffusion systems or for the complex Ginzburg-Landau equation can be extended to situations where spatial embedding is not Euclidean.

Another condition that must be satisfied by solutions of the complex Ginzburg-Landau equation is that they should be continuous functions of the space variable, since singular behavior at a given point in space would have no physical meaning for a chemical system. In the possible case of a singularity in the phase variable, it is required that the amplitude of oscillations vanishes. If we were to imagine two very close points with equal amplitude and opposite phase, then it would be only natural that the amplitude be zero at a given point between them. This is what is know as a *phase slip* or a "kink", a phenomenon with interesting properties which plays an important role in the development of turbulence [73, 74]. However, in a network model it is unreasonable to think of a continuous limit, and we may dispense of this restriction. Therefore, the use of phase oscillators may be a valid approximation, since no requirements on the amplitude are necessary.

The system investigated in the previous Chapter may be considered as a limiting case of such a situation, one in which all elements interact with each other identically. In this chapter, we will consider a system of oscillators which interact through a network, so that each element is connected to a random subset of the elements in the entire system. Our emphasis will be placed on the dynamical behavior that can be observed, and in trying to describe them in general terms as they occur in networks with different properties.

3.1 Oscillators in a network

That each element interacts with a certain fraction of the other elements means that only a fraction of the terms will be retained in the summation in Eqs. (2.2). These terms coincide with the corresponding non-zero elements in the adjacency matrix representing the network of interactions. Therefore, to adapt the system (2.2) to a network representation, it suffices to multiply each interaction term by the corresponding element of the adjacency matrix T. For consistency, we additionally modify the normalization factor by dividing by the connectivity or density of edges in the network ρ. The equations of motion are thus

$$\frac{\partial \phi_i}{\partial t} = \frac{1}{N\rho} \sum_{j=1}^{N} T_{ij} \sin(\phi_j - \phi_i + \alpha) \,, \tag{3.1}$$

where the matrix elements T_{ij} are 1 if there is a directed edge connecting element j to element i, and 0 otherwise. When each element is connected to all others, all $T_{ij} = 1$ (although $T_{ii} = 0$ for all i). In this case $\rho = 1$, and we recuperate Eqs. 2.2.

As a choice for the structure of T, standard networks of the Erdös-Rényi type will be used. In such networks, (directed) links connecting two elements $(i \to j)$ are chosen independently at random with some probability ρ. Explicitly, the elements of matrix T are

$$T_{ij} = \begin{cases} 0 & \text{if} \quad i = j \\ 1 & \text{with prob.} \quad p \\ 0 & \text{with prob.} \quad 1 - p \,, \end{cases} \tag{3.2}$$

where the first condition excludes loop edges. The network of interactions is therefore an unweighted, directed random graph. In the limit of large networks we will have

$$p \approx \rho \equiv \langle T_{ij} \rangle = \frac{\sum_{j=1}^{N} T_{ij}}{(N-1)\, N} \,, \tag{3.3}$$

and the mean degree of the network is $\langle k \rangle = \rho N$. The probability p is an expectation value for the connectivity of the network ρ, and the two values coincide in the infinite-size limit. In this Chapter, we will only consider realizations of the adjacency matrix T for which the network is strongly connected, meaning that there exists at least one directed path from each element to all others.

A state in which all phases are identical (which is a solution of the system (2.1) in the previous chapter for all values of α) is no longer a solution of system (3.1) for $\alpha \neq 0$. Indeed, if all phases are identical, then each term in the sum of 3.1 will have the same value $\sin \alpha$. In this case we get

$$\dot{\phi}_j = \frac{k_j^{in}}{N\rho} \sin \alpha \,, \tag{3.4}$$

where k_j^{in} is the incoming degree of node j. Since this degree is in principle different for each element, this equation can only be satisfied when $\alpha = 0$ or $\alpha = \pi$, and $\dot{\phi}_j = 0$ for all j. Otherwise, each element would have different velocities $\dot{\phi}_i$, and the phase-synchronized state would rapidly disintegrate.

However, there may still be solutions in which all elements have the same velocity, that is $\dot{\phi}_i = \Omega$. In these cases, a frozen configuration would be reached in which the phase-distances d_{ij} between all pairs of elements, as defined in Eq. (2.24), are constant in time, and the system rotates with constant velocity as a rigid body. In particular, for $\alpha = 0$, the frozen configuration reached is one with $d_{ij} = 0$ for all i, j for (almost) any kind of connected network [42, 62], and therefore, for all values of ρ. This would be a phase- and velocity-synchronized state, and the global order parameter would be $|Z| = 1$.

When α is slightly increased from zero, we can expect the distribution of the phase values in the frozen configuration to spread, although velocities may remain constant. Since this is the more general case, in the remainder of this thesis, we will refer to such a velocity-synchronized state as simply *synchronized*, unless stated otherwise. In this case, the magnitude of the global order parameter would be reduced, yet still reach a constant finite value.

Nevertheless, the existence of such a stationary state cannot be so far guaranteed, and persistent dynamics may develop in the system. The configuration of the elements would therefore no longer be frozen, and the velocities of the elements would not be constant in time. A possible scenario is that the system is locked into a periodic attractor. This terminology does not refer to the periodicity of the elements themselves, but to a periodic change in the configuration, that is, the phase-distances d_{ij} between the pairs of elements. In fact, the dynamics of the attractor in the absence of a stationary synchronized state could also be quasiperiodic, or even chaotic. In such cases, it is still useful to consider the time-averaged value of the order parameter as a measurement of overall coherence in the system.

In Fig. 3.1 we plot the long-term time averaged magnitude of the global order parameter, defined as

$$\begin{aligned} W &= \int_{T}^{T+\Delta T} |Z(t)| dt \\ &= \langle |Z(t)| \rangle \ , \end{aligned} \tag{3.5}$$

where T and ΔT are both as large as possible.

As can be seen in Fig. 3.1, a transition to an incoherent stationary dynamics takes place at a certain value of α, which becomes smaller as the connectivity of the network is decreased. This transition, however, becomes less abrupt for smaller connectivity values, allowing for intermediate states in which the system remains in a partially coherent state with non-vanishing $|Z| < 1$. As we shall see, the smoothness of this transition for connectivity values $\rho < 1$ is due to the appearance of dynamic states.

3.2 Local signals vs global signals

The introduction of network interactions means that each element is no longer coupled to a global field. Instead, each element interacts with the elements with which it is connected in the network. This means that it will still be effectively coupled to a field that is local to its position in the network.

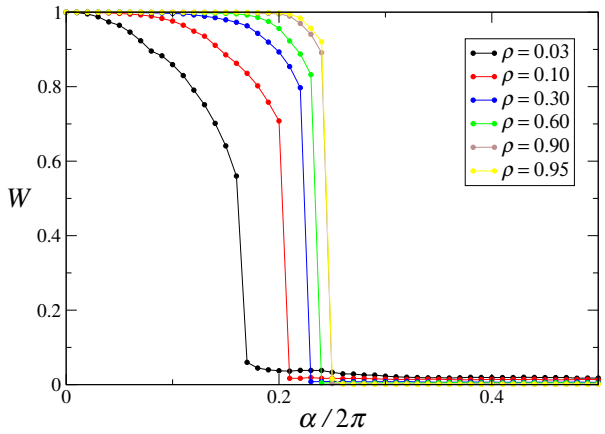

Figure 3.1: Average magnitude of the global order parameter as a function of the phase shift value α for different values of the network connectivity ρ. $N = 200$.

In addition to the global order parameter Z defined in Eq. (1.36), it is convenient to introduce the following *local* order parameters

$$z_i = \frac{1}{N}\sum_{j=1}^{N} T_{ij} e^{i\phi_j} \,, \tag{3.6}$$

which measure the coherence of the signal received by each element through its incoming connections [62]. With these quantities, the Eqs. (3.1) may be expressed in a complex form similar to 2.5 as

$$\dot{\phi}_i = \frac{1}{2i}\left(z_i e^{i\alpha} e^{-i\phi_i} - c.c.\right) \,, \tag{3.7}$$

where it is clear that each element is coupled to its own individual field, generated by its neighbors in the network. In the limit of $\rho = 1$, all local signals z_i reduce to the global signal Z, and Eqs. (3.7) reduce to 2.5.

If we calculate the mean value of the local signals over all elements we get

$$\begin{aligned} \langle z_i \rangle &\equiv \frac{1}{N^2}\sum_{j=1}^{N}\sum_{i=1}^{N} T_{ij} e^{i\phi_i} \\ &= \frac{1}{N}\sum_{j=1}^{N} \frac{k_j^{out}}{N} e^{i\phi_j} \,, \end{aligned} \tag{3.8}$$

where k_j^{out} is the outdegree of the j-th node. The mean value of the local signal has the same form of the global signal, in which each element is weighted by its number of outgoing connections. With this in mind we may define a set of auxiliary quantities

$$\begin{aligned} \tilde{z}_i &\equiv Z - z_i \\ &= \frac{1}{N}\sum_{j=1}^{N}(1 - T_{ij}) e^{i\phi_j} \,. \end{aligned} \tag{3.9}$$

The matrix whose elements are $(1-T_{ij})$ has the interesting property of being the adjacency matrix of a network consisting of the matrix elements that are "missing" in T. Using these quantities we can write the evolution Eqs. (3.7) in yet another form as

$$\dot{\phi}_i = \frac{1}{2i}\left(Ze^{i\alpha}e^{-i\phi_i} - c.c.\right) - \frac{1}{2i}\left(\tilde{z}_i e^{i\alpha}e^{-i\phi_i} - c.c.\right) . \tag{3.10}$$

The first term coincides with the globally coupled system studied in the previous chapter. The second term corresponds to a coupling with a local field that takes into account the edges that need to be removed from the globally coupled case to obtain the network represented by T. In the case of high connectivity, that is $\rho \lesssim 1$, we can understand Eq. 3.10 to express the dynamics of the system explicitly as a perturbation of the globally coupled case, where the interaction between a few pairs of elements has been "knocked out". Just as we did with z_i, we may calculate the mean value of $\tilde{z}_i$ as

$$\begin{aligned} \langle \tilde{z}_i \rangle &\equiv \frac{1}{N^2}\sum_{j=1}^{N}\sum_{i=1}^{N}(1-T_{ij})e^{i\phi_i} \\ &= \frac{1}{N}\sum_{j=1}^{N}\left(1-\frac{k_j^o}{N}\right)e^{i\phi_j} . \end{aligned} \tag{3.11}$$

The average value of the local signals $\langle \tilde{z}_i \rangle$ are of order $(1-\rho)$. We therefore can interpret Eq. 3.10 to represent a system of the form

$$\text{NETWORK} = \text{GLOBAL COUPLING} - (1-\rho) \times \text{MISSING LINKS} . \tag{3.12}$$

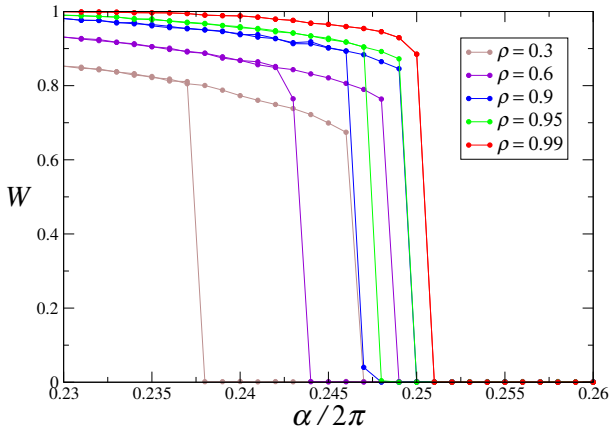

Figure 3.2: Hysteresis plot for the average magnitude of the global order parameter as α is both decreased and increased around the transition.

The presence of a perturbation term in the globally coupled equations will affect the transition between the attractors that would otherwise be present. Such a term

may act by breaking the degeneracy in the system, and thus the destabilization of the attractors would take place through different mechanisms. In this case, we may expect that a transition region will be present between the synchronous and the incoherence attractor, in which the sharpness of the transition may be smoothed out, and hysteresis may occur.

In Fig. 3.2 we show the time-averaged magnitude of the global order parameter Z in the transition region for different values of the network connectivity ρ, both when α is increased and decreased. As can be appreciated, there is a hysteresis region which grows wider as the connectivity of the network is reduced.

As was done for the global order parameter in Eq. (3.5), we can define a long-term average local signal for each node as

$$w_i = \int_T^{T+\Delta T} |z_i(t)| dt \,, \tag{3.13}$$

where T and ΔT are both as large as possible.

An important aspect of the desynchronization transition in system (2.5) as outlined in the previous chapter is that, since the global field acting on all elements is zero for values of $\alpha > \pi/2$, interactions between elements essentially vanish. This is not the case in the system (3.7). As can be observed in Fig. 3.3, the mean value of the average local signals, given by

$$w = \frac{1}{N} \sum_{i=1}^{N} w_i \,, \tag{3.14}$$

does not vanish for any value of α when the connectivity $\rho < 1$. Therefore, it is natural to expect that complex dynamics take place in replacement of the desynchronized state when a network is introduced. Indeed, that the desynchronized state in the globally coupled system is neutrally stable is due to the high degeneracy. Introducing network interactions breaks this degeneracy (as also could, for example, heterogeneities in the natural frequencies of oscillators), and dynamic states appear.

3.3 Lyapunov exponents

Since the phase space of the system is N-dimensional, there will be N Lyapunov exponents describing the dynamics of the system within a given attractor. However, it is clear that the dynamics of system (3.1) are invariant if we shift the phases of all elements by a the same value, that is $\phi_i \to \phi_i + const$ for all i. This means that if we compare the dynamics of the system in a given attractor for a given trajectory and a trajectory for which the phases of all elements have been shifted by a common value, then these trajectories will remain at a constant distance, and the Lyapunov exponent associated with this translation will be zero.

This zero Lyapunov exponent will always be present. Since it conveys no information on the properties of the attractor or the dynamics of the system, we will ignore it, and concentrate only on the remaining $N-1$ exponents. Therefore, throughout this work, when we refer to the maximal Lyapunov exponent, we mean the maximum of the $N-1$ Lypaunov exponents that do not correspond to rigid

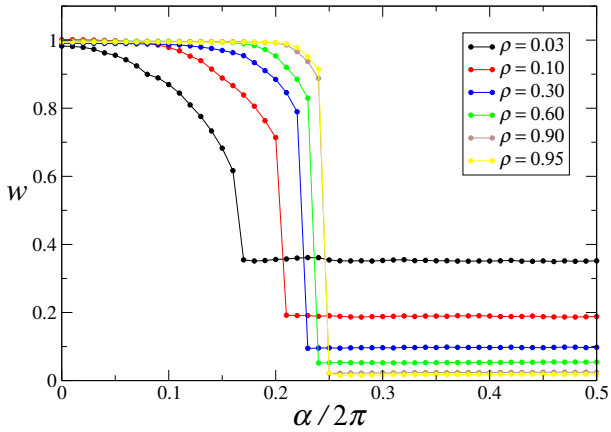

Figure 3.3: Mean value of the local signals, average over all elements, as a function of the phase shift for different values of the network connectivity ρ. $N = 200$.

translations. For all practical purposes, this amounts to discarding the first zero exponent.

The transition leading to the destabilization of the synchronous state can be visualized by tracking the value of the maximal Lyapunov exponent (MLE). In Fig. 3.4 this exponent is plotted as a function of the phase shift for different values of the network connectivity ρ. This plot is obtained by varying α in increasing direction. However, as shown in Fig. 3.2, hysteresis is only present in very narrow intervals, and the behavior would not be significantly different if α were varied in the opposite direction.

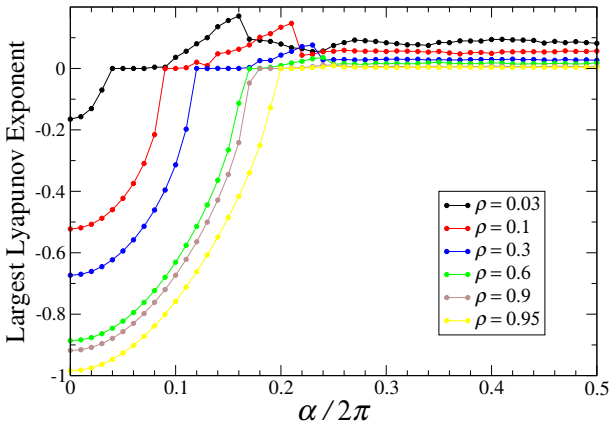

Figure 3.4: Maximum Lyapunov exponent as a function of the phase shift value for different values of the network connectivity ρ. The curves are obtained by increasing α from 0 to π. $N = 200$.

Although changing the connectivity of the network produces different results, all the curves have a common behavior. The maximal Lyapunov exponent is negative for small values of α, which could have been expected from the fact that $\alpha = 0$ only

has a synchronous attractor [42]. In the vicinity, the maximal Lyapunov exponent increases steadily, reaching zero for a certain critical value $\alpha = \alpha_c$, which decreases as the connectivity is diminished. In this range, the negative maximal Lyapunov exponent indicates the convergence of the system towards a stable stationary state. Above the critical point, a plateau follows where the maximal Lyapunov exponent remains equal to zero, and soon grows positive as α is further increased.

The MLE remains positive for all further values of α, reaching a maximum at $\alpha = \alpha_{max}$. This maximum moves to the left as the connectivity is decreased, and the height of the peak increases. As α is further increased, the maximum Lyapunov exponent settles around an approximately steady value, which is also higher for lower connectivity values.

All other Lyapunov exponents λ_j can be computed for each attractor. In the following we do this for different values of ρ at $\alpha = \pi$. To obtain smoother curves, for a single value of $\alpha = \pi$ we perform this calculation for a system of $N = 1000$ elements. This is shown in Fig. 3.5, where histograms of all $N = 1000$ Lyapunov exponents are shown for different values of ρ. All exponents are zero for $\rho = 1$, and a single peak is registered (out of visualization scale in the plot). As the connectivity is lowered, the exponents spread apart in a bell-shaped distribution, and the mean value moves to the left. However, a significant portion of the exponents remain to the right of 0. In fact, this portion is approximately the same for all curves (except, of course, $\rho = 1$).

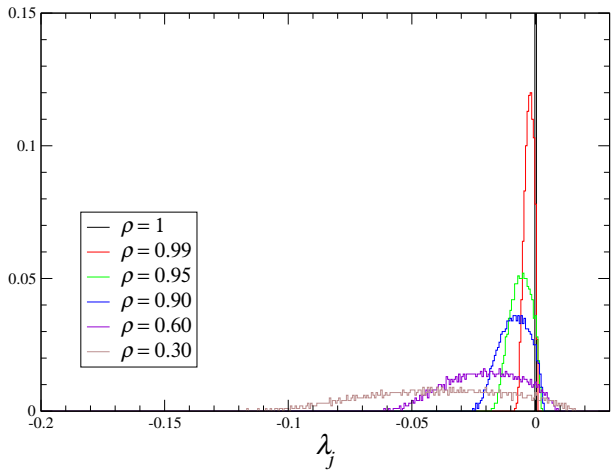

Figure 3.5: Distributions of all Lyapunov exponents for different values of the network connectivity for $\alpha = \pi$. The curve for $\rho = 1$ is a single peak at zero with height 1, and has been cut for illustrative purposes. $N = 1000$.

In fact, if we look at the curves of the values of the exponents in decreasing order, as shown in Fig. 3.6 for the different values of the network connectivity, we see that the shape of the curves is conserved. Furthermore, they cross the zero-axis at almost exactly the same point. This suggests that there is a certain scale invariance between all curves.

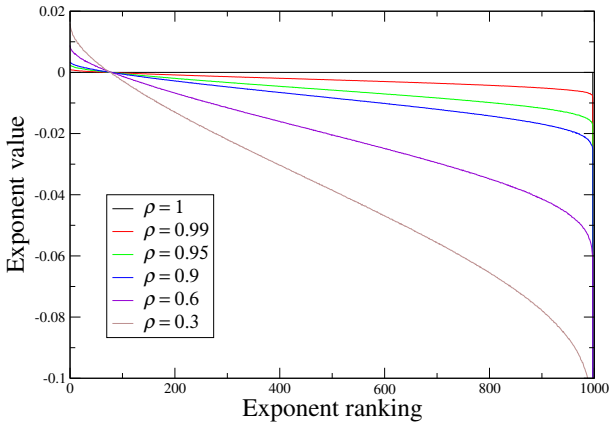

Figure 3.6: Curves for the values of the ordered Lyapunov exponents for $\alpha = \pi$. All exponents are set in decreasing order so that their value is plotted against their rank. $N = 1000$.

Keeping in mind the idea expressed in (3.12), it seems natural to assume that the scaling between curves will be proportional to a function of $1 - \rho$. In Fig. 3.7 the distributions have been scaled by

$$\lambda_i' = \frac{\lambda_i}{\sqrt{1-\rho}}\,. \tag{3.15}$$

In this figure it can be seen that the distribution of the scaled exponents for higher values of the connectivity are very similar, indicating that the scaling of the dynamics may indeed follow this law, at least approximately. As the connectivity is further reduced ($\rho \leq 0.6$ in Fig. 3.7), this scaling breaks down and the distributions become wider.

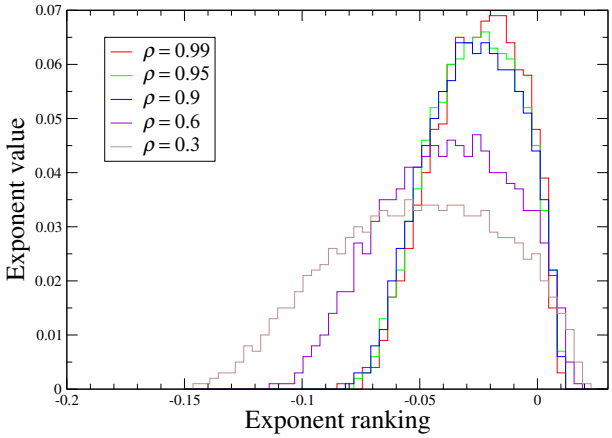

Figure 3.7: Distributions of all the Lyapunov exponents after rescaling as indicated by Eq. (3.15). $\alpha = \pi$, $N = 1000$.

3.4 Kaplan-Yorke dimension

Another interesting quantity to calculate is the Kaplan-Yorke dimension. In Fig. 3.8 we see this dimension as a function of α for different connectivity values. The dependence of this dimension is non-monotonous, typically having a maximum for an intermediate value of α along the transition. This value coincides with α_{max} at which a maximum is found for the MLE. The maximum dimension reached decreases as the connectivity is decreased, while the location of this maximum moves towards the left. For values close to unity, the maximum value of the Kaplan-Yorke dimension in this peak can be quite large, comparable to the value of the dimension of the system N, and the location of this peak approaches $\alpha = \pi/2$. As seen in the previous chapter, for the singular case in which $\rho = 1$, an abrupt transition at this point occurs when the dimension jumps to $D_{KY} = N$.

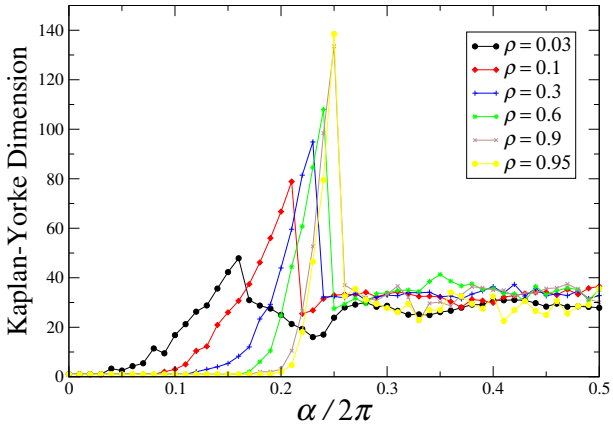

Figure 3.8: Kaplan-Yorke dimension of the attractor as a function of the phase shift value for different network connectivities. $N = 200$.

Beyond this peak there is an abrupt transition to an attractor whose dimension is still quite high, but its value presents no significant changes as the value of α is further increased. Interestingly, the value of the dimension of the attractor in this region of the transition landscape shows no appreciable dependence on the connectivity.

The fact that the dimension of the attractor above a critical value of α does not change when changing α or ρ could have been expected from the curves shown in Fig. 3.6. Nevertheless, it is still remarkable that the dimension of the attractors is approximately independent of the connectivity of the network and the phase shift value (in the range $\alpha > \alpha_{max}$), since they are the only parameters of the system, other than its size. This means that there exists a dynamic regime of high-dimensional chaos in which the dimensionality of the attractor is determined by the size of the system. The characteristics of this attractor are robust to major changes in the functions determining the interactions between elements.

In Fig. 3.9 we show the ratio of the calculated Kaplan-Yorke dimension of the attractor to the size of the system for a value $\alpha = \pi$ as the system size is increased. These values have been found by averaging over five different realizations of the

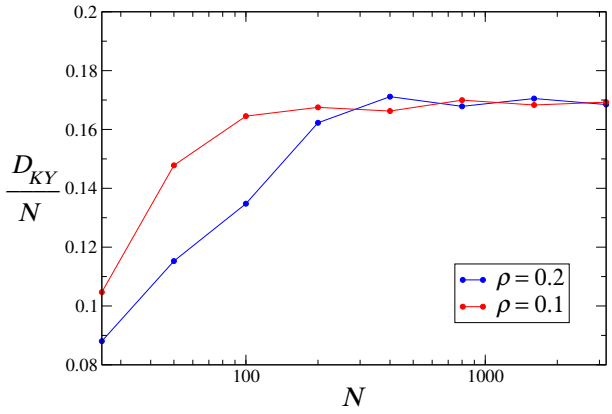

Figure 3.9: Ratio of the Kaplan-York dimension of the attractor at $\alpha = \pi$ to the size of the system, as a function of the size. Each point is the result of an average over 5 realizations of the network (except for $N = 1600$ and $N = 3200$, which are obtained from single realization for each curve).

network for each system size (except for the two largest values, where only one realization is used for each). As can be seen, as the size of the system is increased, an approximately stationary value is reached, meaning that the dimension of the attractor is roughly proportional to the system size. Furthermore, this value seems to not have a strong dependence on the connectivity of the system.

This extensive quality of the chaotic behavior allows us to draw a parallel between the dynamics of the system and the turbulent behavior in spatially distributed oscillator systems. As is known for oscillatory media and reaction-diffusion systems of oscillatory nature, a transition to turbulence can be found as a function of the parameters. The extensive nature of the embedding dimension of the attractor is a well-know property of turbulent systems [92, 93, 94]. In this sense, we can understand that the kind of high-dimensional chaos that our system exhibits is analogous to the phase turbulence observed in oscillatory media. Of course, since our system has no defined spatial extension, the idea of spatio-temporal chaos is not applicable. Instead, the role of distance must be played by the length of a path that connects different elements.

3.5 Velocity-synchronized states

As seen in Fig. 3.4, the maximal Lyapunov exponent is negative for a certain range of values of α at all connectivity values. This implies the existence of an attracting configuration that is frozen in time. Such a state is only possible if the velocities of all elements are equal, and the system may rotate with a fixed velocity.

Such a state exists up to a critical value of alpha, at which the first Lyapunov exponent reaches zero. In Figs. 3.4 and 3.8 we have seen that this critical value becomes smaller as the value of the connectivity is reduced. In Fig. 3.10 we calculate this critical value α_c as a function of the connectivity. The critical value of α grows

with the connectivity ρ, reaching $\pi/2$ when the connectivity is 1, as was found in the previous chapter. In the other extreme, it appears to approach 0 when the connectivity does. Of course, the connectivity cannot be zero for a connected network, and this extrapolation is only meaningful in the limit of infinite system size.

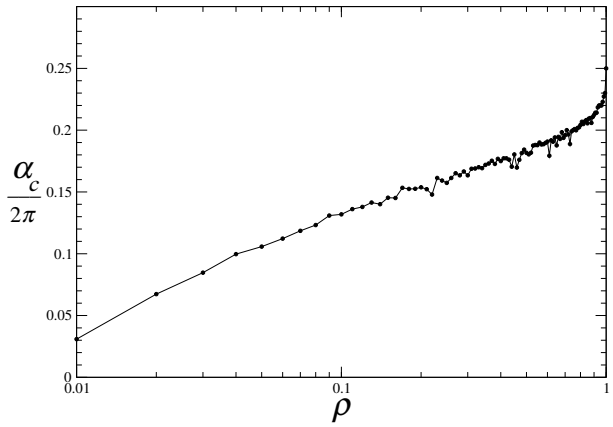

Figure 3.10: Critical value of α for which the velocity-synchronized state ceases to exist, as a function of the connectivity of the network ρ. The ordinate axis is plotted on a logarithmic scale, and each point is averaged over 5 different network realizations.

Below the critical value α_c for each connectivity value, a stable state is attained by the system. This means that a frozen configuration is reached, and that perturbations from this configuration are damped as the system relaxes back to it. The properties of this stable configuration may change as the parameters are changed.

As a way to characterize the distribution of phases in the stable configuration, we measure the average value of the distance d_{ij} defined in (2.24), over all pairs of elements in the long-time limit. Thus parameter $\overline{d}$ is defined as

$$\overline{d} \equiv \lim_{t\to\infty} \langle |d_{ij}(t)| \rangle = \lim_{t\to\infty} \frac{1}{2N(N-1)} \sum_{i=1}^{N} \sum_{j=1}^{N} |d_{ij}(t)| \,. \tag{3.16}$$

This quantity is plotted in Fig. 3.11 as it depends on the value of parameter α in the velocity-synchronized state for different values of the network connectivity. As can be seen, increasing the value of the phase shift causes the distribution of phases to spread. This becomes more accentuated as the connectivity is diminished. Coherence is therefore diminished, and the modulus of Z in the synchronized state decreases, as seen in Fig. 3.3.

In this partially coherent synchronized states all velocities are identical. This means that there is a solution of the form

$$\Omega = \frac{1}{N\rho} \sum_{j=1}^{N} T_{ij} \sin(\phi_j - \phi_i + \alpha) \,, \tag{3.17}$$

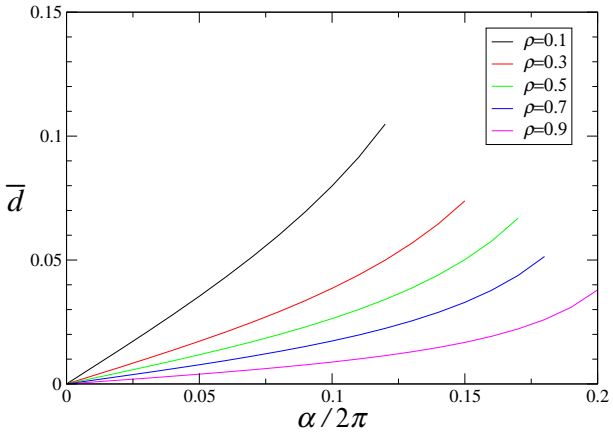

Figure 3.11: Average phase-distance $\overline{d}$ in the velocity-synchronized state for values of $\alpha < \alpha_c$ for different values of the connectivity ρ. $N = 1000$.

where all terms inside the sin function are constant. Ω is therefore approximately the expectation value of $\sin(\phi_j - \phi_i + \alpha)$. If we assume that the stationary distribution of phases in the synchronized state is symmetric and narrow, we get

$$\Omega \approx \langle \sin(\phi_j - \phi_i + \alpha) \rangle \approx \sin \alpha \,, \tag{3.18}$$

In Fig. velocitysynchronizedstates we plot the velocities of the synchronized states as a function of α in the range $\alpha < \alpha_c$. This is shown for different values of the network connectivity, although all curves almost coincide.

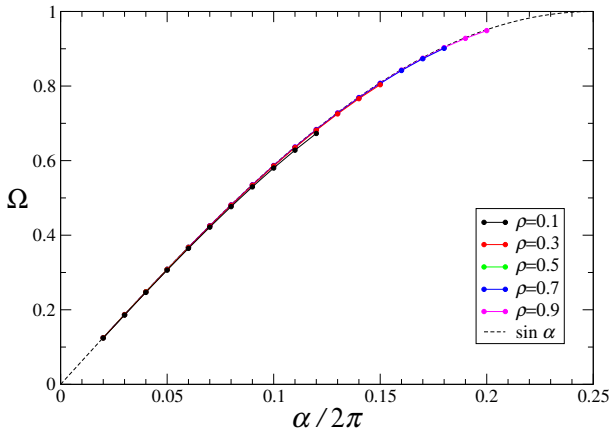

Figure 3.12: Velocity of the synchronized states as a function of α for $\alpha < \alpha_c$. the function $\sin \alpha$ is plotted in dashed lines. $N = 1000$.

3.6 Dynamical states

In the previous chapter, the presence of a number of zero Lyapunov exponents was said to denote the neutral stability of the attractor. This is because the attractor

is a fixed point, where the dynamics are frozen. Thus, perturbations along the zero Lyapunov exponents are not damped, nor do they grow. In the present case, since there is no fixed point solutions to the equation of motion, any possible attractor is necessarily dynamic. Therefore, the fact that the largest Lyapunov exponent reaches zero at $\alpha = \alpha_c$ indicates the presence of a limit cycle.

A limit cycle corresponds to an attractor in which the configuration of the system changes periodically. However, as α is increased beyond α_c, the maximal Lyapunov exponent remains equal to zero, whereas the dimension of the system increases. This implies that several Lyapunov exponents are zero. In such a case, quasi-periodic dynamics take place.

Since all elements are identical, and their interactions are mediated by the same phase shift, all heterogeneity in the system is given by the network interactions. In this sense, the dynamics of each element is entirely determined by the network architecture. Furthermore, since each element can only be affected by the elements with which it is connected, the aspects of the network that decide the dynamics of each elements are mostly local. Of course, an element i connected to element j will affect its dynamics, and if j is connected to k, a certain degree of transitivity between i and k is in principle present. However, since the connectivity between different pairs of nodes is uncorrelated, these sort of "long range" interactions seem to be too weak in this system to be relevant.

3.6.1 Very low connectivity

We examine the particular case of the dynamics for $\alpha_c < \alpha < \alpha_{max}$ for very low connectivity values. In Fig. 3.13, the long term average velocities ν_i of all elements are plotted against their in-degree in the network, i.e., how many incoming connections they have, for the case of $\rho = 0.007$ and $\alpha = 0.07\pi$. It is remarkable that all elements with more than one incoming connection have the same velocity, whereas all elements with one single incoming connection (there is 7 of them for in this network) rotate with a different velocity. It is clear then that the dynamical properties of these elements with one connection are entirely determined by this defining topological feature.

This is not very surprising when one takes a look at the evolution of Eqs. (3.1). Elements with only one incoming connection will have only one term in their equations of motion. For values of α before the destabilization of the velocity- synchronized state, that is $\alpha \lesssim \alpha_c$, a stationary state with $\phi_i = \Omega$ exists for all i. This value of Ω is determined by all elements and all interactions between them, and is therefore a global property. Nevertheless, as the value of α is increased towards the critical value α_c and Ω grows beyond a given value[1], those elements for which their evolution equation has only one term will not be able to reach this velocity. These elements will therefore fall out of synchrony, and begin to orbit with a given velocity. Furthermore, this will happen simultaneously for all elements with one

[1]The critical velocity should be approximately of order $(\rho N)^{-1}$ for very low connectivities. This is due to the presence of elements with only one incoming connection, so that the approximations in (3.18) are not valid.

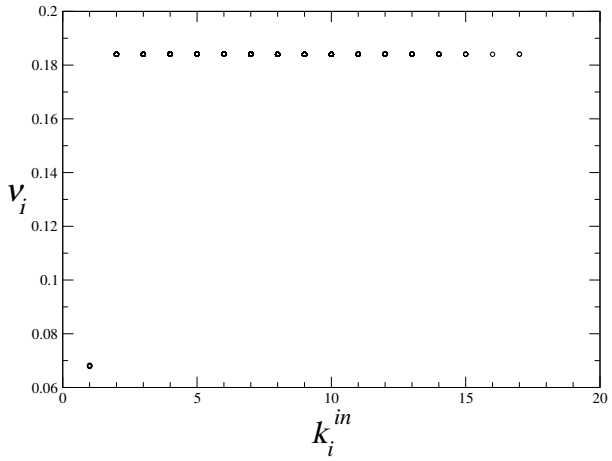

Figure 3.13: Long-term average velocities of each element as a function of its number of incoming connections. $\alpha = 0.07\pi$, $\rho = 0.007$, $N = 1000$.

incoming connection, and their velocities will therefore be approximately the same. This means that all the elements with one incoming connection become disengaged or disentrained from the rest of the system simultaneously, and form a dynamical block by themselves.

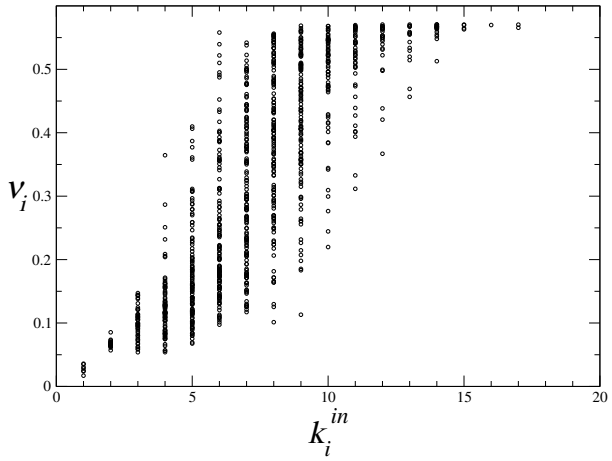

Figure 3.14: Long-term average velocities of each element as a function of its number of incoming connections. $\alpha = 0.33\pi$, $\rho = 0.007$, $N = 1000$.

In Fig. 3.14 we make a similar plot for the same network as in Fig. 3.13, this time for a value of $\alpha = 0.33\pi$, slightly smaller than α_{max} for this value of the connectivity. The spread in velocities is much larger here, and essentially all elements are disentrained. Nevertheless, a clear correlation between velocity and degree can be seen in this figure, where elements with more incoming connections have a larger velocity. This reinforces the results observed in Fig. 3.13 near the

destabilization of the synchronized state.

In stark contrast, the situation is very different when $\alpha > \alpha_{max}$. A plot of the velocities off all elements as a function of their degree is shown in Fig. 3.15 for a value of $\alpha = 0.34\pi$. In this case, all correlation between the velocity and the degree is lost, and the long-term average velocities are distributed in a seemingly random manner around zero.

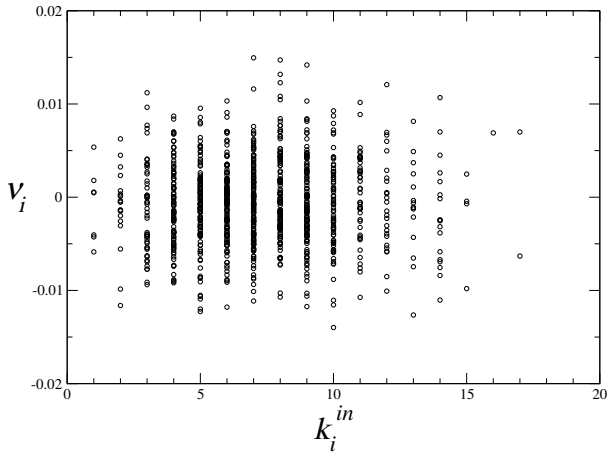

Figure 3.15: Long-term average velocities of each element as a function of its number of incoming connections. $\alpha = 0.34\pi$, $\rho = 0.007$, $N = 1000$.

3.7 Heterogeneous phase shifts

So far we have analyzed the case in which all interactions between connected pairs of elements are equal, specifically, they have the same associated phase shift. In many systems of interest, the interactions do not show this homogeneity. In particular, for cases where the interaction is restricted by a given spacial distribution of the elements, or affected by a given distance, the interactions may have a given transmission delay, which may be very different between different pairs of elements, not only because of their distance, but also due to the transmission mechanisms.

In many systems, e.g., in a factory, the pattern of interactions between elements may be unalterable without breaking down the functioning of the entire system. In such a case, the structure of the interaction network may be a fixed condition of the system. However, the transmission delays and transport velocities may still be something that can be adjusted to affect and still sustain operation.

In our model, such a delay would be represented by a specific phase shift in the interaction between two elements. In this section, in an attempt to make the model more general, we consider the case in which each connection in the network has its own associated phase shift. In order to avoid making unnecessary assumptions and minimize the number of free parameters, we choose to determine these phase shifts randomly and with no correlation to the network structure.

The evolution equations are thus transformed to

$$\dot{\phi}_i = \frac{1}{N\rho} \sum_{j=1}^{N} T_{ij} \sin(\phi_j - \phi_i + A_{ij}) \,, \tag{3.19}$$

where $A_{ij} = \alpha + a_{ij} \times \delta$. The individual elements of the matrix a_{ij} are randomly drawn from a uniform distribution in the range $[0, 1]$. The case of $\delta = 0$ reduces to the Eq. (3.1), whereas the case $\alpha = 0$ represents a system where all the phase shifts are randomly chosen, and control parameter δ determines their magnitudes.

Interestingly enough, the main characteristics of the transition landscape of the system do not change significantly by replacing the uniform phase shift with randomly chosen ones. In Fig. 3.16, we show the mean, maximum and minimum of the long-term average velocities ν_i as a function of the magnitude of the phase shifts. The case of homogeneous phase shifts is compared to the case of $\alpha = 0$ with varying δ, in both cases for the same network. The curves are quite similar if we compare the parameters α and $\langle a_{ij} \rangle \times \delta$. It seems therefore that the important quantity to determine the global dynamics of the system for a given network is the mean value of the phase shifts involved.

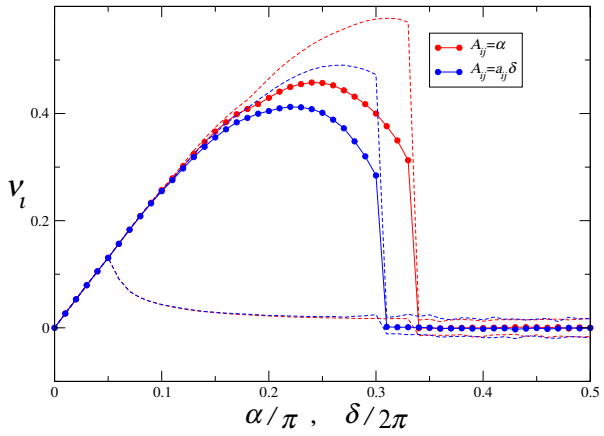

Figure 3.16: Comparison of the dynamics for heterogeneous and homogenous phase shifts. We can see that the mean value of the phase shifts is the relevant quantity.

The fact that each connection has a different associated phase shift generally implies that the equilibrium configuration of the synchronous state is different to that in the case of a homogeneous phase shift for the same network. It would therefore be natural to assume that the destabilization of this configuration occurs differently as well. However, this heterogeneity seems not to affect the general correlations between the local network properties of an element and its dynamics. In Fig. 3.17 we show the velocities ν_i of all elements as a function of their degree in the network for phase shifts such that α and $\langle a_{ij} \rangle \times \delta$ are approximately of the same value in respective plots. Here we can see that the distribution of velocities in terms of the local degree of incoming connections seems to be preserved when introducing heterogeneity in the phase shifts. The velocity values in both situations depicted in

Fig. comparisondeltaalpha are also of the same order. Equivalent behavior has also been found for other values of α and δ.

3.8 Final comments

In this chapter we have studied a model for oscillators in a network, and the different dynamics that develop as the value of a phase shift in the interactions is varied. This model emerges naturally when extending the model in the previous chapter to the network case. This modification to the model seems to break the degeneracy of the globally coupled case, thereby replacing the stationary incoherent states with regimes of persistent dynamics.

The transition between the fully synchronized states and the incoherent state occurs less abruptly with the appearance of intermediate, partially coherent stationary state. The phase-synchronized state is replaced by a velocity-synchronized state in which the phases of the elements are distributed in a range that becomes larger as the value of the phase shift is increased and the connectivity decreased.

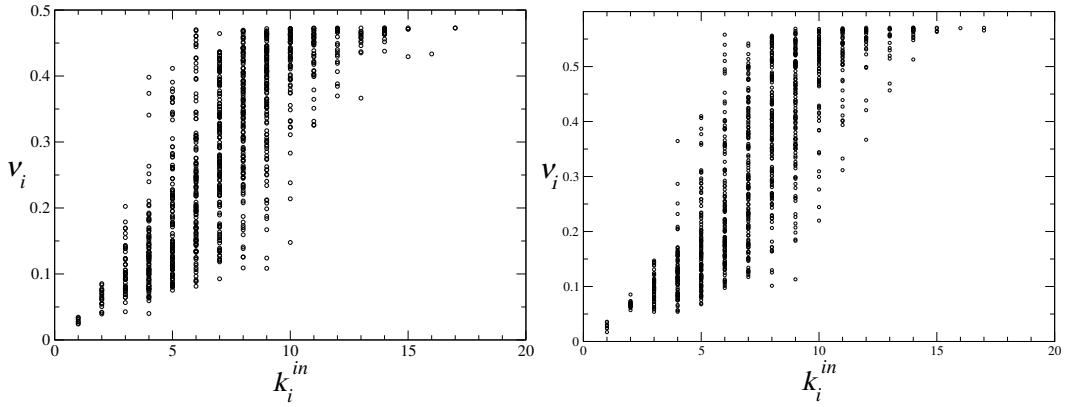

Figure 3.17: Long-term average velocities of each element as a function of its number of incoming connections for (left) $\alpha = 0$, $\delta = 0.65\pi$; and (right) $\alpha = 0.33\pi$, $\delta = 0$. $\rho = 0.007$, $N = 1000$.

Large values of the phase shift lead to chaotic dynamics in which the embedding dimension of the attractor is very large. An important property of the considered model is that individual elements are not chaotic. Instead, chaos emerges as a result of the coupling between them. The dynamics of individual elements is extremely simple, and it is the pattern of interactions that induces complex dynamics. However, a chaotic regime is present in which the embedding dimension becomes approximately independent of the specific properties of the pattern of interactions.

The presence of network interactions can be effectively considered as a structural perturbation to the limiting case of globally coupled elements. In these terms, the perturbation is the elimination of individual interactions between certain pairs of elements from the globally coupled case. This allows us to find approximate scaling laws for the dynamics in terms of the connectivity of the network. In the particular case of the high-dimensional chaotic attractor, these perturbations seem

to only affect the temporal scales of the dynamics, whereas qualitative aspects of the attractors remain unchanged. The embedding dimension of the high-dimensional chaotic attractor seems to be independent of these perturbations.

The fact that this dimension does not depend on the parameters of the system indicates that an extensive kind of high-dimensional chaos is present, in which the dimension is a function of the size of the system. In our system we have measured that this dependence is approximately linear when the size is large enough.

Because of these reasons, an analogy can be made to the turbulent regime observed in oscillatory reaction-diffusion systems, where the phase value in all points of the system behaves chaotically in space and time. It is a well known fact that the embedding dimension of the attractor in turbulent chemical systems (as well as hydrodynamic) scales proportionally to the size of the system. This can be proven for simple systems and has been corroborated by numerical computations [94, 95].

While our investigations have been performed for a particular model, we conjecture that the results should be general, and similar behavior will be found in other network-organized systems of various origins. Indeed, it can be shown that the considered model is closely related to the generic phase network model obtained by phase reduction of amplitude oscillator dynamics on networks in the vicinity of the supercritical Hopf bifurcation. The instability leading to the network turbulence in the model is the analog of the Benjamin-Feir instability of uniform oscillations in the complex Ginzburg-Landau equation.

Chapter 4

Global feedback control

In the previous chapter we have studied a system of oscillators interacting through a network where interactions are mediated by phase shifts. In this system, we have found that high dimensional chaos can develop when the phase shift values are large enough.

At the beginning of the previous chapter, we made a comparison between a network of interacting oscillators and extended oscillatory systems. Indeed, models for oscillatory media are usually built upon the premise that a continuous system of oscillatory nature can be described as a lattice of single oscillatory elements with neighbor-to-neighbor coupling. In light of this, the use of a network as a pattern of interactions could be regarded as a generalization of systems embedded in Euclidean space to more complex topologies.

A lot of progress has been made in the last decades in the direction of control of turbulence in oscillatory media. Particularly interesting results have been found for the use of a global feedback control as a method to suppress turbulence, as discussed in Sec. 1.6.2. Global feedback is a convenient kind of control, given that it is very simple, it has few parameters and can be easily implemented in experimental setups. But the most appealing aspect of it is that the control signal is generated by the system itself. In this manner, the dynamics can self-organize and adapt without any need of supervision or interference.

Such a mechanism is easily capable of restoring uniform oscillations in an otherwise turbulent system. However, the most interesting aspect of global feedback as a method to control turbulence is that not only uniform oscillations can be restored, but also a rich variety of complex patterns and coherent structures can be found when exploring the parameter space. By manipulating a very small number of parameters (intensity, time delay or a phase shift in the application of the feedback) a great variety of self-organized structures can be induced, such as standing waves, spirals, phase clusters, intermittent turbulence, target patterns, etc.

The formation of patterns in the transition between order and chaos is not a property exclusive to chemical systems. Many prominent scientists have advocated that the emergence of dynamical order in the form of coherent complex structures may be a general phenomenon at the edge of chaos. In this context, the use of a global feedback is a very convenient way to tune the system to this region and keep it there.

In this chapter we will consider the effects of a global feedback as a mechanism to control the network turbulence observed in the previous chapter. In analogy to extended oscillatory systems, we want to find whether a similar transition between turbulence and synchronization can be observed in network systems. And if so, what would be the network analogous of the coherent structures observed in the spatially extended counterparts?

The focus of this chapter will be set on the dynamic properties of the system at different stages of the transition and their relationship to structural properties of the network. For this, we will consider a single realization of the interaction network and its associated phase shifts, and concentrate on what kind of dynamics we can observe in the system when we introduce a global feedback. As such, the character of this chapter will be exploratory rather than explanatory, and it should not be taken as an exhaustive study of the possible kinds of behavior of networks synchronization and chaos.

4.1 Global feedback control

We have seen that system (3.19) may exhibit high dimensional chaos under very general conditions for matrices T and A. However, we are interested in seeing how chaos can be suppressed or controlled, and what complex dynamics we may encounter in the process. For this reason, we will from here on consider only a single realization of T and A which will remain fixed for the rest of this chapter. The values of ρ and δ will therefore also remain fixed at $\rho = 0.006$ and $\delta = 0.8\pi$, and α will be assumed zero throughout. tThe number of elements will be fixed at $N = 1000$.

$\rho = 0.006$ is one of the lowest connectivity values that one can set for a network of the Erdös-Rényi type with 1000 nodes and still have it be strongly connected.[1] We thus choose a network T that satisfies this condition, and determine that a magnitude $\delta = 0.8\pi$ for the spread in the values of the phase shifts is sufficient to observe turbulent behavior as discussed in Sec. 3.4. For these values, the dynamics is chaotic and the attractor has a Kaplan-Yorke dimension of $D \approx 137$.

We introduce now a global feedback term that will act on all elements, in addition to the interactions that take place through the network. We may reinterpret the global order parameter Z to be a global signal, conformed by the addition of the signals from all individual elements. As such, this signal may be applied back to the system with a regulated intensity as external forcing.

[1] See Sec. 1.4.1.

The equations of motions are then written in the form

$$\dot{\phi}_i = \frac{1}{\rho N} \sum_{j=1, j\neq i}^{N} T_{ij} \sin(\phi_j - \phi_i + a_{ij} \times \delta) \; + \; \frac{\mu}{2i}(Ze^{-i\phi_i} - \text{c. c.}) \,, \qquad (4.1)$$

where μ is the parameter that specifies feedback intensity. For the remains of this chapter, μ will be the only parameter to be manipulated, except when explicitly stated.

By construction, the system exhibits high-dimensional chaos at $\mu = 0$. On the other hand, the second term coincides with the global coupling term as studied in Chapter 2 ($\alpha = 0$). If this were the only present interaction, it would bring the system to synchronization. Therefore, we also expect this for system (4.1) for large values of μ. It is thus clear that global feedback is an effective way to restore uniform oscillations in a disordered system as 3.19.

4.2 Lyapunov exponents and Kaplan-Yorke dimension

In this chapter we will concern ourselves with the transition scenario between these two extreme cases. As we have done in the previous chapter, we use the Lyapunov exponents to describe the dynamics of the system in a concise way. As such, we will study the dependence of these exponents, and in particular the largest of them, as they change in function of our control parameter μ. As in the previous chapter, we will ignore the first zero Lyapunov exponent (which corresponds to uniform shifts in all phases) and consider only the remaining $N - 1$ Lyapunov exponents.

We also consider the Kaplan-Yorke dimension as a way to characterize the properties of the attractor as it changes with the control parameter. In Figs. 4.1 and 4.2 we plot the dependence of the maximal Lyapunov exponent and the Kaplan-Yorke dimension on the the global feedback intensity μ

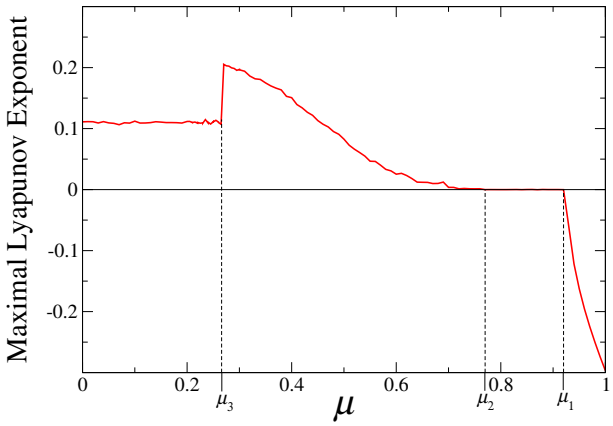

Figure 4.1: Dependence of the maximal Lyapunov exponent on the control parameter μ. $\delta = 0.8\pi$, $N = 1000$.

In these figures we can see that the transition from synchronization to chaos can be divided in different stages. For large values of the global feedback intensity

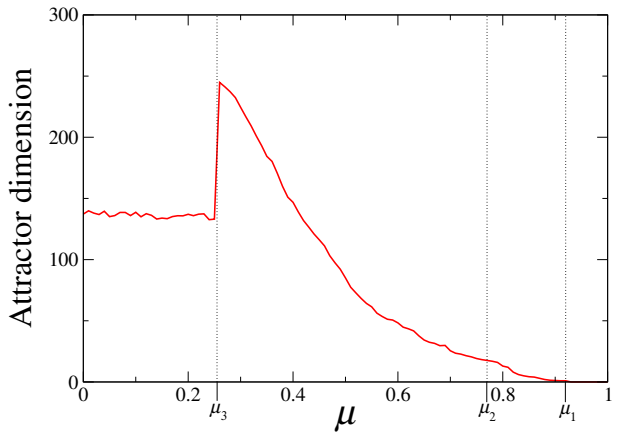

Figure 4.2: Dependence of the Kaplan-Yorke embedding dimension on the control parameter μ. $\delta = 0.8\pi$, $N = 1000$.

(and for all values outside of these figures), the maximal Lyapunov exponent is negative, signaling that the system goes to a stable attractor in which the phase distances between all pairs of elements remain constant. Such a state is identified as synchronous, in that all elements are entrained in global rotations with a constant frequency. Correspondingly, the dimension of the attractor is zero[2]. When we decrease the intensity of the global feedback, the synchronous state becomes unstable at a value $\mu_1 \approx 0.92$, when the maximal Lyapunov exponent reaches zero.

Below this value there is a plateau, and the maximal Lyapunov exponent remains constant and equal to zero for a certain range of values. This indicates that the stable synchronous attractor has been replaced by a periodic or quasi-periodic attractor. However, the dimension of the attractor begins to grow in this range already, indicating that a number of Lyapunov exponents that were negative for higher values of μ become zero in this range. Indeed, from the definition of the Kaplan-Yorke dimension (1.18), it follows that if the k highest Lyapunov exponents are zero, then the dimension is equal to k. As we shall see later, this takes place through a sequence of saddle-node bifurcations, associated with an increasing number of elements incurring in phase-slips, or fast excursions in the phase space between almost synchronous configurations.

When reaching a value $\mu_2 \approx 0.77$ the largest exponent becomes positive, marking the onset of chaos. Decreasing the value of μ further increases the magnitude of the largest exponent and the Kaplan-Yorke dimension. This increase is monotonous in the range $0.27 < \mu < 0.77$, and in the lowest extreme the dimension may reach values as high as $D = 244.8$, significantly higher than that in absence of the global feedback.

In the last stage of this transition, there is an abrupt change in the attractor, and both the largest exponent and the Kaplan-Yorke dimension drop to the values

[2]This is a result of ignoring the first zero Lyapunov exponent. Any configuration is equivalent to that obtained by any homogeneous displacement of all phases, and therefore any state defines a straight line of equivalent configurations in the phase space.

expected in the absence of feedback for the turbulent regime, as seen in Sec. 3.4. Remarkably, this occurs for a non-zero critical value of the global feedback intensity, and further changes in the value of μ seem to have no effect in this macroscopic variables. This suggests that this sudden drop is associated with a breakdown of the global feedback as a control mechanism.

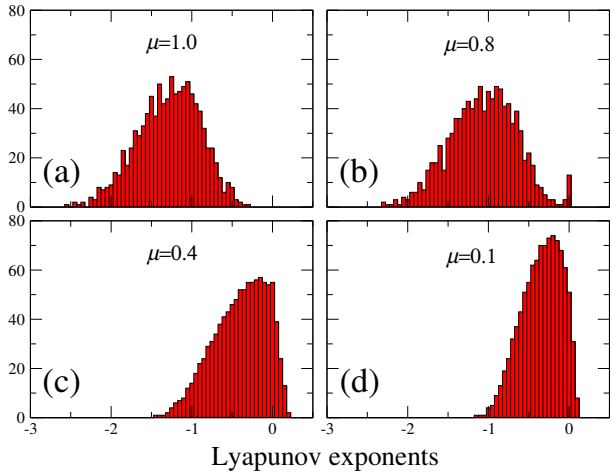

Figure 4.3: Histograms of Lyapunov exponents for different values of the control parameter μ. $\delta = 0.8\pi$, $N = 1000$.

Additionally, four histograms of the distributions of all $N-1$ Lyapunov exponents are shown in Fig. 4.3 for different values of μ. For large values of the global feedback intensity ($\mu > \mu_1$) the distribution of Lyapunov exponents is approximately symmetric. At $\mu = 1.0$ it is roughly centered at -1.3 (Fig. 4.3a). In the region $\mu_2 < \mu < \mu_1$ we can see the presence of degenerate zero Lyapunov exponents, as demonstrated in panel 4.3b for $\mu = 0.8$, where a small but clear peak is present at 0. As we move into the chaotic region, the distribution of exponents moves towards the right and, as seen in Fig. 4.3c, a large number of Lyapunov exponents are then positive (approximately 10% of them). The distribution also becomes clearly asymmetric. In the final stage, for values below μ_3 (panel 4.3d) the distribution of Lyapunov exponents becomes more narrow, and the fraction of positive exponents is reduced to approximately 6%.

This last type of distribution corresponds to the ones showed in Fig. 3.5. Although in this figure, the proportion of positive Lyapunov exponents is slightly bigger (arround 7.5%), it can be noted that this proportion is diminished as the connectivity of the network is reduced. In our present case, the connectivity is orders of magnitude smaller than the smallest value in Fig. 3.5, and therefore, this discrepancy is accounted for. Nevertheless, it is remarkable that for such disparate connectivity values and regardless of a finite global feedback intensity, this proportion is maintained to a large degree.

The results displayed in these figures indicate that there are several interesting aspects of the transition from synchronization to chaos. Below we study this transition using different statistical tools to better describe and understand the complex

behavior observed in networks at the edge of chaos.

4.3 Velocity distributions and dynamical regimes

The action of the global feedback on the system is to drive it towards synchronization. Indeed, as we have seen in chapter 2, if only this type of global coupling were present, the system would undergo complete phase synchronization with $|Z| = 1$ and constant velocity (and equal to zero in the present case). This would happen with no threshold on the feedback strength.

When network interactions are present, the completely synchronized state is only possible in the limit of infinite μ, due to the presence of phase shifts that introduce a level of frustration in the system [27, 28]. Instead, for large but finite values of the global feedback intensity, a dynamical state can be reached in which all elements are entrained in global oscillations with the same non-zero velocity. This means that $\dot{\phi}_i = \Omega = const$ for all i, but phases are distributed in a certain region of the circle. If this state is stable, then perturbations from it are damped. Thus, it will be characterized by negative maximal Lyapunov exponents. As follows from Fig. 4.1 and 4.3a, frequency synchronization takes place if global feedback is strong enough, i.e. if $\mu > \mu_1$.

If this state is not stable, then the velocities of all or some elements will not satisfy $\dot{\phi}_i = const$, meaning that dynamic activity will persist in the system indefinitely. We thus monitor the behavior of the long-term average velocities ν_i of each element, defined as

$$\nu_i = \frac{1}{\Delta T} \int_T^{T+\Delta T} \dot{\phi}_i(t) dt = \frac{1}{\Delta T} \left[\phi_i(T + \Delta T) - \phi_i(T) \right] , \tag{4.2}$$

where T and the integration interval ΔT are as large as possible.

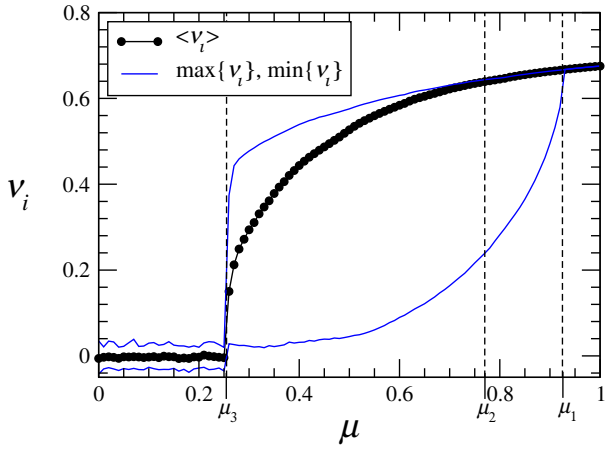

Figure 4.4: Mean time-averaged velocity of the network (dots) as function of the feedback intensity μ. Thin lines show the maximum and minimum velocity values. $\delta = 0.8\pi$, $N = 1000$.

In Fig. 4.4 we have computed the long-term average velocities ν_i of all elements, and plotted the mean, the maximum and the minimum as functions of the global

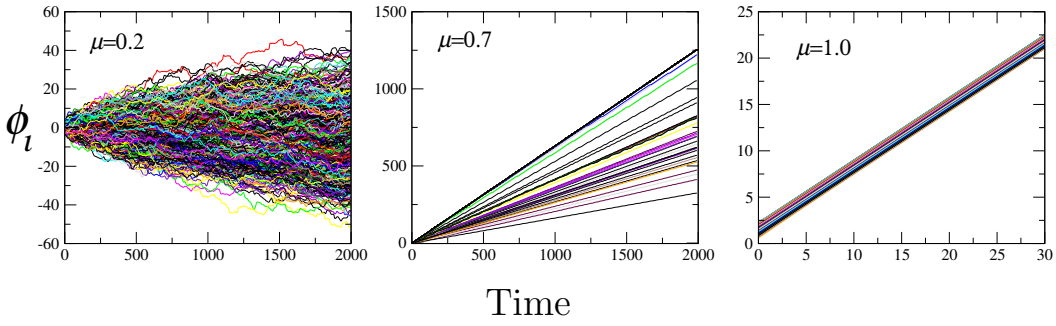

Figure 4.5: Temporal evolution of all individual phase values for different values of the global feedback intensity μ. $\delta = 0.8\pi$, $N = 1000$.

feedback intensity μ. As expected, for large values all three of them coincide, meaning that the system is in a state of synchronization in which all elements have the same velocity, and rotate like a rigid body in a fixed configuration with constant velocity. A characteristic realization of these dynamics can be seen in the rightmost panel of Fig. 4.5.

On the other extreme, when $\mu < \mu_3$, the mean velocity is close to zero, and dispersion is small. A realization of the dynamics for parameter values in this range is shown in the leftmost panel of Fig. 4.5, where the phases of all elements appear to diffuse with no regularity.

In the transition region between these regimes, in the range $\mu_3 < \mu < \mu_1$, the velocities of individual oscillators are spread broadly. However, as can be seen in the middle panel of Fig. 4.5 for a typical realization in this regime, the average velocities of all elements are well-defined, and do not change in time. For values of μ closer to μ_3, the spread in velocities is increased, but the behavior remains qualitatively the same. This seems to be a sort of "ordered disorder": in contrast to the regime $\mu > \mu_1$, dynamical properties are highly heterogenous; but, in contrast to the region $\mu < \mu_3$, a dynamical order is persistent. Recalling Fig.s 4.1 and 4.2, it is interestig to note that it is in this region where the maximal Lyapunov exponent and the dimension maximize.

Clearly, the dynamics in this transition region are far from being a simple superposition of the dynamics in both extremes. Instead, we observe that the interplay between network and global interactions gives rise to a new kind of dynamics. In the following, we present different methods to shed light on on some interesting aspects of the dynamics in this transition region.

4.4 Transition region

In previous sections we have identified the different stages along the transition from synchronization to chaos. In the following, we present some tools to describe and characterize different aspects of this transition.

4.4.1 Active and synchronous elements

The dynamics of the system in the range $\mu_3 < \mu < \mu_1$ is such that each element has a well defined average velocity. As an initial step, we investigate the distribution of such velocities. This is done in Fig. 4.6, where different histograms of velocities ν_i are plotted for different values of μ in the long-time regime. It is important to note that these histograms are independent of initial conditions, and only a function of the parameters.

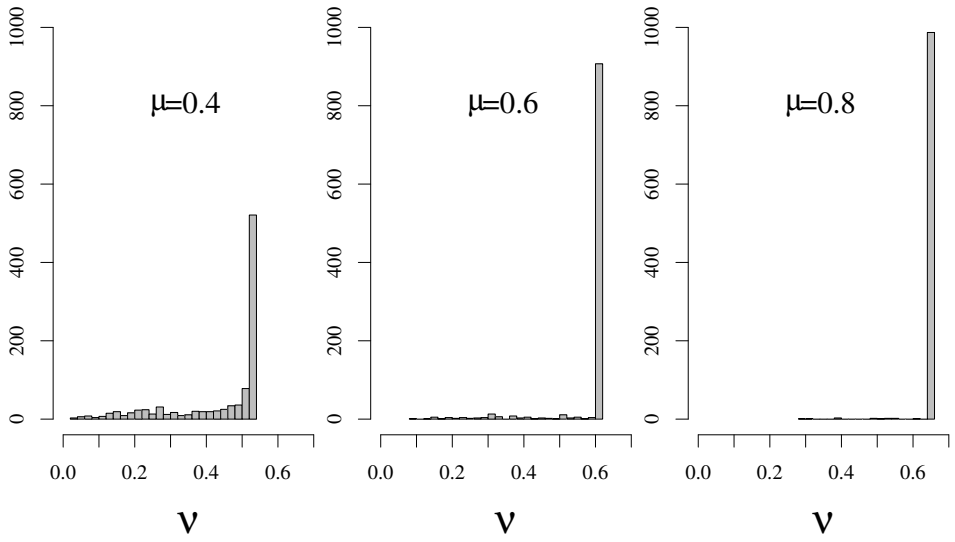

Figure 4.6: Distributions of time-averaged velocities of all network elements for three selected values of feedback intensity μ. $\delta = 0.8\pi$, $N = 1000$.

A notable aspect about these histograms is that, although the overall spread in velocities is large, most elements have the same long-term average velocity. As seen in the rightmost histogram in Fig. 4.6 for values of μ close to μ_1, almost all elements have velocities falling in a single peak in the distribution, while only a very small number of elements fall outside of it. This means that most of the elements remain in a fixed configuration, rotating almost like a rigid body. The system is essentially in the same synchronous configuration as it would be for values $\mu \gtrsim \mu_1$, only some elements have become disentrained, and rotate with their own velocities with respect to those still entrained.

If we were to look at the dynamics of the system in a rotating frame of reference with velocity equal to the value at which the peak in the histogram is, we would see that the elements whose velocity is in the peak remain frozen, or at most vibrate around a well-defined fixed position, whereas elements with a different velocity perform persistent rotations around the circle with different frequencies. For this reason, we classify elements whose velocity is in the peak as conforming a *synchronous condensate*, while elements with distinct velocities will be referred to as *active*.

This nomenclature is valid as long as a well defined peak can be identified in the

distribution of velocities, which, as can be seen in the last histogram, is the case for the largest part of the transition region, for values even lower than $\mu \approx 0.4$. Therefore, this is an appropriate way to describe the dynamic roles of the elements in this transition region.

This classification is further clarified if we look at the instantaneous dynamics of active and synchronous elements. The time-dependence of the phases of all elements is plotted in Fig. 4.7 with high time resolution for a value of $\mu \leq \mu_1$. Here it is clear that the phases of elements in the synchronous condensate increase steadily at constant velocity and almost unperturbed. Active elements follow this behavior closely, but repeatedly undergo rapid phase slips, performing a 2π rotation and returning to their point of "almost equilibrium". Each active element undergoes phase slips with a different frequency, giving rise to different long-term average velocities, as seen in Fig. 4.6

The fact that active elements perform such rapid phase slips means that the instantaneous velocity $\dot{\phi}_i(t)$ of these elements will have very high variations. As seen in Fig. 4.8, all elements in the synchronous condensate exhibit only weak temporary deviations from the common velocity. In contrast to this, each active element is characterized by repeated velocity pulses, ocurring at regular intervals with different frequency. Each of such pulses corresponds to a full 2π phase rotation, i.e. a phase slip with respect to the condensate. Phase slips imply a strong variation in the signals produced by active elements on elements connected to them. In this sense, large variations in the velocities of active elements are reminiscent of the spiking behavior in neural models [103].

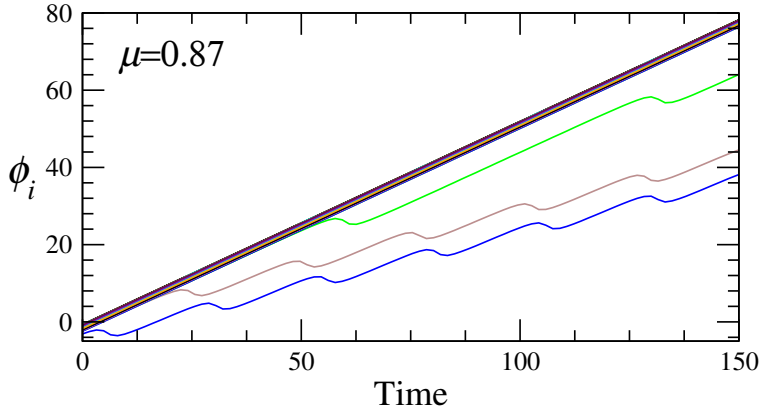

Figure 4.7: Temporal-evolution of all individual phase values for $\mu = 0.87$. $\delta = 0.8\pi$, $N = 1000$.

To elaborate on the distinction between active and synchronous elements, it is useful to study how the destruction of the synchronized takes place. For this, we note that we may rewrite Eqs. (4.1) in the form

$$\dot{\phi}_i = \frac{1}{2i}\left[(z_i + \mu Z)e^{-i\phi_i} - \text{c. c.}\right], \tag{4.3}$$

where the *local signal* z_i is the signal perceived by element i through its incoming network connections. Due to the heterogeneity in the phase shifts, we need to

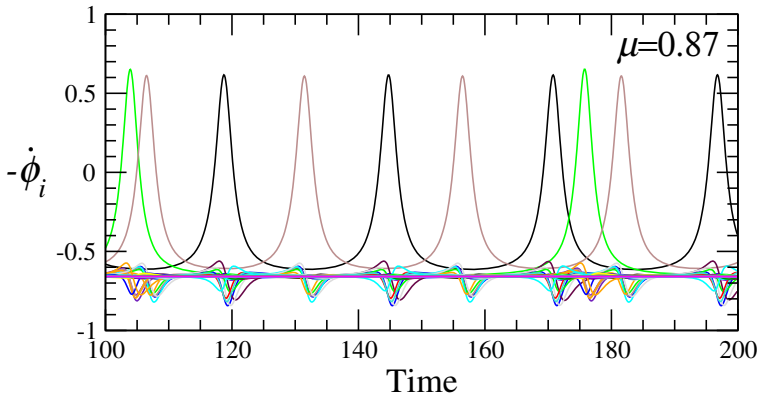

Figure 4.8: Instantaneous velocities of all elements for $\mu = 0.87$. $\delta = 0.8\pi$, $N = 1000$.

reformulate the definition of the local signal with respect to that given in (3.6) as

$$z_i = \frac{1}{\rho N} \sum_{j=1, j\neq i}^{N} T_{ij} e^{i(\phi_j + a_{ij}\times\delta)} \,. \tag{4.4}$$

z_i is equivalent to the sum in the first term of Eq. (4.1) corresponding to the i-th element.

When moving to a frame of reference that co-rotates with the synchronous condensate, we introduce the relative phases of elements in the form

$$\psi_i = \phi_i - \Phi \,, \tag{4.5}$$

where Φ is the phase of the global signal $Z = R\exp(i\Phi)$. With this change of variables, Eqs. (4.3) become

$$\dot{\psi}_i = -\dot{\Phi} + \frac{1}{2i}\left[(\widetilde{z}_i + \mu R)e^{-i\psi_i} - \text{c. c.}\right] , \tag{4.6}$$

where the transformed local signals $\widetilde{z}_i$ are defined as

$$\widetilde{z}_i = \frac{1}{\rho N} \sum_{j=1, j\neq i}^{N} T_{ij} e^{i(\psi_j + a_{ij}\times\delta)} \,. \tag{4.7}$$

$\dot{\Phi}$ is constant only in the synchronized state, i.e., for $\mu > \mu_1$. However, when $\mu \lesssim \mu_1$ there is only a few elements that are active, while the majority of elements remain in an almost frozen configuration. Therefore, variations in $\dot{\Phi}$ are expected to be very small, and we can approximate it as a constant $\dot{\Phi}(t) \approx \Omega$. Furthermore, when a synchronized state is reached, all $\widetilde{z}_i$ are also constant. We can introduce a new set of local variables as

$$R_i \exp(\Psi_i) \equiv \frac{\widetilde{z}_i}{\mu} + R \,. \tag{4.8}$$

With this definition, Eq. (4.6) takes the form

$$\dot{\psi}_i = -\Omega + \mu R_i \sin(\Psi_i - \psi_i) \,. \tag{4.9}$$

A solution to this equation, and therefore the existence of a synchronized state, is only possible if $\mu R_i \geq \Omega$. This is always the case when the global feedback intensity is very strong ($\mu \to \infty$), as the network interactions become negligible[3]. However, as the intensity of the global feedback is decreased, this condition will eventually not be fulfilled by a certain element. This element can no longer be entrained and will begin to orbit around the condensate. The quantity R_i can therefore be associated with a threshold value for each element, determining its dynamic characteristics.

The validity of Eq. (4.9) relies on $\dot{\Phi}$ and $\widetilde{z}_i$ being constant. However, since near this critical point only one or a few elements are not entrained, the variations in these quantities will be small (of order N^{-1}). Eqs. (4.9) may thus be approximately valid for the majority of the elements, even if the synchronized state is not attainable.

The above analogy with spiking neurons is not far-fetched. The transition to orbiting in Eq. (4.9) has the normal form of the saddle-node bifurcation on the invariant cycle, which is characteristic for Hodgkin's Class I excitable neuron models [97, 98]. Non-entrained elements can pertain to two different classes: elements that are supra-threshold, which perform rotations periodically, generating spikes repeatedly and acting as pacemakers on the rest of the system; and elements that are close to their threshold and are effectively excitable, performing rotations when a strong perturbation arrives. Elements in the synchronous condensate are therefore sub-threshold, and perturbations coming from active elements are not enough to trigger a phase-slip.

It is important to note that whether element i satisfies $\mu R_i \geq \Omega$ depends not only on its connections and their respective phase shifts, but also on Ω, which is a macroscopic quantity determined by all elements in the system and their interactions. Moreover, the specific value of each of the $\widetilde{z}_i$ depends on the synchronized configurations of each node's neighbors, which is determined as a global equilibrium point. In this sense, it is clear that the orbiting of certain elements is an emergent property, not determined by local network topology but through interactions that involve all elements in the system.

Spontaneous spiking is periodic for $\mu_2 < \mu < \mu_1$, as evidenced by the fact that the maximal Lyapunov exponent is zero ($\lambda_1 = 0$) inside this interval. Actually, as seen in Fig. 3b, several Lyapunov exponents can be zero inside this interval, indicating that active elements are orbiting independently, and the attractor is quasi-periodic. For each spontaneously spiking element there is a zero Lyapunov exponent, so that the Kaplan-Yorke dimension is equal to the number of spontaneously spiking, supra-threshold elements. For lower feedback intensities, collective dynamics of the system becomes chaotic, and this association may no longer valid.

4.4.2 Active subnetworks

Since elements in the synchronous condensate are in a fixed configuration, the signals they exchange present little variation. The action of elements in the synchronous condensate on a given element amounts to a local field of almost constant magnitude which rotates with almost constant frequency. In contrast, the action of an active

[3]It is clear from Eq. (4.1) that Ω is finite.

element on another element connected to it presents very high variations as it goes around the circle every time it performs a 2π phase-slip. Hence, elements in the synchronous condensate can be thought of as generating a background signal on which active elements interact. Active elements are thus responsible for most of the dynamics of the system.

In Fig. 4.9 we can see how the number of active elements depends on the global feedback intensity μ. The growth in the number of active elements is monotonous as the value of the global feedback is decreased. When we get closer to the left end of the transition region, i.e., when μ is close to μ_3, the number of active elements approaches the total number of elements in the system. Here, distinguishing a peak in the distribution of velocities may not be possible, and our classification breaks down. Nevertheless, this only happens very close to μ_3, and this framework is suitable for the largest portion of the transition region. Thus, the transition from synchronization to chaos takes place gradually through the progressive emergence of individual active elements, which eventually takes over the entire system.

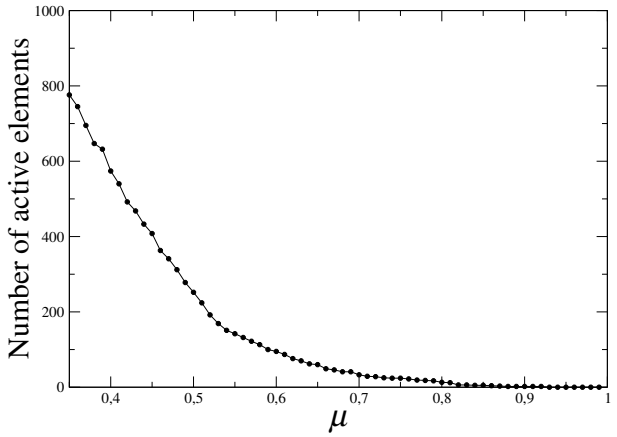

Figure 4.9: Number of active elements as a function of μ. For values below $\mu = 0.3$, the distinction between active and synchronous elements may no be clearly drawn. $\delta = 0.8\pi$, $N = 1000$

Active elements are distinguished from elements pertaining to the synchronous condensate by their dynamical properties. There remains the question of the topological properties of the nodes they occupy in the underlying network, and how they interact with each other through it. Given that the number of active elements increases as the global feedback intensity is decreased, it is inevitable that some active elements eventually be connected to each other. Since the signals received from an active element are strong and have much larger variations that signals coming from the synchronous condensate, this direct interaction of active elements may lead to interesting dynamics and the formation of active substructures in the network. We may therefore consider the activation of a given set of elements as the emergence of an active subnetwork. The properties of these active subnetworks may in turn be controlled by the global feedback intensity.

To construct the subnetwork of active elements, it suffices to disregard elements

in the synchronous condensate and their connections. For this, we let the system evolve for a long time for a given value of the global feedback intensity μ, and we identify the non-entrained active elements in the system. By retaining only the active elements and the connections between them in the underlying network, we obtain a new subnetwork corresponding only to the active elements. This subnetwork may not be connected, it may posses some isolated elements, or may show some localized structures of different sizes. By repeating this process for different values of the global feedback intensity we can investigate how the structure of the active subnetworks change.

This is what is seen in Fig. 4.10, where each one of the panels represents a different long-time realization for different values of μ. Initially, for values of μ close to μ_1, the active elements are isolated and scattered over the system. As the value of μ is decreased, more elements aggregate to this network, and eventually form connected substructures[4]. Continuing to increase μ leads these structures to grow and merge, and eventually one giant component emerges which groups the majority of active elements. In this sense, by manipulating the intensity of the global feedback, we can control the size and number of such active structures.

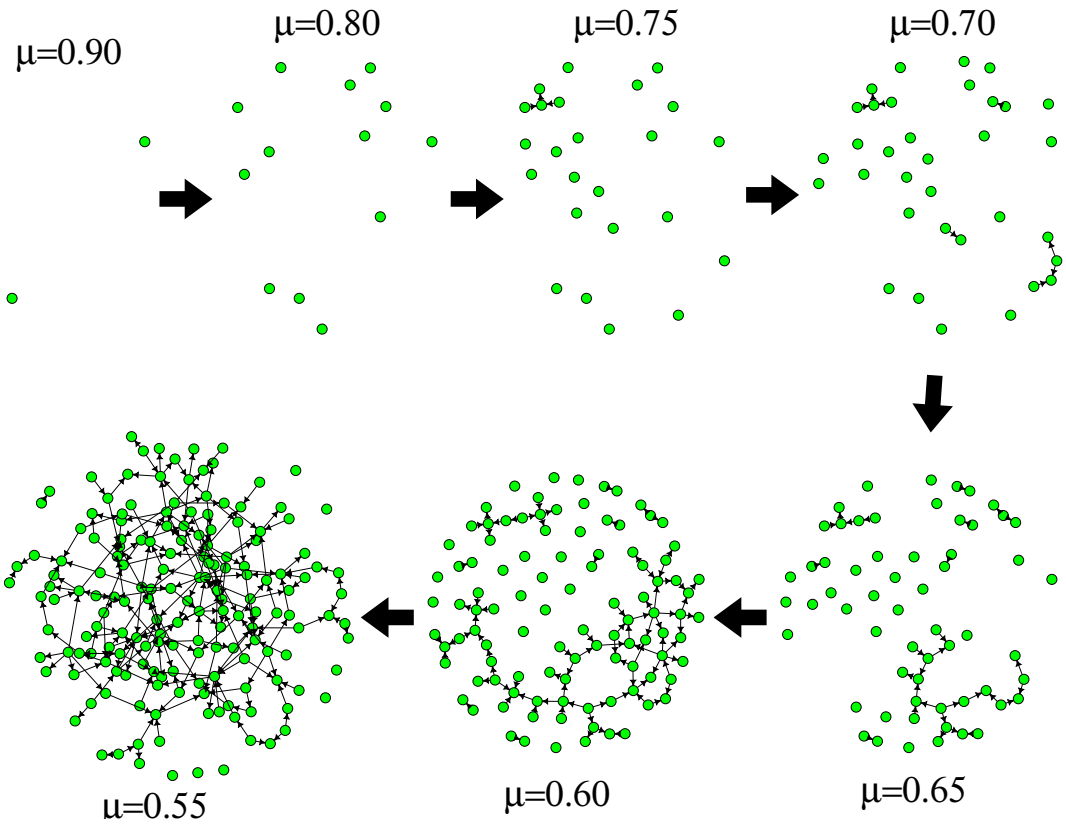

Figure 4.10: The sequence of active subnetworks observed under gradual decrease of the feedback intensity μ. $\delta = 0.8\pi$, $N = 1000$.

[4]By connected, we mean here *weakly connected*, i.e., all elements interact with some other elements in the component. In other words, the corresponding undirected structure is connected.

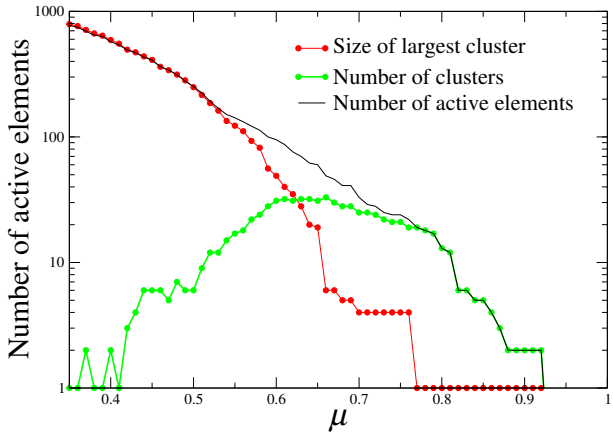

Figure 4.11: Size of largest cluster (red) and number of clusters (green) in the subnetworks of active elements as a function of the global feedback intensity.$\delta = 0.8\pi$, $N = 1000$.

Except in the last panel, the relative spatial location of the nodes from panel to panel is preserved. As was seen in Fig. 4.9, the number of active elements increases monotonically as the global feedback is decreased. Fig. 4.10 also indicates that this growth takes place through aggregation of nodes to the subnetwork of active elements. In the process of decreasing μ, an increasing number of nodes become active, but no active elements return to the synchronous condensate. Aggregating elements will eventually form connected components or *clusters*,[5] which can only grow.

In Fig. 4.11, we plot the number of such connected clusters and the size of the largest of them as compared to the number of active elements when the feedback intensity is reduced. It can be seen that initially, and for a certain range of the parameter, the number of clusters is equal to the number of active nodes. Therefore, only isolated active elements are present in the system. Below a value of $\mu \approx \mu_2$, the largest connected component begins to grow, and the number of clusters eventually decreases, indicating that the clusters merge with one another. For values of μ below $\mu \approx 0.5$, essentially all active elements belong to a certain cluster, and only a small number of clusters with one or a few elements can be found. This can already be seen in the last panel of Fig. 4.10.

Apart from the size and number of connected components in the active subnetwork, the topological properties of such subnetworks may be affected by the intensity of the global feedback. In the following we calculate the diameter of the subnetwork for each value of μ. The diameter requires a specific definition for disconnected networks. For each pair of elements in the active subnetwork, the minimal directed path between them is computed if it exists. The diameter is taken to be the maximum of these minimal paths amongst all pair of elements. This represents the maximum diameter amongst the diameters of each individual connected component.

[5]This use of the term "cluster" is unrelated to the concept used in Chapter 2, and is standard in the network literature [42].

In Fig. 4.12 we plot this quantity for each subnetwork of active elements as a function of the global feedback intensity. The diameter grows as the number of active elements increases until reaching a maximum, and then decreases to a value of 8, which is the diameter of the full network. It is remarkable that this quantity reaches very high values for intermediate values of μ. The diameter is larger for active subnetworks than it is for comparable standard random networks. For example, at $\mu = 0.49$ the subnetwork of active elements has a diameter of 29, it has 293 elements and 494 links, and its mean degree is 3.37. The subnetwork formed by a subset of 293 elements randomly chosen from the full network has an expected diameter of approximately 23.

Subnetworks of active elements attain particularly long paths with fewer edges than would be expected for randomly chosen elements. This means that, even though the underlying network has a random structure, and the phase shifts involved in the interactions are randomly distributed the subnetwork of active elements is *not* random in the Erdös-Rényi sense. Instead, even though active elements are part of the underlying network, and are therefore restricted in the topological properties that any subset of them may have, a process takes place that selects for the occurrence of long paths in the active subnetworks, thus resulting in subnetworks with special properties.

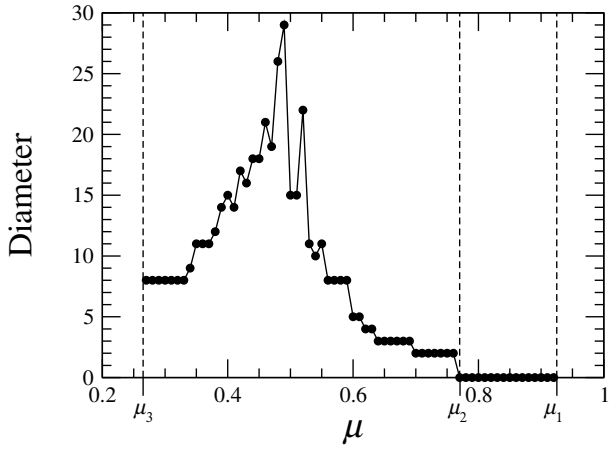

Figure 4.12: The largest diameter of active subnetworks as function of the feedback intensity μ. $\delta = 0.8\pi$, $N = 1000$

The activation of a given node is not an uncorrelated process. It is determined by the underlying network of interactions and the phase shifts associated with each edge in the network, inasmuch as they determine the configuration of the synchronous condensate. One could imagine that the local topological properties of a given node in the network would be a determining factor in the dynamics of the node. However, the interdependence between the properties of the whole network and the given set of phase shifts makes no clear factors to determine the activation of a given node. Indeed, for a given underlying network of interactions, the topological properties of the active subnetworks show a great dependence on the specific values of the phase shifts.

As a small digression, we present in Fig. 4.13 the calculated average path length of the subnetwork of active elements for different values of magnitude of the phase shifts δ as a function of the number of elements in the active subnetworks, which are obtained by varying the value of μ for each value of δ. For comparison, the expected average path length of a subnetwork with the corresponding number of nodes which are chosen randomly is also presented. As we see, not only the values of the path lengths are quite different from those of a randomly chosen subnetworks, but there is also a clearly systematic dependence on the values of the phase shifts. That active subnetworks with the same number of elements and drawn from the same underlying network of interactions may have very different average path lengths for different values of δ is a confirmation that the factors that decide the activation of each element are not only topological. Indeed, any topological measurement intending to determine the causes for the activation of different elements will fail to explain the behavior observed in Fig. 4.13.

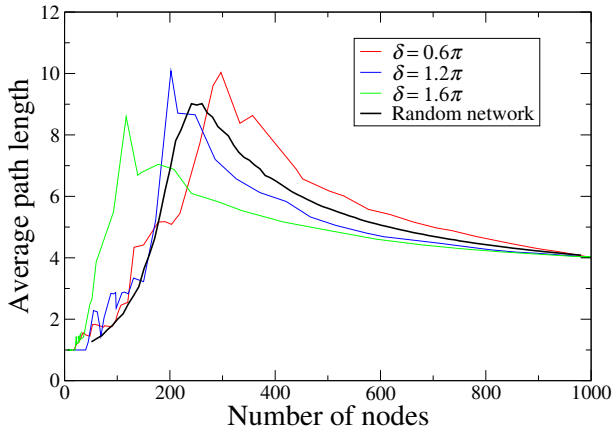

Figure 4.13: Average path length of the within connected components of the active subnetwork as a function of the number of active elements for different values of parameter δ. $N = 1000$

The transition scenario depicted Fig. 4.4 has common aspects with the one presented in Fig. 3.16. By construction, the case of $\mu = 0$ coincides with the regime of large δ presented in the previous Chapter. In the other extreme, large μ yields synchronization, which is what is seen in Fig. 3.16 for small δ and α. This may indicate that the transition from synchronization to chaos seen by decreasing the global feedback intensity might be qualitatively the same as the one seen in the absence of noise by increasing the values of the phase shifts.

Nevertheless, an important difference between these cases is that the role played by the phase shifts is different. As seen in Fig. 4.13, changing the value of the phase shifts may lead to very different active subnetworks. To illustrate this, we may construct plots similar to the ones shown in Figs. 3.13, 3.14 and 3.17 for different values of μ and δ. In Fig. 4.14, the long-term average velocities of each element is plotted against its number of incoming connections in the network for two different values of δ, and for values of μ such that there is only one active element in the

system in respective cases. As can be seen, the first elements to become active have different topological properties in the network for different values of δ.

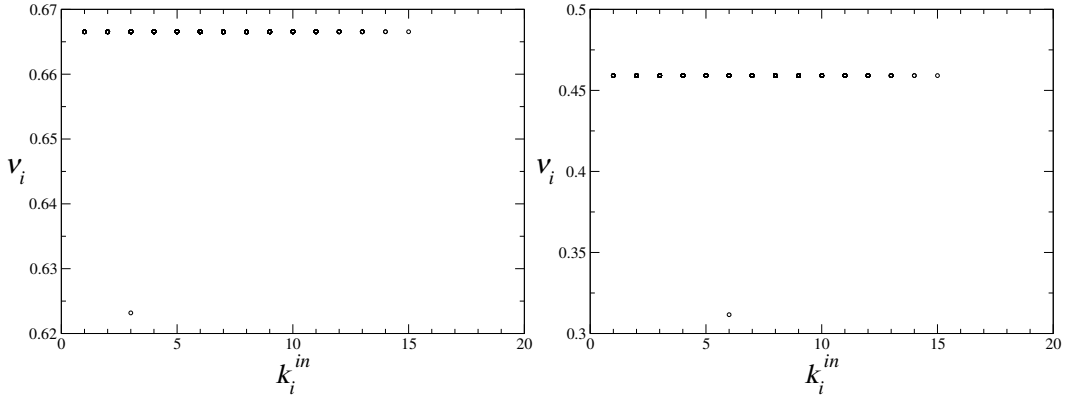

Figure 4.14: Long-term average velocities of each element as a function of its number of incoming connections. Left: $\mu = 0.92$ and $\delta = 0.8\pi$; Right: $\mu = 1.4$ and $\delta = 1.2\pi$. For both panels, $\rho = 0.007$, $N = 1000$.

Finally, it is worth noting that, as can be seen in Fig. 4.12, the diameter of the largest component only becomes bigger than 0 at approximately $\mu = \mu_2$, when the maximal Lyapunov exponent becomes larger than zero. This indicates the presence of the first connected components of active elements, meaning that active elements begin to interact with one another directly. The fact that this occurs at approximately the onset of chaos in the system suggests that small connected substructures of active elements can already display complex dynamics. Understanding the nature of these dynamics is the object of the following section.

Dynamics and wave propagation

Active subnetworks are also dynamical structures. As we have seen, active elements perform repeated rotations with respect to the synchronous condensate at different intervals and different frequencies, emitting velocity spikes to their neighbors in the network. It is to be suspected that certain correlations may exist between the frequencies and the way elements are connected to each other in the active subnetwork.

As we have shown before, for high values of the global feedback close to μ_1, only a few elements are active, and they are isolated from each other. In terms of Eq. (4.9), these elements can be considered as being in a supra-threshold periodic state. In this sense, each one of these elements will act as a pacemaker, sending signals down their connections. Since these active elements are isolated, their connections lead to elements that are entrained in the condensate. However, a synchronous element connected to an active element may be very close to its threshold in the sense of Eq. (4.9). Since the signals it receives directly from active elements have great variability, a small reduction in the feedback intensity may be sufficient for these perturbations

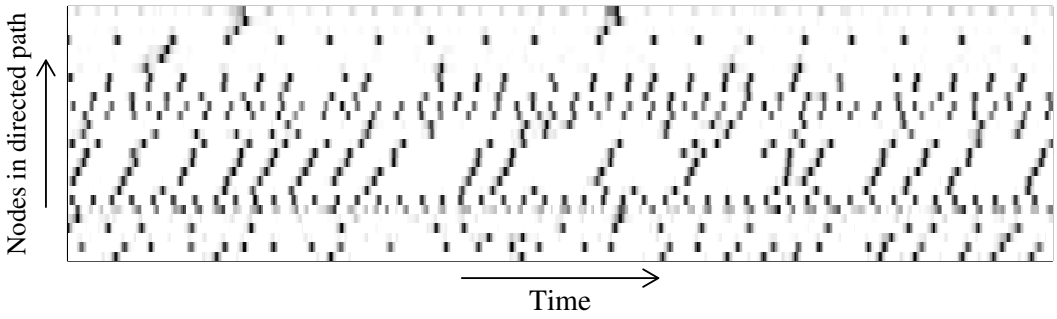

Figure 4.15: Space-time diagram showing the dynamical activity pattern in the chain of 29 elements belonging to the active subnetwork. $\mu = 0.49$, $\delta = 0.8\pi$, $N = 1000$

to temporarily bring the element over its threshold. This element would therefore be in an excitable state, performing rotations with respect to the condensate when a strong enough perturbation reaches it through its incoming connections.

Through this process, an active element may trigger a cascade of phase slips that propagates along the edges of the active networks. This kind of waves of excitation would be the process responsible for the specific topological properties of the active networks. Such a mechanism would effectively work as a selection process for active subnetworks with long paths.

This effect has been shown in Fig. 4.12, where one can see that for a feedback intensity of $\mu = 0.49$, there is a given pair of elements for which the minimal path that connects them is as long as 29 edges. This pair of elements thus determines a chain of nodes such that the minimal path between any (properly ordered) pair of them is also contained in this chain. We can therefore consider this chain as a unidimensional array of active elements, and study the dynamics along it. This is what is shown in the raster plot in Fig. 4.15, where the activity of each element in the chain is shown as a function of time. Here, the absolute value of the velocity of each element with respect to the synchronous condensate is displayed in grayscale, with darker colors representing higher values. The occurrence of a black dot can be readily identified with a "velocity spike" or phase slip of active elements, as those seen in Fig. 4.8.

In different parts of the chain, clear signs of wave propagation can be observed, where persistent cascades of phase slips travel along the direction of the edges in the chain. This propagation seems to be quite robust, even though the dynamics are irregular. The interruption of such propagation is to be expected, since the elements in the chain are very heterogenous: each one of them is connected to different numbers of both active elements and elements in the condensate and receives signals from them. In other parts of the chain, no correlation can be perceived between neighboring elements.

This plot corresponds only to a chain of 29 elements, a subset from 293 nodes that form the subnetwork of active elements at $\mu = 0.49$. The full activity pattern is very complex, and cannot be easily visualized. However, we see here that the

presence of coherent patterns of activity can be observed at different scales, with different characteristic lengths. It is to be inferred that such behavior could be found for a much larger subset of active elements.

Inside an interval of feedback intensities preceding the final feedback breakdown, the considered system can generate a variety of dynamical networks whose sizes and dynamical properties can be controlled by the feedback intensity. These networks are effectively built from oscillatory and excitable elements. They are strongly heterogenous in terms of the oscillation frequencies and excitation thresholds of their elements. As the feedback intensity μ is decreased, the number of active, non-entrained elements grows and they begin to dominate the dynamics of the system. In the next section we analyze the transition corresponding to the final loss of coherence.

4.5 Breakdown of global feedback

In Figs. 4.1 and 4.2 we have seen the presence of a discontinuity in both the maximal Lyapunov exponent and the embedding dimension of the attractor at $\mu_3 \approx 0.26$. The dynamical properties of the system also change sharply, as seen in Fig. 4.4. Below this point, the properties of the system show no significant variation with respect to the global feedback intensity. The global feedback becomes thus ineffective as a control mechanism, in that it is unable to affect the dynamics. Below we provide further analysis of this feedback breakdown transition and the dynamical properties of the network in its vicinity.

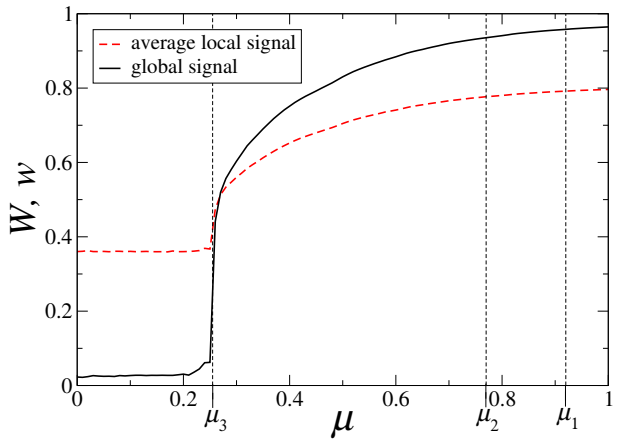

Figure 4.16: Time-averaged magnitude of the global signal (solid line) and mean time-averaged magnitude of local signals (dash line) as functions of the feedback intensity μ. $\delta = 0.8\pi$, $N = 1000$

A breakdown in the global feedback means a breakdown in the global signal Z. The solid black line in Fig. 4.16 shows the dependence of the time-averaged modulus of the global signal W, as defined in (3.5) Indeed, a sharp drop to almost vanishing values can be seen at the critical point $\mu = \mu_3$, below which it remains very small. It can be presumed that this level would be zero if the size of the system

were infinite. Since the modulus of the global signal Z coincides with the Kuramoto order parameter, its vanishing indicates a loss of phase coherence.

Also in Fig. 4.16 the computed dependence of the mean value of the time-averaged local signals w_i as a function of the global feedback intensity μ is plotted in dashes lines. This quantity is calculated as

$$w = \frac{1}{N}\sum_{i=1}^{N} \langle |z_i(t)| \rangle = \frac{1}{N}\sum_{i=1}^{N} w_i \,, \tag{4.10}$$

with $z_i(t)$ given by Eq. (4.4). In this figure we can see that mean local signal decreases together with the global signal as the feedback intensity is decreased approaching the critical point $\mu = \mu_3$. However, its magnitude does not vanish, but it remains strong for all values of μ.

Since our control parameter determines the coupling strength of a global interaction, an important distinction should be made here between this transition and that usually observed in globally coupled systems. In oscillator populations with global, all-to-all coupling, vanishing of the Kuramoto order parameter leads to the loss of interactions between elements. They become almost independent, with the rest interactions of order N^{-1} and vanishing in the limit $N \to \infty$.

In the system we are studying, in contrast, the interactions between elements through the network never vanish. Instead, the feedback breakdown leads the system to the high-dimensional chaotic state of network turbulence. Previously, analogous global feedback transitions have been investigated by Y. Kawamura and Y. Kuramoto [99] for continuous active media described by the complex Ginzburg-Landau equation. It is remarkable that, as seen in Figs. 4.1 and 4.2, the maximal Lyapunov exponent and the embedding dimension *increase* as the critical point $\mu = \mu_3$ is approached and abruptly drop below it.

Time-dependent spectra

The transition observed at $\mu = \mu_3$ is characterized by an abrupt change in the magnitude of the interaction and by a discontinuity in the dynamical properties of the attractor. To compare the dynamics observed at both sides of the transition we resort to the construction of time-dependent spectrum plots.

To confect such plots we first calculate the autocorrelation function $S(\tau, t)$ of the global signal is calculated within a sliding time window of width T,

$$S(\tau, t) = \frac{1}{T}\int_{t}^{t+T} Z(t')Z^*(t'+\tau)dt' \,, \tag{4.11}$$

After that, the time-dependent spectral density $S(\omega, t)$ of the global signal is determined by the Fourier transform,

$$S(\omega, t) = \left| \frac{1}{T}\int_{0}^{T} S(\tau, t)e^{-i\omega\tau}d\tau \right| .$$

With this procedure we may calculate the spectrum of the signal at different times and observe its variation. The power spectrum $S(w, t)$ is displayed in a grayscale

plot, such that vertical lines represent the spectrum at each location of the time window. This type of methods is widely used in the analysis of electro-encephalographic data to identify the presence of coherent activity in the brain [100, 101].

In our investigations we use a sliding window of width $T = 110$, which is chosen arbitrarily to provide most illustrative results. Using smaller window size leads to noisy results, and larger window sizes result in excessive averaging. In Fig. 4.17 we display spectral density plots for the global signal at several selected values of the global feedback intensity, both above and below the transition.

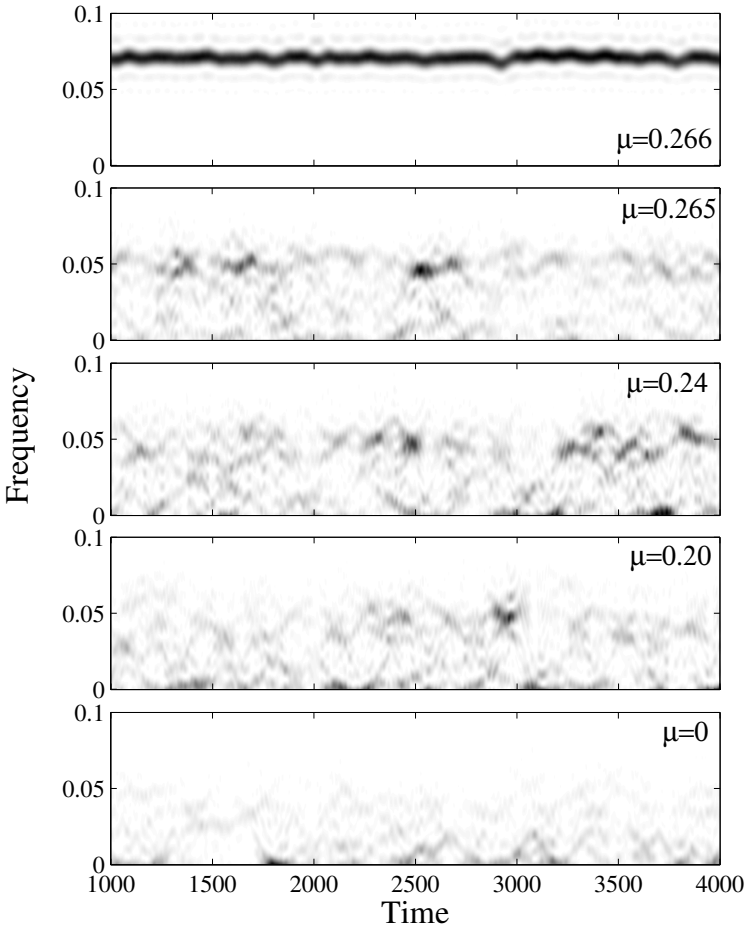

Figure 4.17: Time-dependent spectral densities of the global signal at different feedback intensities μ. The absolute magnitude of the signal is much larger at $\mu = 0.266$, than in other plots shown.

Above the transition ($\mu = 0.266$, first panel) a peak in the spectrum persists in time for a well-determined characteristic frequency. This indicates the occurrence of coherent rotations in the system at a constant frequency.

Immediately below the transition point (second panel, $\mu = 0.265$) such a persistent peak is absent. Nevertheless, irregular occurrences of repeated peaks within a defined range of frequencies in the spectrum can be observed. Such peaks indicate the occurrence of transient regimes of coherence, in which global rotations happen

sporadically but persistently. This sort of intermittent behavior also occurs at a similar frequency as that characteristic above the transition.

The above described intermittency is retained well below the transition, as can be seen in the third and fourth panel of Fig. 4.17. However, as the feedback intensity is gradually decreased, bursts of coherence become more rare and their characteristic duration decreases. In the absence of feedback, as illustrated in the last panel for $\mu = 0$, the transients of coherence disappear.

The gray scale used in these plots is such that pure black is assigned to the maximum value of the power spectrum for a given plot, and pure white to the minimum. This means that the scale is not the same for all panels. As was seen in Fig. 4.16, the magnitude of the global signal is much stronger on the right side of the transition than it is on the left, and therefore, the magnitude of the peaks in the power spectra is also different. Nevertheless, the fact that a well-defined frequency is identifiable indicates that coherence is present in both cases, which would not happen in the case of simple fluctuations.

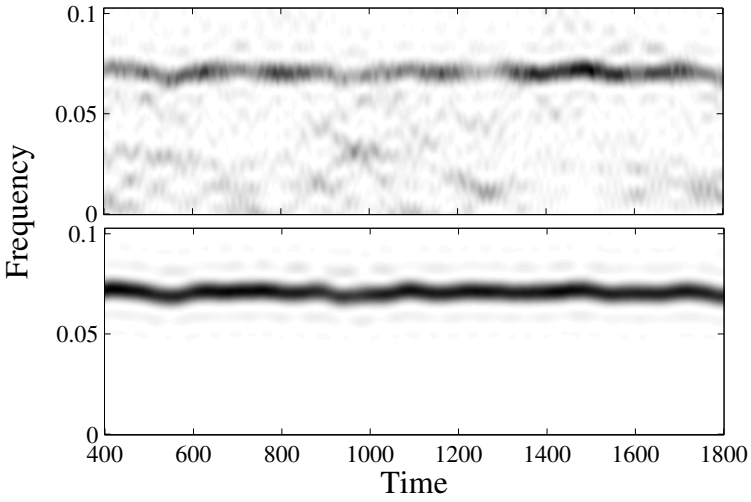

Figure 4.18: Time-dependent spectral density of a single oscillator $s_i(\omega, t)$ above the feedback breakdown transition ($\mu = 0.266$). The spectrum of the global signal is shown in the lower panel as a comparison.

Since the global signal is finite on the right side of the transition, its influence on each element is significant. This influence may be put in evidence by looking at the spectral density of a single element, defined for element j as

$$s_i(\omega, t) = \left| \frac{1}{T} \int_0^T s_i(\tau, t) e^{-i\omega\tau} d\tau \right| , \tag{4.12}$$

where

$$s_i(\tau, t) = \frac{1}{T} \int_t^{t+T} e^{i(\phi_i(t') - \phi_i(t'+\tau))} dt' . \tag{4.13}$$

In Fig. 4.18 the spectral density for a single randomly chosen element on the right side of the transition ($\mu = 0.256$) is compared to the spectrum of the global signal.

Here we can see that the spectrum of the global signal is clearly imprinted in the spectrum of each element. This means that the dynamics of all elements are governed by the global dynamics. This should indeed be expected if we take into account that all oscillators effectively experience external forcing generated by the global feedback, and their spectra therefore reflect the presence of such forcing.

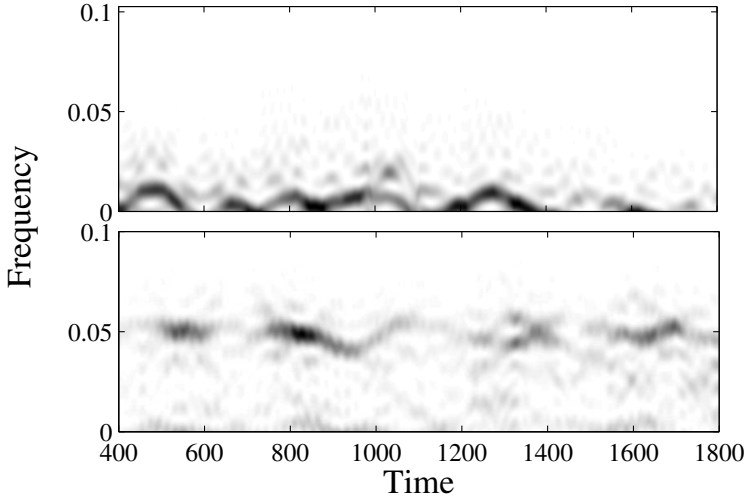

Figure 4.19: Time-dependent spectral density of a single oscillator $s_i(\omega, t)$ below the feedback breakdown transition ($\mu = 0.265$). The spectrum of the global signal is shown in the lower panel as a comparison.

The case below the critical point is rather different. As can be seen in Fig. 4.19, the spectrum of the same element as in Fig. 4.18 holds no similarity with that of the global signal any more. This means that the occurrence of transient burst of coherence is a truly emergent property, in the sense that it is the result of the constructive interaction of many incoherent elements, only observable when looking at the system as a whole.

This aspect of the dynamics below the transition indicates that coherence emerges as a collective phenomenon. There remains however the question of whether some elements have more responsibility in the formation of such events. If this were the case, a possible scenario would be that a certain element or group of elements may act as a pacemakers, which temporarily entrain a number of other elements, giving rise to small periods of synchronicity.

However, inspection of the spectra of all individual elements reveals no reasons to believe that any given element may be more responsible for the occurrence of such synchronous episodes. In fact, a more plausible scenario is that sporadic coherence occurs as a mesoscopic phenomenon, only perceivable when a large number of elements is taken into account.

To shed light on this issue, we have analyzed two different burst of coherence in the spectrum of the global signal at $\mu = 0.255$ shown in Fig. 4.20. For the two instants $t = t_1$ and $t = t_2$ marked with arrows, we have computed the power spectra

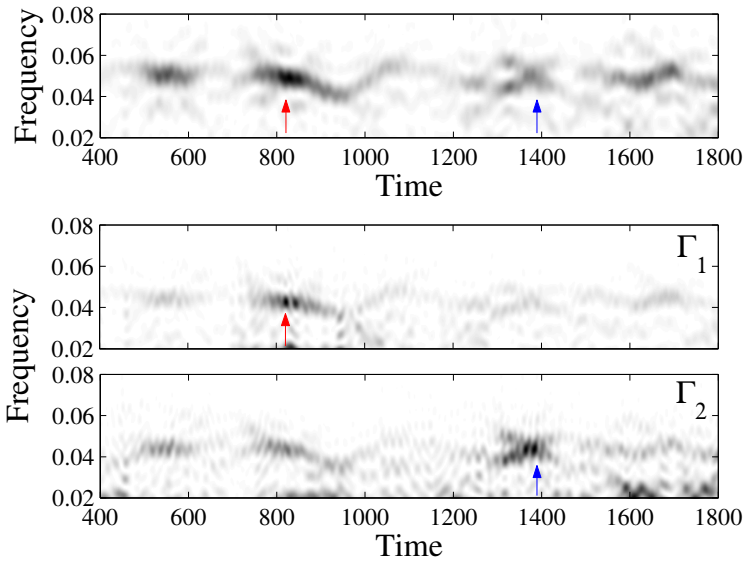

Figure 4.20: (Time-dependent spectrum plot of (above) the global signal and (below) collective signals of two specially selected groups of oscillators. $\mu = 0.265$.

$s_i(\omega, t_1)$ and $s_i(\omega, t_2)$ for all individual elements. From all these spectra and for each instant we have chosen the 50 elements whose spectra are the most similar the spectrum of the global signal. This similarity has been quantified by means of an overlap function of the form

$$h_i(t) = \frac{\int s_i(\omega, t) S(\omega, t) d\omega}{\int s_i(\omega, t) d\omega \int S(\omega, t) d\omega} \,. \tag{4.14}$$

Two groups Γ_1 and Γ_2 are considered, containing the 50 elements for which $h_i(t_1)$ and $h_i(t_2)$ are maximum respectively. For the elements in these two groups, a joined signal is computed as

$$Z_{\Gamma_k}(t) = \frac{1}{50} \sum_{i \in \Gamma_k} e^{i\phi_i(t)} \,, \tag{4.15}$$

and the spectra $S_{\Gamma_k}(\omega, t)$of these signals are determined in the same way as the spectrum of the global signal, that is

$$S_{\Gamma_k}(\omega, t) = \left| \frac{1}{T} \int_0^T Z_{\Gamma_k}(t + \tau) e^{-i\omega\tau} d\tau \right|^2 \,. \tag{4.16}$$

The results for this procedure are shown in Fig. 4.20, where we show the spectra of the joint signals for two groups, Γ_1 and Γ_2, which are chosen at $t_1 = 822$ and $t_2 = 1384$ respectively. In both cases, coherent activity can be seen to emerge in transient bursts for both groups already at the group level. More importantly, the spectrum of the global signal is partially reproduced by both groups. Nevertheless, this spectrum is reproduced by the joint signal much more strongly around the time in which the elements of each group have been selected, whereas for other times,

the spectrum of the global signal is only slightly present or not at all. This suggests that it is likely that only a subset of elements is involved in the generation of each coherent event.

Analyzing composition of the two groups, corresponding to synchronization bursts at $t_1 = 822$ and $t_2 = 1384$, we find that they have only two common elements. Thus, the subset of partially synchronized elements is indeed different in different bursts in the intermittent turbulence regime. The elements of a group represent nodes in the considered network and there are links connecting them. Essentially, each group defines a certain subnetwork which temporally undergoes partial synchronization. Therefore, chaotic intermittency in the considered system can be understood as generating an irregular sequence of synchronization events imposing partial synchronization on different subnetworks. A synchronized subnetwork emerges, persists for some time, dissolves and, after a pause, is replaced by a different synchronized subnetwork.

We have chosen to consider groups of 50 elements, which is a completely arbitrary number. What has been observed for these two groups of elements may be more pronounced for groups of different sizes, and there is no reason to assume that the same number of elements will be optimal for groups selected at different times. Nevertheless, it is important to note that the groups Γ_1 and Γ_2 have 32 and 20 edges connecting elements within the groups, respectively, while the average number of links for a group of 50 randomly chosen elements is 15.75 ± 3.78. This means that the emergence of a coherent burst is indeed induced by groups that are strongly connected.

4.6 Final comments

In this chapter we have analyzed the possibility of controlling turbulence in a model of coupled phase oscillators through a global feedback mechanism. Our attention has been focused on the properties of dynamical patterns and intermittent turbulence characteristic for the transition region.

The results obtained in this Chapter for our system are very much consistent with some of the behavior found in the general model of the complex Ginzburg-Landau equation [76, 75] and in experimental and theoretical studies of the catalytic CO oxidation reaction [77, 78, 102], as discussed at the beginning of this Chapter. In our system, the role of emerging coherent structures is played by active subnetworks. Elements in the active subnetworks spontaneously undergo repeated phase slips, which may induce further phase slips on their neighbors in the network. Therefore, traveling waves of phase slips repeatedly develop and propagate over a subnetwork, spreading from several emergent pacemaker centers.

These traveling waves correspond to the cascades of phase defects in continuous media. In fact, the dynamics described in Fig. 4.15 have an interesting similitude to with the phenomena in Fig. 1.12. Of course, since in our system the interactions between elements are directed, propagation can only take place in one direction.

While each next cascade in the continuous case is typically originating at a different spatial location and involves a different set of the elements of a medium, active networks are permanent in the considered network model. Although the patterns of wave activity in a subnetwork may be quite complex and chaotic, the subnetwork itself remains fixed.

This difference is due to the fact that the considered oscillator networks are strongly heterogeneous, with the heterogeneity imposed both by the structure of the network of connections and the phase shifts in interactions between individual elements. As a result, some elements become easily excitable and others turn into pacemakers. Together, such connected elements form permanent active subnetworks.

When wave patterns in active subnetworks are observed, the rest elements, representing the majority of a network, are in a synchronous state and form a condensate. As the feedback intensity is decreased, the number of active subnetworks increases and each network typically grows in size. In a percolation transition, individual subnetworks merge to form a giant active component, already comprising a substantial fraction of all network elements.

As the feedback intensity is further decreased and approaches the critical point, the Kuramoto order parameter (almost) vanishes, indicating the loss of persistent synchronization. Since this order parameter yields at the same time the magnitude of the global signal, we conclude that breakdown of the feedback control takes place. Analogous feedback-breakdown transitions have been previously studied for continuous oscillatory media under global feedback control [99]. In contrast to the global signal, local signals corresponding to network interactions do not vanish after the transition. Therefore, it is different from the desynchronization transition in globally coupled systems where, after the transition, interactions between elements almost vanish and the oscillators become effectively independent.

The time-dependent spectral analysis of the global signal has shown that, after its breakdown, the feedback is able to induce sporadic bursts of synchronization in the system. This behavior is reminiscent of what has previously been seen in the oscillatory systems comprising global and nonlocal coupling [96]. Our analysis suggest that different groups of elements are responsible for each next synchronization burst. Taking into account their connections, this means that different subnetworks of the entire network are spontaneously exhibiting (partial) synchronization. *Each synchronization episode involves a different subnetwork and such episodes are alternating with complex asynchronous states.*

This looks similar to the behavior characteristic for the developed hydrodynamic turbulence, where different coherent structures are built and replace one another in an irregular sequence. In networks, spatial ordering is absent and therefore spatiotemporal patterns cannot develop. Instead, coherent structures represent various dynamical subnetworks which get accentuated. The simplest form of coherence is partial synchronization, but other, more complicated kinds of coherent dynamics in the emerging networks are also possible.

Chapter 5

Conclusions

The most attractive feature of phase oscillator models is their simplicity. This is not only convenient because of their tractability, but also because it allows us to represent large classes of systems with very few assumptions and parameters. By sparing ourselves the complications introduced by particular details of a given system, we also avoid obtaining spurious or circumstantial results that may be artifacts of the specific characteristics of the chosen model. For this reason, the simplicity of phase oscillator models is often interpreted as their potential for describing general classes of systems, rather than as a capitulation to the intractability of more complicated systems [5, 59]

Throughout this Thesis we have studied a few systems of identical interacting oscillators. Our intention has been to examine the different kinds of behavior that are present between order and disorder. We have done this with the hope that the choice of simple elements may account for more general results, rather than just simpler ones. For this reason, we do not interpret our results as specific to the particular systems we studied, but as phenomena that may be common to a larger class of systems of oscillatory nature.

In Chapter 2 we have studied a system of globally coupled elements for which a desynchronization transition could be induced. Under these circumstances we have observed that the presence of external noise acting on all elements simultaneously may induce the formation of highly coherent clusters. For this system we have chosen to use the most general kind of noise possible: uncorrelated isotropic gaussian noise. For such general assumptions, we already see that the noise is very effective in inducing order in the system. Even when this kind of noise is not appropriate for modeling various situations encountered in the physical and chemical world, we would expect that the presence of correlations and anisotropy, except in pathological cases, would further accentuate this phenomenon.

The scope of this model would therefore not be restricted to systems under the action of exogenous random forcing, but systems for which parameters fluctuate in

time might also be considered within this category. The presence of a noise term like the one considered could be interpreted as the variability of a global parameter, like temperature, lighting conditions, etc., which would affect the instantaneous frequency of each element differently, depending on the stage of the cycle in which they are in. This means that the spontaneous appearance of coherent dynamics could be observed in a variety of systems in the presence of fluctuations.

The system here studied is completely degenerate, in that all elements are identical and so are their interactions. Nevertheless, this kind of dynamics has shown a certain degree of robustness to variability in the population of oscillators. This variability has been chosen here to be represented by heterogeneities in the individual frequencies of each element, but could also be introduced as a noise in the individual dynamics of each element, or as a small variability in the pair-wise interactions [86]. All of these kinds of alterations have qualitatively similar results. This means that the formation of such ordered states is not a result of degeneracy, and could in principle be observed in experimental or even natural systems.

High heterogeneities in the interactions would however destroy such forms of order [62, 65]. As it was shown in Chapter 3, the introduction of network interactions leads to the appearance of an incoherent state in which no macroscopic rotation occurs, but dynamics are highly chaotic. In network systems, contrary to the globally coupled case, the forces perceived by each element do not cancel out, and remain strong and highly variable even when the system becomes completely incoherent. This type of interaction leads the system to a special kind of chaotic dynamics that we have chosen to call *network turbulence* because of analogous aspects with hydrodynamic and chemical turbulence. Some dynamical properties of such network turbulence have proven to be independent of the specific interaction network and the parameter values, indicating that it is a universal behavior that only depends on the size of the system.

The transition between synchronization and turbulence has been explored by use of a global feedback, whose intensity we can manipulate to tune the system between different dynamical states. In this exploration we have seen that the transition takes place gradually, through the progressive emergence of active elements which perform rotations against a background of uniform oscillations. These elements initially act as isolated pacemakers which interact with the background and knock other elements out of synchrony. This is a dynamical selection process which gives rise to the emergence of self-organized active substructures in the network whose dynamics may be very complex. The resulting subnetworks are localized structures, within which the propagation of waves takes place and can be controlled by the global feedback. These emergent active subnetworks are therefore analogous to the coherent structures that are observed in oscillatory media in the interface between turbulence and synchrony.

In the turbulent regime, the presence of intermittency has been found as subsets of coherent elements sporadically emerge, resulting in transient bursts of synchronization. These bursts involve different groups of elements in each occurrence, which are formed by highly interconnected elements. This situation is reminiscent

of neuronal dynamics in the brain, where electro-encephalographic data reveals that transient coherent activity takes place in different areas of the cortex when a given task is performed [101, 103]. Bursts of localized coherence in the brain are directly related to the processing of information and cognitive functions. It is believed that the functionality of the brain is in a sense codified in the temporal and spacial structure of these bursts [104, 103]

Our results show that such dynamics already occur in random networks of extremely simple elements. It is conceivable that evolution may have led to the development of specific neural networks that make use of this intermittency, making the occurrence of such synchronous episodes efficient and robust.

For this reason, an interesting way in which our work could be extended would be to implement an evolutionary algorithm to engineer networks for which such synchronous episodes are fostered, perhaps even trying to reproduce target dynamical patterns of coherent activity. For this, a measurement of coherence between elements should be devised, such that the success or failure of a given network in attaining a desired functionality may be quantified. We have made a attempts in this direction with no substantial success, but research in this direction shall be continued.

Another relevant extension to our work would be that of including a phase shift for the feedback term, or even a real time delay. This should provide a second control parameter that would allow not only the size and number of active subnetworks to be selected, but also their dynamics and structure. Both theoretical and experimental studies on oscillatory media have proven this to be a successful control method [77, 78, 72], and preliminary simulations have indicated that it is a promising strategy for our system as well.

Bibliography

[1] A. S. Mikhailov & V. Calenbuhr, "From Cells to Societies: Models of Complex Coherent Action" (Springer, Berlin, 2nd ed. 2006).

[2] P.A. Tass, "Phase Resetting in Medicine and Biology" (Springer, Berlin, 1999).

[3] P. A. Tass, *Biol. Cybern.* **89**, 81 (2003).

[4] S. Lmmer, H. Kori, K. Peters & D. Helbing, *Physica A* **363**, 39-47 (2006) .

[5] Y. Kuramoto, "Chemical Oscillations, Waves, and Turbulence" (Springer, Berlin 1984).

[6] A. Díaz-Guilera & A. Arenas, In: Proceedings of the Workshop on Bioinspired design of networks (BIOWIRE 2007) (Springer, Cambridge, 2008).

[7] W. C. Lindsey & J.H. Chen, *Euro. Trans. Telecommun.* **7**, 25 (1996).

[8] E. Ott, C. Grebogi, & J. A. Yorke, *Phys. Rev. Lett.* **64**, 1196 (1990).

[9] E. D. Sontag, "Mathematical Control Theory: Deterministic Finite-Dimensional Systems" (Springer, Berlin, ed. 2, 1998).

[10] K. Pyragas, *Phys. Lett. A* **170**, 421 (1992).

[11] S. Kauffman, "The Origins of Order: Self-Organization and Selection in Evolution" (Oxford University Press, New York, 1993).

[12] S. Kauffman, "At Home in the Universe: The Search for Laws of Self-Organization and Complexity" (Oxford University Press, New York, 1995).

[13] C. G. Langton *Physica D* **42**, 12-37 (1990).

[14] M. Mitchell, P. T. Hraber, & J. P. Crutcheld. *Complex Systems* **7**, 89-130 (1993).

[15] M. G. Earl & S. H. Strogatz *Phys. Rev. E* **67**, 036204 (2003).

[16] A. S. Mikhailov, "Foundations of Synergetics I. Distributed Active Systems" (Springer, Berlin, 2nd ed. 1994).

[17] G.V. Osipov, J. Kurths & C. Zhou, "Synchronization in oscillatory networks" (Springer, Berlin,2007).

[18] A. Pikovsky, A. Rosenblum & J. Kurths, "Synchronization: A Universal Concept in Nonlinear Sciences" (Cambridge Univ. Press, Cambridge 2001).

[19] S. C. Manrubia, A. S. Mikhailov, & D. H. Zanette, "Emergence of Dynamical Order: Synchronization Phenomena in Complex Systems" (World Scientific, Singapore, 2004).

[20] E. Ott, "Chaos in Dynamical Systems" (Cambridge University Press, 1993).

[21] P. Grassberger & I. Procaccia, *Physica D* **9**, 189 (1983).

[22] M. V. Berry, *J. Phys. A*, **12**, 781 (1979).

[23] G. Benettin, L. Galgani, A. Giorgilli, J.-M. Strelcyn, *Meccanica* **21** (1980).

[24] I. Shimada & T. Nagashima, *Prog. Theor. Phys* **61**, 1605 (1979).

[25] A. Wolf, J. B. Swift, H. L. Swinney & J. A. Vastano, *Physica D* **16**, 285 (1985).

[26] P. Frederickson, J. Kaplan, E. Yorke & J. York, *J. Diff. Eqs.* **49**, 185 (1983).

[27] H. Daido, *Phys. Rev. Lett.* **68**, 1073 (1992).

[28] D. H. Zanette, *Europhys. Lett.* **72**, 190 (2005).

[29] J. A. Acebrón , L. L. Bonilla, C. J. Pérez Vicente, F. Ritort & R. Spigler, *Rev. Mod. Phys.* **77**, 137 (2005).

[30] F. C. Hoppensteadt & E.M. Izhikevich, "Weakly Connected Neural Networks" (Springer-Verlag, New York, 1997).

[31] E. M. Izhikevich, *Phys. Rev. E* **58**, 905 (1998).

[32] D. Hansel, G. Mato, & C. Meunier, *Phys. Rev. E* **48**, 3470 (1993).

[33] H. Kori & Y. Kuramoto, *Phys. Rev. E* **63**, 046214 (2001).

[34] H. Kori, Doctoral dissertation, Kyoto University (2003).

[35] P. Tass, *Phys. Rev. E* **56**, 2043 (1997).

[36] D. Golomb, D. Hansel, B. Shraiman & H. Sompolinsky, *Phys Rev. A* **45**, 3530 (1992).

[37] M. D. Fricker, J. A. Lee, L. Boddy & D. P. Bebber, *Topologica* **1** 004 (2008).

[38] J. M. A. Tanchoco (ed.), "Material flow systems in manufacturing" (Springer-Verlag, New York, 1994).

[39] D. Helbing (ed.), "Managing Complexity: Insights, concepts and applications" (Springer, Berlin, 2008).

[40] D. J. Watts, "Small Worlds: The Dynamics of Networks between Order and Randomness" (Princeton University Press, Princeton 2003).

[41] T. A. B. Snijders, *Jour. Math. Soc.* **21**, 149-172 (1996).

[42] A. Arenas, A. Daz-Guilera, J. Kurths, Y. Moreno & C. Zhoug, *Phys. Rep.* **469** 93-153 (2008).

[43] R. Albert, A.-L. Barabási, it Rev. Mod. Phys. **74**, 47-97 (2002)

[44] M. E. J. Newman, *SIAM Rev.* **45** 167-256 (2003).

[45] P. Erdős, & A. Rényi, *Publicationes Mathematicae* **6**, 290 (1959).

[46] J. Spencer (ed.), "Paul Erdős: The Art of Counting" (MIT Press, Cambridge, 1960).

[47] L. d. F. Costa, F. A. Rodrigues, G. Travieso, P. R. V. Boas, *Adv. Phys.* **56** 167-242 (2007).

[48] A.-L. Barabási & R. Albert, *Science* **286**, 509 (1999).

[49] S. Dorogovtsev, J.F.F. Mendes, *Adv. Phys.* **51**,1079-1187 (2002).

[50] S. H. Strogatz, *Nature* **410** 268-276 (2001).

[51] S. Boccaletti, V. Latora, Y. Moreno, M. Chavez & D.-U. Hwang, *Phys. Rep.* **424**, 175 (2006).

[52] Ch. Hyugens. English Translation: "The pendulum clock" (Iowa State University Press, Ames (1986).

[53] A. Winfree, *J. Theoret. Biol.* **16**, 15 (1967)

[54] S. H. Strogatz, "Obituaries: Arthur T. Winfree", January 30, 2003. SIAM News, http://www.siam.org/news/news.php?id=289.

[55] N. Wiener, "Cybernetics: Or Control and Communication in the Animal and the Machine" (John Wiley & Sons, New York, 1948).

[56] A.T. Winfree, "The Geometry of Biological Time" (Springer-Verlag, Berlin, 1980).

[57] Y. Kuramoto, in: H. Arakai (Ed.), International Symposium on Mathematical Problems in Theoretical Physics, Lecture Notes in Physics, Vol. 39 (Springer, New York, 1975).

[58] Y. Kuramoto, *Progr. Theoret. Phys. Suppl.* **79** 223 (1984).

[59] S. H. Strogatz, *Physica D* **143** 120 (2000).

[60] Y. Kuramoto, I. Nishikawa, *J. Statist. Phys.* **49**, 569 (1987).

[61] H. Daido, *J. Statist. Phys.* **60**, 753 (1990).

[62] J. G. Restrepo, E. Ott & B. R. Hunt, *Chaos* **16** 015107 (2005).

[63] D. H. Zanette, *Physica D* **237** 818828 (2008).

[64] A. E. Motter, C. S. Zhou & J. Kurths, *Europhys. Lett.* **69**, 334340 (2005)

[65] Y. L. Maistrenko, O. V. Popovych & P. A. Tass, *Lect. Notes Phys.* **671**, 285306 (2005).

[66] E. E. Holmes, M. A. Lewis, J. E. Banks & R. R. Veit, *Ecology* **75**, 17-29 (1994).

[67] S. Alonso, A. V. Panfilov, *Phys. Rev. Lett.* **100**, 218101 (2008).

[68] R. Kapral & K. Showalter (eds.), *Chemical Waves and Patterns* (Kluwer, Dordrecht, 1995).

[69] A. S. Mikhailov & K. Showalter, *Phys. Rep.* **425** , 79 (2006).

[70] M. Falcke, H. Engel, & M. Neufeld, *Phys. Rev. E* **52**, 763 (1995).

[71] M. Bär, M. Hildebrand, M. Eiswirth, M. Falcke, H. Engel & M. Neufeld, *Chaos* **4**, 499 (1994).

[72] M. Bertram, Doctoral Dissertation, Technische Universität Berlin (2002).

[73] O. Rudzick & A. S. Mikhailov, *Phys. Rev. Lett.* **96**, 018302 (2006).

[74] D. A. Egolf & H. S. Greenside, *Phys. Rev. Lett.* **74**, 1751 (1995).

[75] D. Battogtokh, A. Preusser, & A. S. Mikhailov, *Physica D* **106**, 327 (1997).

[76] D. Battogtokh & A. S. Mikhailov, *Physica D* **90**, 84 (1996).

[77] M. Kim, M. Bertram, M. Pollmann, A. von Oertzen, A. S. Mikhailov, H. H. Rotermund & G. Ertl, *Science* **292**, 1357 (2001).

[78] M. Bertram & A. S. Mikhailov, *Phys. Rev. E* **63**, 066102 (2001).

[79] F. Mertens, R. Imbihl, & A. Mikhailov, *J. Chem. Phys.* **99**, 8668 (1993).

[80] F. Mertens, R. Imbihl, & A. Mikhailov, *J. Chem. Phys.* **101**, 9903 (1994).

[81] J.-n. Teramae & D. Tanaka, *Phys. Rev. Lett.* **93**, 204103 (2004).

[82] H. Nakao, A. S. Mikhailov, *Phys. Rev. E* **79**, 036214 (2009).

[83] Y. L. Maistrenko, O. V. Popovych, O. Burylko & P. A. Tass, *Phys. Rev. Lett.* **93**, 084102 (2004).

[84] H. Nakao, K. Arai & Y. Kawamura, *Phys. Rev. Lett.* **98**, 184101 (2007).

[85] E. Moro & A. Sánchez, *Europhys. Lett.* **44**, 409 (1998).

[86] Zanette D. H. *Eur. Phys. Jour. B* **69**, 269 (2009).

[87] N. J. Balmforth & R. Sassi, *Physica D* **143** 2155 (2000).

[88] B. Madore & W. Freedman, *American Scientist* **75** 252-259 (1987).

[89] M. Woltering,R. Girnus, & M. Markus, *J. Phys. Chem. A* **103**, 4034-4037 (1999).

[90] A. J. Steele, M. Tinsley, & K. Showalter *Chaos* **16**, 015110 (2006).

[91] I. S. Aranson & L. Kramer, *Rev. Mod. Phys.* **74** 99 (2002).

[92] D. Ruelle & F. Takens, *Comm. Math. Phys.* **20**, 167 (1971).

[93] S. Newhouse, D. Ruelle & F. Takens, *Comm. Math. Phys.* **64**, 35 (1978).

[94] T. Bohr, M. H. Jensen, G. Paladin & A. Vulpiani, "Dynamical Systems Approach to Turbulence" (Cambridge University Press, Cambridge, 1998).

[95] D. Ruelle, *Comm. Math. Phys.* **87**, 287-302 (1982).

[96] V. Casagrande, A. S. Mikhailov, *Physica D* **205**, 154 (2005).

[97] B. Ermentrout, *Neural Comp.* **8**, 979 (1996).

[98] G. Mato, & I. Samengo, *Neural Comput.* **20**, 2418 (2008).

[99] Y. Kawamura & Y. Kuramoto, Phys. Rev. E **69**, 016202 (2004).

[100] G. Dragoi & G. Buzsaki, *Neuron* **50**, 145157 (2006).

[101] E. Rodríguez *et al.*, Nature **397**, 430 (1999).

[102] M. Falcke, M. Bär, H. Engel, & M. Eiswirth, *J. Chem. Phys.* **97**, 4555 (1992).

[103] M. I. Rabinovich, P. Varona, A. I. Selverston & H. D. I. Abarbanel, *Rev. Mod. Phys* **78**, 1213 (2006).

[104] U. Lindenberger, S.-C. Li, W. Gruber, & V. Muller, *BMC Neuroscience* **10**, 22 (2009).

Published works

During the course of the research and development of the work presented in this thesis, the following articles were produced

- "Networks at the edge of chaos: Global feedback control of turbulence in oscillator networks"
  S. Gil & A. S. Mikhailov, *Phys. Rev. E*, **79**, 026219 (2009).

- "Common noise induces clustering in populations of globally coupled oscillators"
  S. Gil, Y. Kuramoto & A. S. Mikhailov, *Europhys. Lett.*, **88**, 60005 (2009).

Acknowledgments

In the first place, I would like to thank Prof. Dr. Alexander S. Mikhailov, for having guided me through these three and a half years with so much dedication and disposition, and for opening for me the doors to the Fritz Haber Institute, where I could develop this work in absolutely ideal circumstances. I would also like to thank Prof. Dr. Harald Engel for his trust and support.

Scientific collaboration with Prof. Dr. Yoshiki Kuramoto has been very important for this work, as have also been the discussions with Prof. Dr. Keneth Showalter, Prof. Dr. Raymond Kapral and Prof. Dr. John (Jack) Hudson in several visits to our Group.

I am also very grateful to all the people whose paths I crossed during my stay in the Complex Systems group. In no particular order, I would like to thank Pablo Kaluza, Oliver Rudzick, Holger Flechsig, Sergio Alonso, Yuichi Togashi, Hiroya Nakao, and also Hiroshi Kori, Vanessa Casagrande, Michael Stich. All of them have helped me in different ways along the road.

Many thanks are also due to each and every current and former member of the Physical Chemistry Department. In particular, I thank Katrin Domke, Pablo Sánchez Bodega, Waruno Mahdi, Ingeborg Reinhardt, Marion Reimers and Dieter Bauer for their friendship, support, help and good humor. And of course, without Manya Hettwer and Elisabeth Stankewitz, my life at the Fritz Haber Institute would have been much harder.

To my parents, Inés Martínez de San Vicente and Carlos Gil, for their eternal support and encouragement in everything I do.

To Maureen, once again, for everything else.